Thesis for the Degree of Doctor of Philosophy

Combustion reactivity of ilmenite with coal volatiles under steam reforming atmosphere

Tsedenbal Battsetseg

Graduate School of Science and Technology,

Gunma University

September 2020

要旨

ケミカルルーピング石炭燃焼技術は、金属酸化物（酸素キャリア）の格子酸素で石炭を燃焼するため、従来の空気吹き石炭燃焼では不可避である、窒素による生成ガスの希釈が無く、分離装置の導入なしに燃焼炉出口で高濃度の CO_2 が得られるため、発電効率を損なうことなく CO_2 を高効率に分離・回収可能な発電技術として注目されている。このプロセスは、主に石炭ガス化炉、揮発分燃焼炉、空気炉の 3 つから構成される。まず、石炭ガス化炉において石炭を熱分解・ガス化する。ガス化ガスと揮発分は、分散板を介してガス化炉上部に設置された揮発分燃焼炉に運ばれ、酸素キャリアにより燃焼され CO_2 に転換する。これによって、燃焼炉からは、高濃度の水蒸気と CO_2 が排出され、分離・回収される。また、揮発分燃焼炉からオーバーフローでガス化炉に落下したキャリアは空気炉に運ばれ、消費されたキャリアの格子酸素を回復させることにより再生される。ケミカルルーピング石炭燃焼技術では、これら一連の化学プロセスが繰り返される。

通常、石炭の熱分解・ガス化では、燃料ガスの他、高分子炭化水素（タール）や炭素析出物、硫黄ガスなどが発生する。これらの汚染物質が CO_2 回収・貯留に悪影響を及ぼすことが懸念される。さらにケミカルルーピングプロセス運転障害や酸素キャリアの失活、大気汚染などの問題を起こす可能性がある。

本論文では主に石炭ケミカルルーピング燃焼プロセスの揮発分燃焼炉に着目し、酸素キャリアの酸化前処理、反応時の水蒸気濃度（Steam/Carbon(S/C) 比）、石炭の熱分解・ガス化により生成する硫黄不純物が、酸素キャリアによる揮発分の燃焼に及ぼす影響を明らかにすることを目的として、天然鉄チタン鉱物であるイルメナイト ($FeTiO_3$)を酸素キャリアとして、水蒸気改質条件及び硫黄ガス雰囲気下における酸素キャリアと石炭揮発分との燃焼反応性を詳細に評価した。また、比較試料として、人工酸素キャリア Fe_2O_3/Al_2O_3 についても検討した。酸素キャリアによる石炭揮発分の水蒸気改質実験は固定層流通式二段反応器を用いて、1173K で行った。

イルメナイトを酸化前処理することにより揮発分の CO_2 転換率が著しく増加し、タールの生成がほとんど見られなくなることを見出した。イルメナイトは酸化前処理すると比較的緻密な微構造を形成するが、水蒸気改質実験後には、内部及び表面が多孔

質化していた。また、イルメナイトは、広範な水蒸気濃度において高い反応性が維持され、S/C 比の増加に伴って炭素析出が大幅に減少することが明らかとなった。イルメナイトは、高 S/C 雰囲気下でも還元状態の $FeTiO_3$ が比較的に安定であるのに対して、Fe_2O_3/Al_2O_3 の還元状態 $FeAl_2O_4$ は高 S/C 雰囲気下では再酸化され、水素ガス収量が大幅に増加した。

さらに、固定層流通式二段反応器を用いて、水蒸気改質雰囲気下におけるイルメナイト及び Fe_2O_3/Al_2O_3 の石炭揮発分との反応性への H_2S の影響について検討した。その結果、低濃度の H_2S 存在下では、イルメナイトによる揮発分の燃焼が著しく促進され、H_2S なしと比べて CO_2 への転換率が向上することを見出した。さらに、様々な H_2S 濃度下において、イルメナイトの 8 サイクル酸化還元テストを行なった結果、低濃度の H_2S 存在下においてイルメナイトの初期還元反応速度が著しく上昇することがわかった。この結果より、イルメナイトの鉄成分の内部から表面への移動を H_2S が促すことで、イルメナイトの燃焼反応性が向上したと推定できる。一方、高濃度の H_2S 存在下では、還元さにより生成した金属鉄が硫化し、硫化鉄（$Fe_{1-x}S$）が析出するため、イルメナイトの燃焼反応性が低下するものの、析出した硫化物が次の酸化処理でほぼ完全に除去されることを確認した。H_2S とキャリアとの反応性は、キャリアの酸化状態（格子酸素）に大きく依存し、格子酸素が豊富な条件では、ほとんどの H_2S が酸素キャリアで酸化され SO_2 ガスとして揮発分燃焼炉から排出されるが、格子酸素が乏しい条件では、イルメナイトの硫化反応が進行し、硫黄成分が空気炉に持ち込まれるため、実際のプロセスでは、空気炉から SO_2 として放出されることが懸念される。Fe_2O_3/Al_2O_3 酸素キャリアでは、イルメナイトと比べて硫黄析出量が遥かに多く、より硫化しやすい傾向があり、H_2S による鉄硫化物（$Fe_{1-x}S$）の生成の影響により、水蒸気改質雰囲気下における石炭揮発分との燃焼反応性が著しく低下した。

これらの結果より、ケミカルルーピング石炭燃焼プロセスにおいて、十分な量のイルメナイトを高酸化状態に保つことによって、石炭の熱分解・ガス化により生成した揮発分を完全に燃焼することができ、また、高い硫黄被毒耐性を持たせることが可能であることを明らかにした。また、イルメナイトは、人工キャリアと比較して水蒸気との反応性が低いため、高い S/C 比で炭素析出を抑制しながら、安定的な運転が可能であることが示唆された。

ABSTRACT

Coal chemical-looping combustion is one of the most promising technologies for generating electricity from coal with high CO_2 capture. This process consists of three fluidized reactors. Coal is firstly gasified in the coal gasification reactor. Then the gasified products and coal volatiles are burned with the lattice oxygen of metal oxide particles (oxygen carrier) in the volatiles combustion reactor and converted into CO_2. In this way, CO_2 is inherently captured with high purity from in the volatiles combustion reactor. Finally, the depleted lattice oxygen in the metal oxides is compensated for in the air reactor.

Apart from H_2, CO, and CH_4, coal volatiles usually contain various pollutants such as condensable higher hydrocarbons (tar), carbon deposit, and sulfur gas. CO_2 capture and storage may be negatively affected by these pollutants. Moreover, they can damage oxygen carriers and decrease their reactivity, in addition to causing environmental and operational problems.

In this thesis, the combustion reactivity of ilmenite with the coal volatiles under steam reforming and sulfur gas atmosphere was investigated in order to evaluate the behavior of sulfur impurities, higher hydrocarbons (e.g., tar) and carbon depositions. A synthetic oxygen carrier of Fe_2O_3/Al_2O_3 was used for comparison. Steam reforming experiments of coal volatiles with oxygen carriers were carried out in a two-stage fixed-bed reactor. The effect of pre-oxidation and of steam ratios on the conversion reactivity of ilmenite was investigated at 1173 K.

It was found that the CO_2 conversion reactivity of ilmenite was greatly enhanced after pre-oxidation, and there was no tar formation. The internal and external porosity of ilmenite also increased after steam reforming of coal volatiles. Ilmenite showed good performance under the various steam conditions, so that carbon deposition decreased considerably as steam ratios increased. The reduced phase $FeTiO_3$ of ilmenite was maintained with the addition of steam, and its reactivity was relatively stable compared with the reduced phase $FeAl_2O_4$ of Fe_2O_3/Al_2O_3.

The effect of H_2S on the combustion reactivity of ilmenite and Fe_2O_3/Al_2O_3 with coal volatiles under a steam reforming environment was investigated in a two-stage fixed bed reactor. Ilmenite's combustion reactivity with carbon volatiles was greatly promoted in the presence of H_2S, and more CO_2 was obtained than without using H_2S. However, the reactivity activation of ilmenite decreased with a higher concentration of H_2S due to the formation of sulfur deposits (e.g., $Fe_{1-x}S$) on the reduced iron particles. Furthermore, eight-cycle redox tests of ilmenite were performed with various concentrations of H_2S. The presence of H_2S greatly enhanced the initial reaction rate of ilmenite. This could be due to that H_2S promotes the migration of more active iron species from the bulk structure of ilmenite to the external surface. While a higher amount of H_2S causes sulfidation on ilmenite, decreasing its combustion reactivity, all the sulfur accumulation on ilmenite can be removed by oxidation.

ACKNOWLEDGEMENTS

I wish to express my sincere gratitude to all the people who contributed to the work presented in this thesis. Particularly, I am deeply grateful to:

Professor Takayuki Takarada, my master's supervisor, for giving me the opportunities to start and pursue this chemical looping research work and to participate in many international conferences, and also for his invaluable knowledge and continued support.

My supervisor Professor Hiromi Shirai, Associate Professor Kazuyoshi Sato and Assistant Professor Naokatsu Kannari for their supervision and guidance, experimental support and discussion, and encouragement during my PhD studies at Gunma University.

All the students in Sato & Kannari laboratory for creating me a friendly and supportive study environment.

All the staffs at the Department of Environmental Engineering Science and in the Student Support Center for their helps and support.

Kota Sakamoto in the Instrumental Analysis Center of Gunma University for his technical support in XPS analysis.

Dr. Atul Sharma at National Institute of Advanced Industrial Science and Technology and Dr. Tomonao Saito in the Japan Coal Energy Center (JCOAL) for their helpful advice and information.

I also acknowledge and appreciate the financial support provided by the New Energy and Industrial Technology Development Organization (NEDO).

Last but not least, I would like to thank my family and my lovely kids for their endless love, encouragement and motivation.

TABLE OF CONTENTS

Chapter 1 INTRODUCTION

1.1 CO_2 emissions and power generation

Carbon dioxide (CO_2) is a major greenhouse gas which prevents some of the solar heat from escaping back to the space, keeping the earth warm. The level of CO_2 released into the atmosphere has increased significantly from 280 ppm in 1750 to 413 ppm in 2019 due to the human activity and industrialization [1]. The global energy-related CO_2 emissions reached to 33.1 Gt CO_2 in 2018 [2], mostly due to combustion of fossil fuels, e.g. coal, oil and natural gas. They are mainly from four sectors: power (40%), industry, e.g. iron and steel production, cement making, chemicals and refining (24%), transport (22%) and buildings (8%) [3]. However, the greatly increased amount of CO_2 is causing to earth's temperature to rise rapidly and global warming.

A substantial effort is required to arrest the growth in CO_2 emissions. The United Nations climate conference, held in December 2015, reached the Paris Agreement COP21, that sets a goal of limiting global warming to less than 2 degrees [4]. According to the Paris Agreement, world average temperature is expected to rise approximately 6 degrees in 2050, unless we take any measures against CO_2 emissions. In order to stay the rise of the world mean temperature to below a 2 degree, the cumulative carbon budget is required about 40% lower over the period to 2060, and contributions from various technology across all sectors are needed. Figure 1 shows the estimation of annual global CO_2 emissions until 2060 and reductions by technology for a 2 degree scenario (2DS) [3]. The largest contributors are energy efficiency and renewables, which account for a 40% and 35% share, respectively. CO_2 capture and storage (CCS) is also a key technology to a 2DS, providing 14% of cumulative CO_2 emissions reduction through 2060 compared to current ambitions (RTS). In addition, a combination of CCS with fuel and electricity efficient technology is expected to contribute 32% in the shift to beyond 2 degree scenario (B2DS).

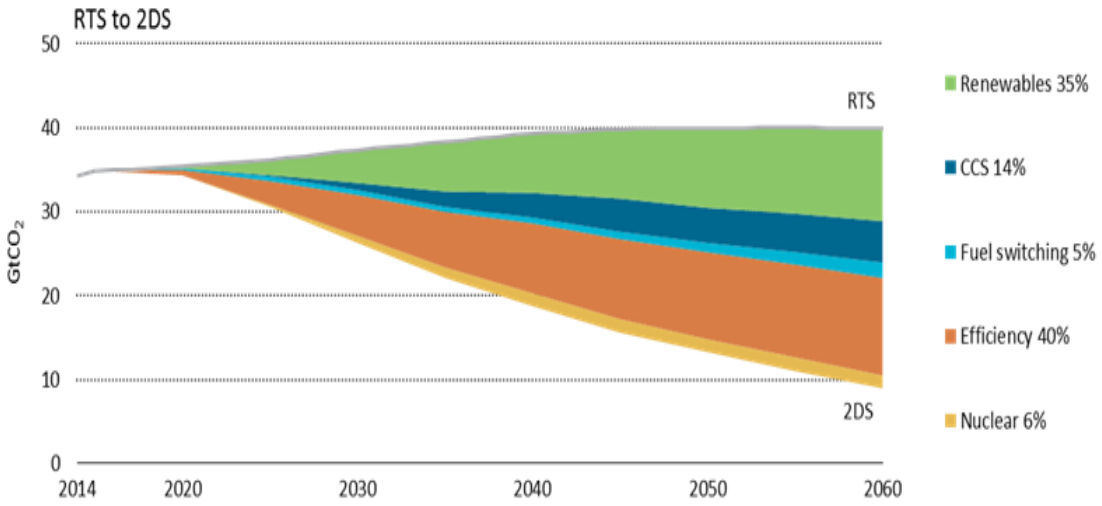

Figure 1. Technology contribution to CO_2 emissions reduction for the 2DS [3]

According to the summary of international energy agency, energy demand worldwide continues to increase and more than doubles by 2060. As the largest source of greenhouse gas emissions, the energy sector must be at the heart of global action to tackle climate change. In the 2DS, the global energy sector needs to reach net-zero CO_2 emissions in 2060, and deep and rapid emissions cuts in the power sector have to be made, especially in coal-fired power plants.

On the other hand, coal is an excellent energy source in providing stable low-cost electricity due to its wide distribution with rich reserves all over the world. In 2014, coal accounted for 9500TWh, 41% of all world energy production [5]. Proved reserves of coal are estimated at around 3.2 trillion barrels of oil equivalent, accounting for half of all proved reserves of fossil fuels. That is sufficient to meet current demand for over 100 years[2]. Coal remains the backbone of the power system in many countries. However, future use of coal faces a significant challenge of net zero emissions. Its continued usage must be compatible with stringent environmental policies. For instance, it can be used only with CCS in the most efficient way. In the 2DS it is estimated that coal-fired power generation without CCS declines and is almost completely phased out by 2045 [6]. At a minimum, new coal power plants that are built should be equipped with CCS.

1.2 Carbon capture and storage (CCS)

1.2.1 Overview of CCS

CO_2 capture and storage (CCS) is a vital technology to capture CO_2 from power stations or industry processes without emitting it to the atmosphere, transport it to sites suitable for geological sequestration, and store it stably underground for a long period of time. Capturing and fixing CO_2 into deep underground can thus mitigate climate change. Overview and the potential of CCS is given in the Intergovernmental Panel on Climate Change (IPPC) Special Report on Carbon Dioxide Capture and Storage [7].

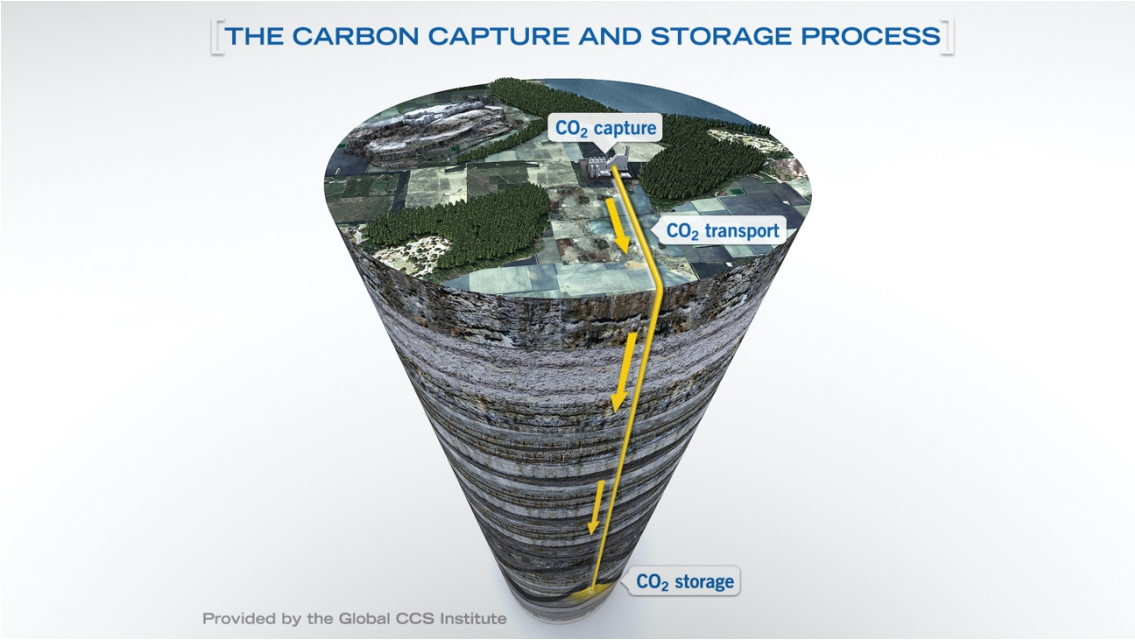

Figure 2. The overview of CCS process, *provided by Global CCS Institute* [8]

CCS technology involves three major steps:

1. **Capture:** From the flue gas emitted from power plants and large-scale factories, CO_2 is separated and captured as high-purity CO_2.

2. **Transport:** Once separated from the other elements of the flue gas, the CO_2 is compressed and transported to a suitable location for geological storage. Today, CO_2 is transported most often by pipelines, but also by ship and road tanker, for use in the oil industry where it is injected into mature fields to enhance oil

recovery, as well as for use in the food and beverage industry. However, the scale of transportation required for widespread deployment of CCS is far more significant than present levels.

3. **Storage:** CO_2 is injected into deep underground rock formations, often at depths of one km or more. Injected CO_2 is blocked upward migration by tick and impermeable layers (known as the caprock) so that CO_2 stored safely and stably. The caprock acts as an upper seal and prevent leakage of CO_2. Once injected, a range of technologies is used to monitor movement of the CO_2 underground. Monitoring, reporting and verifying processes are important to ensure that the CO_2 is safely and permanently stored.

1.2.2 CCS projects in Japan

According to the Global CCS Institute CO_2RE database [9], there are 23 large-scale integrated CCS projects in operation or under construction across the world, capturing CO_2 emissions. The most significant project developments are illustrated in Figure 3.

Figure 3. The key CCS project developments across the world [10]

Today, Japan has the following CCS projects [9] in operation or under construction.

1. The Tomakomai CCS Demonstration Project

Project proponents	The Ministry of Economy, Trade and Industry (METI) and Japan CCS Co.,Ltd.
Location	Tomakomai area, Hokkaido, Japan.
Project status	Operational
CO_2 capture source	CO_2 is to be sourced from a hydrogen production unit at Idemitsu Kosan's Hokkaido Refinery at Tomakomai port.
Capture method	Industrial separation – absorption chemical solvent-based process.
Storage type	Dedicated geological storage – deep saline aquifers. Two separate near shore reservoirs have been identified as storage sites.
CO_2 stored	Approximately 100,000 tons of CO_2 per annum is to be injected over the period 2016-18, with post-injection monitoring continuing.

2. COURSE 50 - CO_2 Ultimate Reduction in Steelmaking Process by Innovative Technology for Cool Earth 50

Project proponents	Kobe Steel, JFE Steel Corporation, Nippon Steel Corporation, Nippon Steel & Sumikin Engineering, Sumitomo Metal Industries and Nissin Steel, the New Energy and Industrial Technology Development Organization (NEDO), the Research Institute of Innovative Technology for the Earth (RITE) and several universities.
Location	Nippon Steel & Sumitomo Metal Corporation, Kimitsu, Chiba. JFE Steel Corporation, Fukuyama, Hiroshima.
CO_2 capture source and capacity	The separation and capture of CO_2 from blast furnace gas. CO_2 capture capacity is 30 tons per day at pilot plants and 3-6 tons per day at bench scale plant
Capture method	Chemical absorption –Physical adsorption
Project status	Operational

3. The EAGLE project (Coal Energy Application for Gas, Liquid and Electricity).

Project proponents	Electric Power Development Company (J-POWER), the New Energy and Industrial Technology Development Organization (NEDO), an independent administrative agency under METI.
Location	J-POWER Wakamatsu Research Institute, Fukuoka.
Project status	Testing completed.
CO_2 capture source	Gases generated during the coal gasification process at J-POWER's 150 tons per day (coal feed rate) oxygen-blown coal gasification pilot plant.
Capture method and type	Pre-combustion capture (gasification) – CO_2 capture from coal gasification gas, testing both chemical absorption and physical absorption methods.
CO_2 capture capacity	Approximately 24 tons per day.

4. The OSAKI COOLGEN project

Project proponents	The Osaki CoolGen Corporation was established in 2009 under joint funding by J-POWER and the Chugoku Electric Power Company.
Location	Chugoku Electric Osaki power station, Osakikamijima, Hiroshima.
Project status	In Construction
CO_2 capture source	CO_2 from the gases generated during the coal gasification process at Osaki CoolGen Corporation's 166MW oxygen-blown coal gasification demonstration plant.
Capture method and type	Pre-combustion capture (gasification) – CO_2 capture from coal gasification gas, testing both chemical absorption and physical absorption capture methods.

5. Saga City Waste Incineration Plant

Project proponents	Toshiba Corporation completed the construction of a carbon capture and utilization system at a municipal waste incineration plant in Saga city.
Location	Saga city waste incineration plant, Saga.
Project status	Operational
CO_2 source	CO_2 from the flue gas of the incinerator.
Capture method and capacity	Post-combustion capture. Approximately 10 tons of CO_2 per day.

6. Nagaoka CO_2 Storage Project

Project proponents	Nagaoka prefecture. The first pilot CO_2 injection test in Japan.
Location	The Minami-Nagaoka onshore gas and oil field, Nagaoka, Niigata.
Project status	Completed
Storage type	CO_2 injected into reservoir of natural gas processing
CO_2 stored	Overall, 10,400 tons of CO_2 were injected between 2003-2005

7. Mikawa Post Combustion Capture Demonstration Plant

Project proponents	Toshiba Corporation, The Mizuho Information & Research Institute
Location	Mikawa thermal power plant in Omuta, Fukuoka.
Project status	In construction
CO_2 source	CO_2 from the flue gas of the 50MW power plants.
Capture method and capacity	Post-combustion capture. Approximately 500 tons of CO_2 per day.

1.2.3 CO_2 capture technologies

The application of CO_2 capture technologies plays a key role in achieving net zero emissions. CO_2 capture can be applied to large-scale energy and industrial processes, including coal and gas-fired power plants, iron and steel production, cement making, chemicals and refining. In normal combustion process, the dry CO_2 concentration is 10-15%. Since less undiluted CO_2 is needed for storage, the separation of CO_2 from any other gases present in the flue gas is the most important step in CCS process. CO_2 can be separated form a carbon emission source either before or after its combustion to produce energy or other products. There are 3 ways to capture CO_2 that can be applied to the power sector, described in Figure 4:

- **Post-combustion:** CO_2 is separated from the flue gas from a conventional power plant. Organic solvents, e.g. monoethanolamine (MEA) is typically employed for CO_2 separation.
- **Pre-combustion:** The fuel is converted to H_2 and CO_2 via gasification and water gas shift reactions. CO_2 is separated from a mixture gas prior to combustion and the remaining H_2 is burnt for power generation.
- **Oxyfuel combustion:** Pure oxygen instead of air is used for fuel combustion to produce a flue gas that is mainly CO_2 and H_2O. Almost pure CO_2 is obtained by condensing steam. However, oxygen separation from air induces extra cost and energy penalty.

  Chemical Looping Combustion (CLC) is usually classified as an oxyfuel combustion process. It is quite revolutionary power generation technology to build a total redesign of the steam boiler, having significant advantages for future power plants with CCS.

The CO_2 capture can also be applied for industrial processes such as the chemical, cement and steel plants, as presented by the 4^{th} path in Figure 4 [7].

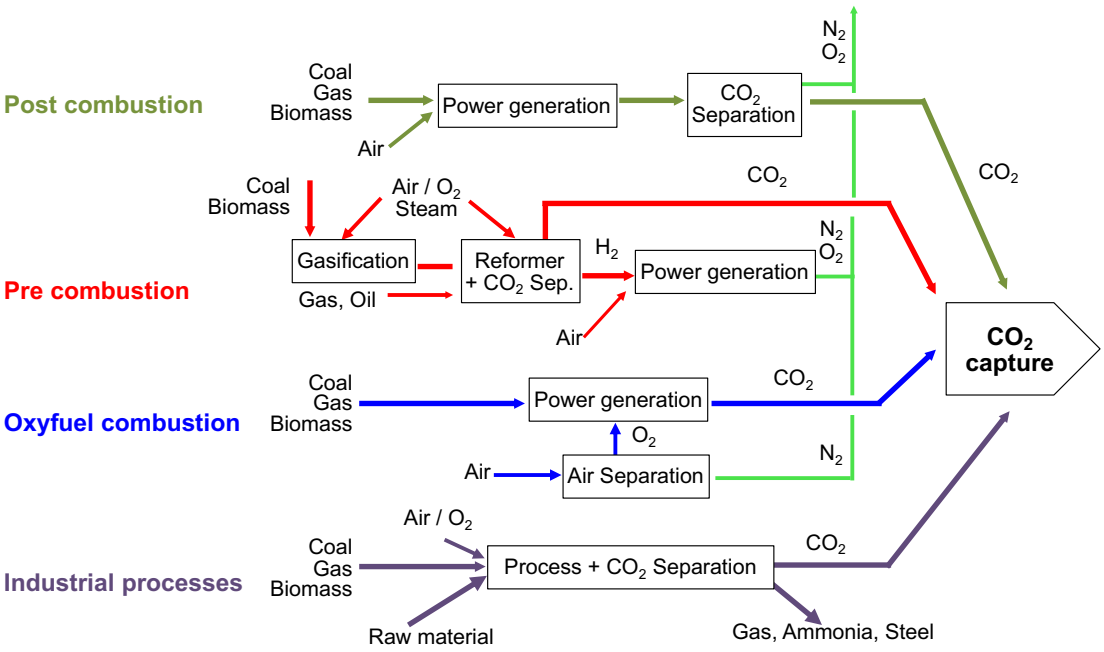

Figure 4. Overview of CO_2 capture in power and industrial processes [7]

Different separation technologies such as solvent absorption, sorbent adsorption, membrane and cryogenic separation technologies can be applied to CO_2 capture (see Appendix Table A1). Some are more effective for high concentration CO_2, and others are better at handling low concentration CO_2. Therefore, depending on the application, a properly integrated and optimized capture system are to be more energy efficient and lower cost.

Among the three major steps of CCS, CO_2 capture is most expensive. Applying CO_2 capture in power plants results in a gain of power generation cost. Figure 5 shows power generation cost by various power plants with CCS [11]. For Supercritical Pulverized Coal (SCPC) plants, power generation without CCS costs around 7JPY/kWh, whereas the unit price of electricity would be almost doubled to 14JPY/kWh in SCPC with 80% of CO_2 capture. Although the price with CCS would slightly decrease in the Integrated coal Gasification Combined Cycle (IGCC) and the Oxyfuel combustion plants, they are still too high for the commercialization. In this context, chemical looping combustion (CLC), which is the topic of this thesis, is the most promising and inexpensive technological option for power generation with CCS. The estimated cost of power generation with CLC would be substantially lower than other power plants with CCS, because no air separation and additional gas separation units are required.

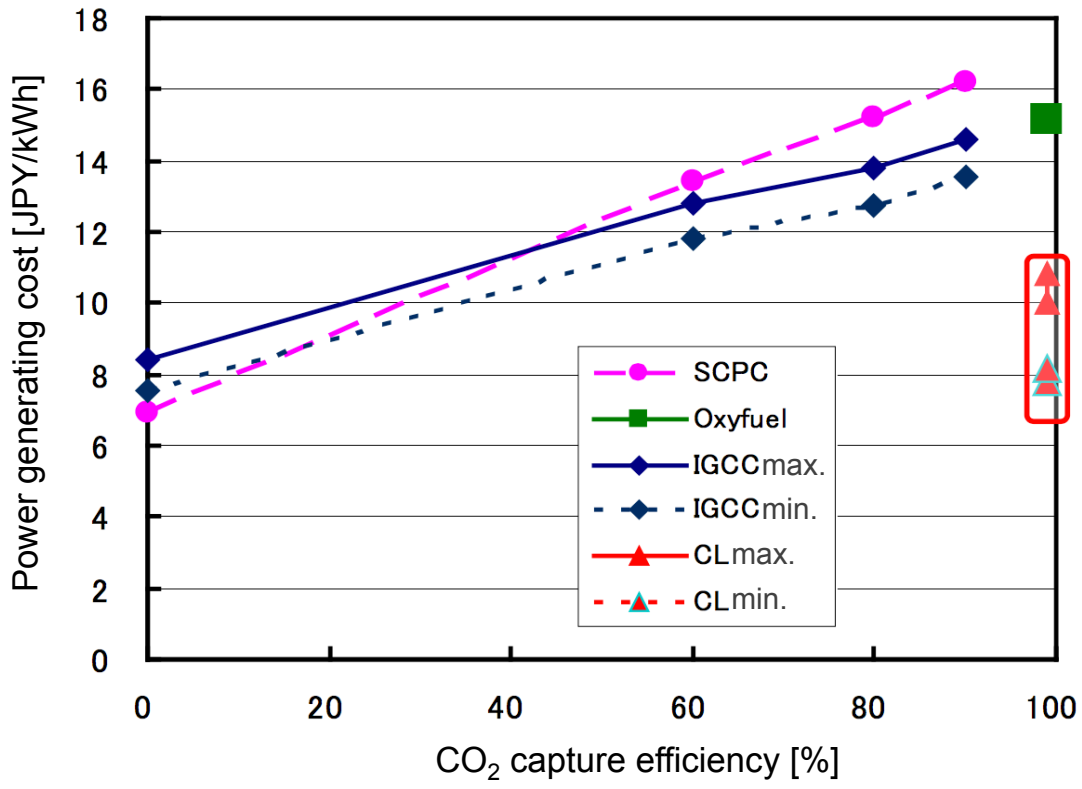

Figure 5. Power generation cost of power plants with CCS [11]

1.3 Chemical looping combustion (CLC)

1.3.1 Overview of CLC

Chemical looping combustion (CLC) is a power generation technology with capturing CO_2 at low cost because expensive gas separation units are not required. CO_2 is inherently captured in CLC. Since fuel and air are never mixed, the exhausting CO_2 is not diluted by atmospheric nitrogen, so that CO_2 can be obtained with more than 90% concentration. The first idea and the principle of CLC can be attributed to Lewis *et al*. [12] and Richter *et al*. [13], respectively, whereas the use of CLC as a CO_2 capture technology was recognized in 1994 by Ishida, *et al*. [14,15]. Lyngfelt *et al*. proposed the use of two interconnected fluidized reactor design for CLC in 2001 [16]. A number of CLC studies have been performed around the world [17].

In the CLC system, metal oxide particles, referred to as an oxygen carrier, are circulated in order to transfer an oxygen from air to fuel, avoiding direct contact between them. Fuel is burnt with the oxygen from an oxygen carrier, while the depleted oxygen content in oxygen carrier is recovered by air. As shown in Figure 6, CLC system basically consists of two fluidized-bed reactors: a fuel reactor for fuel combustion, and an air reactor for oxygen carrier regeneration, with the oxygen carrier circulating between them.

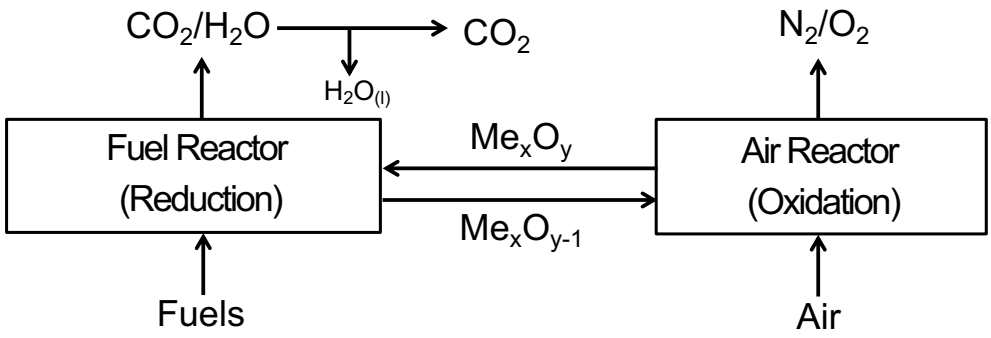

Figure 6. Schematic diagram of chemical looping combustion

Fuel reactor: $\text{Fuel} + Me_xO_y \rightarrow Me_xO_{y-1} + H_2O + CO_2$ (R1)

Air reactor: $Me_xO_{y-1} + O_2 \rightarrow Me_xO_y + \text{Heat}$ (R2)

Redox reactions of the oxygen carrier are applied for fuel combustion and oxygen carrier regeneration. In a fuel reactor, fuel is combusted by oxygen carrier and releases CO_2 and water steam, described in reaction R1. When the oxygen carrier provides its lattice oxygen to fuel, it is then reduced. The reduced carrier transfers to the air reactor. In the air reactor, the carrier is oxidized by air and reactivated to its oxidized form, as shown in reaction R2. A reaction in the fuel reactor is usually endothermic and a reaction in the air reactor is exothermic. However, overall heat in CLC is equal to the heat released from normal combustion.

1.3.2 Oxygen carriers

The performance of the CLC system greatly depends on the type of oxygen carrier.

Basically, the ideal oxygen carriers should have [17]:

- High oxygen transport capacity
- High redox reactivity over the repeated cycles
- High mechanical strength and stability in fluidized beds
  (low tendency to of attrition and fragmentation)
- High fluidizability and resistance to agglomeration and sintering
  (high melting temperature)
- Low cost and long lifetime
- Environmental compatibility and low toxicity

Many kinds of materials have been tested and developed as suitable oxygen carrier for CLC. Materials based on Ni, Cu, Fe and Mn oxides have already shown good reactivity for gaseous fuels [17-24]. The supporting inert materials, which could enhance chemical and physical properties of active metal oxides, e.g., porosity, specific surface area, mechanical strength and attrition resistance, are also important. The reactivity and crushing strength of various oxygen carriers of Cu, Fe, Mn or Ni oxides as an active solid were investigated with Al_2O_3, sepiolite, SiO_2, TiO_2 or ZrO_2 as an inert [19].

As for the choice of oxygen carrier used in coal CLC, an abundant supply, reasonable price, and environmentally benign nature are favorable because partial loss and a complementary supply of oxygen carrier are to be expected with removal of coal ash [25]. Oxygen carriers based on Ni, Fe and Mn have been studied for direct coal CLC. Ni-based oxygen carriers have high reactivity and the CO_2 capture efficiency is high. However, Ni oxides are expensive and toxic as well as easily deactivated by sulfur from coal [26]. Therefore, the use of Ni is not suitable for coal CLC. Mn oxides are relatively cheap and more available as a natural ore. Experiments of Mn ore showed increase of char gasification rate and high CO_2 capture efficiency, owing to Na and K contents in the manganese ore [27]. However, the main disadvantage of Mn ore is low attrition resistant, which causes operation problem and decreases the lifetime of the oxygen carrier [28]. Fe-based carriers have been extensively investigated for CLC with coal because of their abundance, reasonable price, and environmentally benign nature [29-33]. Especially, a natural iron titanium oxide ore, ilmenite has recently received more attention in coal CLC, due to its reasonably high reactivity in fluidized bed systems, as well as, high mechanical strength, and stability against agglomeration and attrition [34-39].

1.3.3 CLC with coal

Application of CLC to coal is more essential due to the massive amount of CO_2 emissions caused by coal-fired power plants. The recent progress in CLC with solid fuels was reviewed by Adánez *et al.* in 2018 [25]. There are two approaches proposed for CLC with coal. Schematic illustrations are shown in Figure 7.

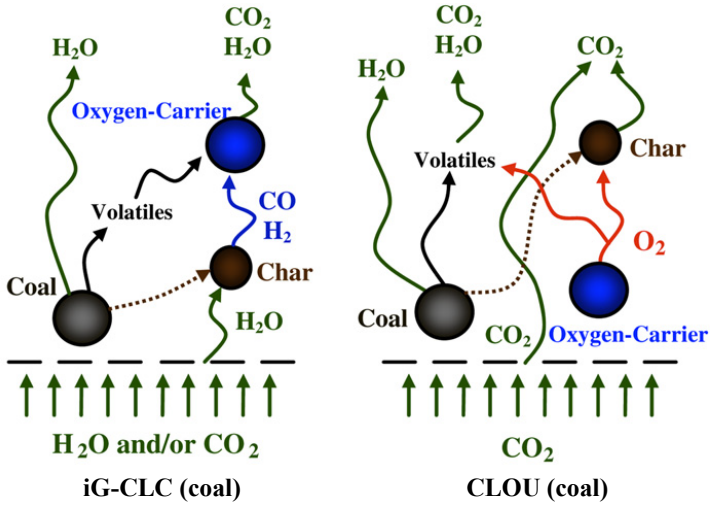

Figure 7. Scheme of the iG-CLC and CLOU processes for coal [25]

The first one is a Chemical Looping with Oxygen Uncoupled (CLOU) process, where coal is burnt with gaseous oxygen from oxygen carrier in the fuel reactor [40]. The CLOU process is based on the use of oxygen carrier, which releases gaseous oxygen in the fuel reactor (R3). Coal is thereby burnt with the gas phase oxygen (R5-R6). However, the suitable oxygen carriers are very limited. Only some Cu-, Mn-, and Co-based oxygen carriers have the oxygen releasing property.

$2Me_xO_y \rightarrow 2Me_xO_{y-1} + O_2$ (R3)

$Coal \rightarrow Volatiles + Char$ (R4)

$Char\ (C) + O_2 \rightarrow CO_2$ (R5)

$Volatiles\ (e.g., CH_4) + O_2 \rightarrow CO_2 + H_2O$ (R6)

Another CLC with coal is in-situ Gasification Chemical Looping Combustion (iG-CLC) [41-45], where coal is in-situ gasified in the fuel reactor and then coal volatiles and gaseous products from char gasification are burnt by the oxygen carrier. One feasible

configuration of iG-CLC, developed by Japan Coal Energy Center (JCOAL), is shown in Figure 8 [46–47]. This project mainly employs iron-based oxygen carriers and undergoes the following main chemical reactions R7 to R12 at 1173K therein. At higher temperature, coal is thermally decomposed into solid carbon (Char) and volatiles (R7). Volatiles usually contain variable amounts of H_2, CO, CO_2, CH_4 and higher hydrocarbons. As a solid–solid reaction between char and oxygen carrier is negligible compared to solid-gas reactions, char formed by coal pyrolysis needs to be gasified by steam (R8). Volatiles and the gasifying products, i.e., H_2 and CO, then enter through a dispersion plate with nozzles to the volatiles reactor, where an oxygen carrier converts them into CO_2 and H_2O according to reactions R9 to R11. The mixture of steam and CO_2 exiting from the volatiles reactor is passed through a cyclone, a heat exchanger and a condenser so that ash and steam can be fully separated from CO_2. The CO_2 is then compressed for storage.

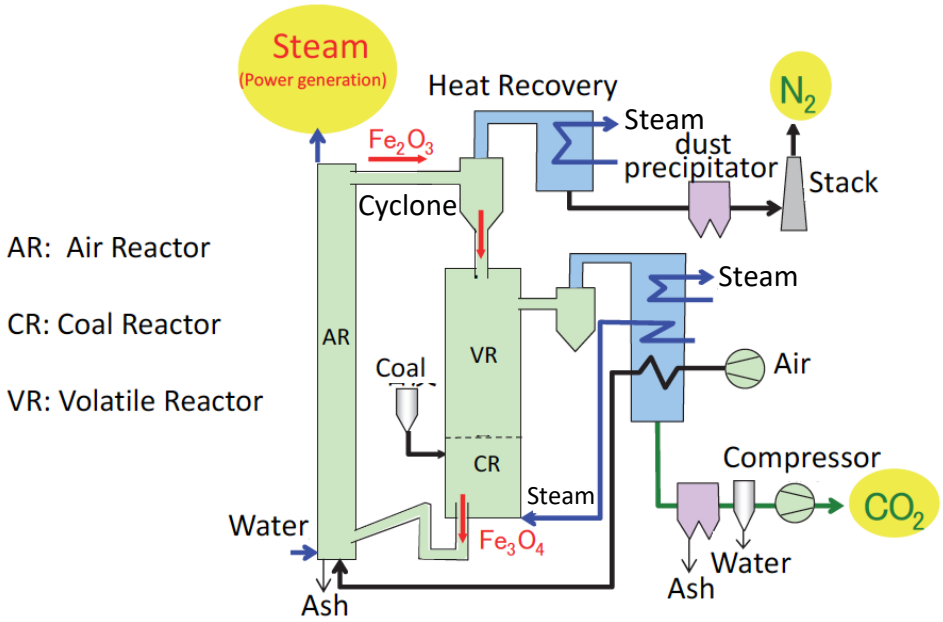

Figure 8. Schematic illustration of the iG-CLC in Japan [46]

$$\text{Coal} \rightarrow \text{Volatiles} + \text{Char} \quad \text{(R7)}$$

$$\text{Char (C)} + H_2O \rightarrow CO + H_2 \quad \text{(R8)}$$

$$\text{Volatiles (e.g., } CH_4) + 3Fe_2O_3 \rightarrow CO_2 + H_2O + 6FeO \text{ (or } Fe_3O_4) \quad \text{(R9)}$$

$$H_2 + Fe_2O_3 \rightarrow H_2O + 2FeO \text{ (or } Fe_3O_4) \quad \text{(R10)}$$

$$CO + Fe_2O_3 \rightarrow CO_2 + 2FeO \text{ (or } Fe_3O_4) \quad \text{(R11)}$$

$$2FeO \text{ (or } Fe_3O_4) + 1/2O_2 \rightarrow Fe_2O_3 \quad \text{(R12)}$$

Meanwhile, the reduced oxygen carrier is transferred through a overflower tube and a loop seal to the air reactor, where it is oxidized by air (R12). The regenerated oxygen carrier is then transported back to the volatiles reactor by a cyclone separation from the reduced air stream. Two reactors are linked together through loop seals to prevent gas leakage from one reactor to another.

From energy efficiency point of view, the oxygen carriers needs to transport heat from air reactor into volatiles and coal reactors in order to support the endothermic reactions (R7-R11). In addition, much of the heat required for steam generation and air pre-heating can offset by the CO_2 stream leaving the volatiles reactor and the reduced air stream leaving from the air reactor. That can be achieved by heat exchangers. The heat generated from air reactor runs a steam cycle which converts the thermal energy into electricity.

To achieve high CO_2 capture, the complete conversion of volatiles and char are desirable in iG-CLC. In real CLC operations, steam may be more practical to be used in the fuel reactor. Oxygen can be provided by steam when CLC process runs under an oxygen deficiency. Steam in CLC can work not only as a gasifying and fluidizing agent, but also as a reformer, inhibitor and oxidizer in coal CLC. Simultaneously, the other components of the coal volatiles may interact with the oxygen carrier or each other in a large number of different reactions, of which some of the most important reactions with steam are as follows:

Hydrocarbons reforming

C_mH_n (e.g.,tar, CH_4) + $mH_2O \rightarrow mCO + (m+n/2)H_2$ (R13)

Carbon gasification

$C + H_2O \rightarrow CO + H_2$ (R14)

Water gas shift reaction

$CO + H_2O \rightarrow CO_2 + H_2$ (R15)

All these reactions simultaneously take place in the fuel reactor and their contribution to CLC largely depends on the nature of oxygen carrier, gas composition, oxygen availability and operating conditions.

1.4 The objectives and scope of this work

When coal is employed as fuel, it is important to consider various factors such as sulfur impurities, nitrogen impurities or higher hydrocarbons and carbon depositions because these pollutants could deteriorate the performance of the CLC units [48-53], as shown in Figure 9. The condensable hydrocarbons, i.e. tars can cause operational problems such as clogging and blockage of downstream equipment in the CLC process. Specially, the nozzles of gas dispersion panel between volatiles and coal reactors can be clogged with tars and soot (carbon deposits). Moreover, the carbon deposited on the oxygen carrier can decrease its reactivity. It also transfers to the air reactor and is combusted by air, which results in a loss of CO_2 capture efficiency. Sulfur contaminant from coal can also damage oxygen carriers and decrease their reactivity, in addition to causing environmental and CO_2 capture and storage problems. Typically, coal volatiles contain all these unwanted components.

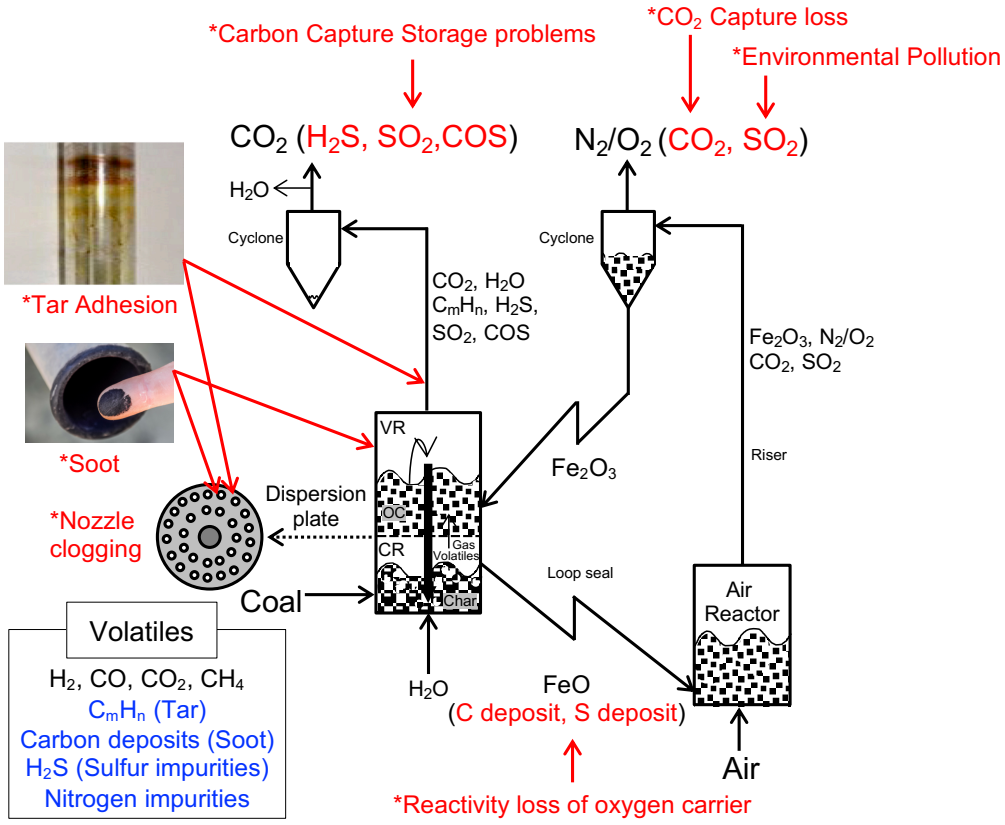

Figure 9. Problems derived from coal during iG-CLC operation

In this work, we used actual volatiles released from coal pyrolysis as fuel and aimed to investigate the combustion reactivity of ilmenite with the coal volatiles under the more realistic steam reforming and sulfur gas environment and to evaluate the behavior of the damaging factors such as tars, carbon depositions and sulfur gases. A synthetic oxygen carrier of Fe_2O_3/Al_2O_3 was employed as a comparative reference. The steam reforming experiments were performed using a two-stage fixed bed reactor. Thermogravimetric analyses were also performed for further investigation of cycle redox reactivity of ilmenite and Fe_2O_3/Al_2O_3.

Generally, the greater amount of oxygen carrier, i.e. lattice oxygen is supplied to the CLC system, the higher CO_2 capture efficiency can be obtained. In fact, the estimated amount of oxygen carrier for full combustion efficiency in the proposed iG-CLC system is several dozens of times higher than its theoretical value. That requires a large-scale operation unit. A detailed investigation on the reactions of coal volatiles and gasification products with oxygen carrier is needed in order to minimize the operation unit of CLC system. In this work, the investigations were mainly performed under an oxygen deficient condition (less than the stoichiometric amount) in order to evaluate a primary reaction tendency of ilmenite with coal volatiles.

This thesis is divided into four chapters.
Chapter 1 covers the introduction and background of this study and includes the fundamental and current development of carbon capture and storage (CCS) and chemical looping combustion (CLC) processes as well as the objective of this study.

Chapter 2 presents investigations on the combustion reactivity of ilmenite with coal volatiles under various steam conditions, including the effect of pre-oxidation and of increased steam ratios, of increased amount of oxygen carrier, as well as redox reactivity tests of ilmenite and Fe_2O_3/Al_2O_3.

Chapter 3 investigates the influence of sulfur gas on the combustion reactivity of ilmenite with coal volatiles under steam reforming atmosphere, in comparison with Fe_2O_3/Al_2O_3. The effect of sulfur gas on the redox reactivity of oxygen carriers was also assessed.

Chapter 4 provides a set of conclusions and recommendations for future work.

References

[1] https://www.co2.earth

[2] IEA (2019), Global Energy & CO2 Status Report 2019, IEA, Paris

[3] IEA (2017), Energy Technology Perspectives 2017, IEA, Paris

[4] FCCC/CP/2015/10/Add.1.https://www.un.org/en/development/desa/population/migration/generalassembly/docs/globalcompact/FCCC_CP_2015_10_Add.1.pdf

[5] Global CCS Institute, The Global status of CCS 2014.

[6] IEA, Share of coal-fired power generation in the Sustainable Development Scenario, 2000-2040, IEA, Paris

[7] IPCC, 2005: IPCC Special Report on Carbon Dioxide Capture and Storage

[8] Global CCS Institute, CCS image library.

[9] Global CCS Institute, CO_2Re Database.

[10] Global CCS Institute, The Global status of CCS 2017.

[11] Y.Yasui, NEDO's effort to reduce the cost of CO_2 capture. https://www.nedo.go.jp/nedoforum2015/en/program/pdf/ts6/akira_yasui.pdf

[12] W.K. Lewis, E.R. Gilliland, M.P. Sweeney, Gasification of carbon-Metal oxides in a fluidized powder bed, Chem. Eng. Prog. 47 (1951) 251–256.

[13] H.J. Richter, K.F. Knoche, Reversibility of combustion processes, in: R.A. Gaggioli (Ed.), Efficiency and Costing, American Chemical Society, Washington, 1983, pp. 71–85.

[14] M. Ishida, H. Jin, A new advanced power-generation system using chemical-looping combustion, Energy 19 (1994) 415–422.

[15] H. Jin, M. Ishida, A new type of coal gas fueled chemical-looping combustion, Fuel 83 (2004) 2411–2417.

[16] A. Lyngfelt, B. Leckner, T. Mattisson, A fluidized-bed combustion process with inherent CO_2 separation; application of chemical-looping combustion, Chem. Eng. Sci. 56 (2001) 3101–3113.

[17] J. Adanez, A. Abad, F. Garcia-Labiano, P. Gayan, L.F. de Diego, Progress in chemical-looping combustion and reforming technologies, Prog. Energy Combust. Sci. 38 (2012) 215–282.

[18] T. Mattisson, A. Lyngfelt, P. Cho, The use of iron oxide as an oxygen carrier in chemical-looping combustion of methane with inherent separation of CO_2, Fuel 80

(2001) 1953–1962.

[19] J. Adánez, L.F. de Diego, F. García-Labiano, P. Gayán, A. Abad, Selection of oxygen carriers for chemical looping combustion, Energy & Fuels 18 (2004) 371–377.

[20] P. Cho, T. Mattisson, A. Lyngfelt, Comparison of iron-, nickel-, copper- and manganese-based oxygen carriers for chemical-looping combustion, Fuel 83 (2004), 1215-1225.

[21] T. Mattisson, M. Johansson, A. Lyngfelt, Multicycle reduction and oxidation of different types of iron oxide particles-Application of chemical-looping combustion, Energy & Fuels 18 (2004) 628–637.

[22] T. Mattisson, M. Johansson, A. Lyngfelt, The use of NiO as an oxygen carrier in chemical-looping combustion, Fuel 85 (2006) 736–747.

[23] T. Mattisson, F. García-Labiano, B. Kronberger, A. Lyngfelt, J. Adánez, H. Hofbauer, Chemical-looping combustion using syngas as fuel, Int. J. Greenh. Gas Control 1 (2007) 158–169.

[24] A. Abad, F. García-Labiano, L.F. de Diego, P. Gayán, J. Adánez, Reduction kinetics of Cu-, Ni-, and Fe-based oxygen carriers using syngas (CO + H_2) for chemical-looping combustion, Energy & Fuels 21 (2007) 1843–1853.

[25] J. Adánez, A. Abad, T. Mendiara, P. Gayán, L.F. de Diego, F. García-Labiano, Chemical looping combustion of solid fuels, Prog. Energy Combust. Sci. 65 (2018) 6–66.

[26] F. García-Labiano, L.F. de Diego, J. Adánez, A. Abad, C. Dueso, Effect of fuel gas composition in chemical-looping combustion with Ni-based oxygen carriers. 1. fate of sulfur, Ind. Eng. Chem. Res. 48 (2009) 2499–2508.

[27] M. Schmitz, C. Linderholm, P. Hallberg, S. Sundqvist, A. Lyngfelt, Chemical-looping combustion of solid fuels using manganese ores as oxygen carriers, Energy Fuels 30 (2016) 1204–1216.

[28] C. Linderholm, A. Lyngfelt, Use of manganese ores as oxygen carriers in chemical-looping combustors for solid fuels, The 4th international conference on chemical-looping (2016).

[29] T.A. Brown, J.S. Dennis, S.A. Scott, J.F. Davidson, A.N. Hayhurst, Gasification and chemical-looping combustion of a lignite char in a fluidized bed of iron oxide, Energy & Fuels 24 (2010) 3034–3048.

[30] S. Rajendran, M. Wong, D. Stokie, S. Bhattacharya, Performance of a Victorian

brown coal and iron ore during chemical looping combustion in a 10 kW_{th} alternating fluidized bed, Fuel 183 (2016) 245–252.

[31] J. Ma, X. Tian, H. Zhao, S. Bhattacharya, S. Rajendran, C. Zheng, Investigation of two hematites as oxygen carrier and two low-rank coals as fuel in chemical looping combustion, Energy & Fuels 31 (2017) 1896–1903.

[32] Y. Saito, F. Kosaka, N. Kikuchi, H. Hatano, J. Otomo, Evaluation of microstructural changes and performance degradation in iron-based oxygen carriers during redox cycling for chemical looping systems with image analysis, Ind. Eng. Chem. Res. 57 (2018) 5529–5538.

[33] Y. Zhongliang, Y. Yanyan, Y. Song, Z. Qian, Z. Jiantao, F. Yitian, H. Xiaogang, G. Guoqing, Iron-based oxygen carriers in chemical looping conversions: a review, Carbon Resour. Convers. 2 (2018) 23–34.

[34] H. Leion, A. Lyngfelt, M. Johansson, E. Jerndal, T. Mattisson, The use of ilmenite as an oxygen carrier in chemical-looping combustion, Chem. Eng. Res. Des. 86 (2008) 1017–1026.

[35] H. Leion, T. Mattisson, A. Lyngfelt, Use of ores and industrial products as oxygen carriers in chemical-looping combustion, Energy & Fuels 23 (2009) 2307–2315.

[36] J. Adánez, A. Cuadrat, A. Abad, P. Gayán, L.F. de Diego, F. García-Labiano, Ilmenite activation during consecutive redox cycles in chemical-looping combustion, Energy & Fuels 24 (2010) 1402–1413.

[37] A. Cuadrat, A. Abad, F. García-Labiano, P. Gayán, L.F. de Diego, J. Adánez, Ilmenite as oxygen carrier in a chemical looping combustion system with coal, Energy Procedia 4 (2011) 362–369.

[38] A. Cuadrat, A. Abad, F. García-Labiano, P. Gayán, L.F. de Diego, J. Adánez, The use of ilmenite as oxygen-carrier in a 500 W_{th} Chemical-Looping Coal Combustion unit, Int. J. Greenh. Gas Control 5 (2011) 1630–1642.

[39] A. Cuadrat, A. Abad, J. Adánez, L.F. de Diego, F. García-Labiano, P. Gayán, Behavior of ilmenite as oxygen carrier in chemical-looping combustion, Fuel Process. Technol. 94 (2012) 101–112.

[40] T. Mattisson, A. Lyngfelt, H. Leion, Chemical-looping with oxygen uncoupling for combustion of solid fuels, Int. J. Greenh. Gas Control 3 (2009) 11–20.

[41] Y. Cao, W.P. Pan, Investigation of chemical looping combustion by solid fuels. 1. process analysis, Energy & Fuels 20 (2006) 1836–1844.

[42] S.A. Scott, J.S. Dennis, A.N. Hayhurst, T. Brown, *In situ* gasification of a solid

fuel and CO_2 separation using chemical looping, AIChE J. 52 (2006) 3325–

[43] H. Leion, T. Mattisson, A. Lyngfelt, The use of petroleum coke as fuel in chemical-looping combustion, Fuel 86 (2007) 1947–1958.

[44] H. Leion, T. Mattisson, A. Lyngfelt, Solid fuels in chemical-looping combustion, Int. J. Greenh. Gas Control 2 (2008) 180–193.

[45] A. Lyngfelt, Chemical-looping combustion of solid fuels – status of development, Appl. Energy 113 (2014) 1869–1873.

[46] S.Y. Lin, T. Saito, K. Hashimoto, Development of the three-tower chemical looping coal combustion technology, Energy Procedia, 114 (2017) 414–418.

[47] T. Saito, S. Lin, Coal Char Reaction with Oxygen Carrier in Chemical Looping Combustion, Energy and Fuels. (2019).

[48] J. Adánez, C. Dueso, L.F. de Diego, F. García-Labiano, P. Gayán, A. Abad, Effect of fuel gas composition in chemical-looping combustion with Ni-based oxygen carriers. 2. fate of light hydrocarbons, Ind. Eng. Chem. Res. 48 (2009) 2509–2518.

[49] P. Gayán, C.R. Forero, L.F. de Diego, A. Abad, F. García-Labiano, J. Adánez, Effect of gas composition in Chemical-Looping Combustion with copper-based oxygen carriers: fate of light hydrocarbons, Int. J. Greenh. Gas Control 4 (2010) 13–22.

[50] A. Larsson, M. Israelsson, F. Lind, M. Seemann, H. Thunman, Using ilmenite to reduce the tar yield in a dual fluidized bed gasification system, Energy & Fuels 28 (2014) 2632–2644.

[51] H. Tian, T. Simonyi, J. Poston, R. Siriwardane, Effect of hydrogen sulfide on chemical looping combustion of coal-derived synthesis gas over bentonite-supported metal-oxide oxygen carriers, Ind. Eng. Chem. Res. (2009).

[52] H. Gu, L. Shen, J. Xiao, S. Zhang, T. Song, D. Chen, Evaluation of the effect of sulfur on iron-ore oxygen carrier in chemical-looping combustion, Ind. Eng. Chem. Res. 52 (2013) 1795–1805.

[53] C. Chung, Y. Pottimurthy, M. Xu, T.L. Hsieh, D. Xu, Y. Zhang, Y.Y. Chen, P. He, M. Pickarts, L.S. Fan, A. Tong, Fate of sulfur in coal-direct chemical looping systems, Appl. Energy. 208 (2017) 678–690.

Chapter 2 THE COMBUSTION REACITVITY OF ILMENITE WITH COAL VOLATILES UNDER STEAM REFORMING

2.1 Introduction and objectives

Carbon dioxide (CO_2) represents the largest contribution to greenhouse gas emissions because of heavy dependence on fossil fuels for power generation. The global atmospheric concentration of CO_2 has increased year by year, reaching approximately 413 ppm in 2019. Therefore, new and advanced technological approaches for reducing CO_2 emissions, e.g. CO_2 capture and storage (CCS), are needed as soon as possible in order to solve current environmental issues and global energy demands. However, the application of CCS in conventional power plants is very limited owing to its enormous expenses and substantial energy losses. Under these circumstances, chemical-looping combustion (CLC) [1] is one of the most attractive technological options in power generation for capturing CO_2 at lower cost [2–5]. Although to date, numerous CLC studies have focused on gaseous fuels, such as natural gas and syngas [6–9], the application of CLC with coal has attracted greater attention in the past decade because of the massive amount of CO_2 emissions caused by coal-fired power plants. The recent progress in CLC with solid fuels up to 2018 was summarized by Adánez *et al.* [10].

One feasible configuration of iG-CLC with coal [11–14] is being proposed and developed by Japan Coal Energy Center (JCOAL) in Japan, shown in Figure 8 [15]. At higher temperature, coal is thermally decomposed into solid carbon (char) and volatiles (R7). Char formed by coal pyrolysis is gasified by steam (R8). The reduction reactions (R9 to R11) of oxygen carrier with volatiles then proceed in the fuel reactor and eventually converts them into CO_2 and H_2O [16]. Among the reactions described above, the char gasification R8 is considered the rate controlling step [17]. Here also, a solid–solid reaction between char and oxygen carrier is negligible because the gasification reaction rate of char with H_2O or CO_2 is much higher than that with the oxygen carrier [18]. The char gasification rate in CLC also depends on the oxygen carrier's reactivity

with the gaseous products, i.e., H_2 and CO, because these gases inhibit the char gasification reaction. In addition, unconverted combustible gases from the fuel reactor may result in a large amount of energy loss. Therefore, complete conversion of volatiles and gasification products with the oxygen carrier is vital for coal CLC in order to achieve high-energy conversion efficiency and CO_2 capture.

Apart from H_2 and CO, coal volatiles usually contain variable amounts of hydrocarbons having molecular weights higher than CH_4. The condensable hydrocarbons, often referred to as tar, consist of a complex mixture of organic non-aromatic and aromatic compounds and can cause operational problems such as clogging and blockage of downstream equipment. Only a limited amount of CLC work has been performed on several hydrocarbons (C_2–C_3) [19–21] or biomass-derived raw gases [22,23]. However, these approaches cannot fully represent the actual coal volatiles.

Generally, an oxygen carrier used in CLC needs to have sufficient reactivity for reduction and oxidation. Using thermodynamic analysis [24], Jerndal *et al.* revealed that certain oxides, such as Cu, Fe, and Mn oxides, are the most suitable oxygen carriers owing to their favorable conversion reactivity. Of these, Fe-based carriers [25,26] have been extensively investigated for direct CLC with coal because of their abundance, reasonable price, and environmentally benign nature that are very important factors given the partial loss of oxygen carrier when coal ashes are removed from the fuel reactor. In this context, the natural iron titanium oxide ore, ilmenite showed competitive performance as an oxygen carrier in CLC [17,27] owing to its sufficient redox reactivity, high mechanical strength, and stability against agglomeration and attrition. Even though it can be used in its raw state, Adánez *et al.* [28] showed that the reactivity of ilmenite is greatly enhanced by heat treatment under an oxidized atmosphere and reaches a maximum value after several cycles. Other authors [16,29,30] investigated the reactivity of ilmenite with various reducing gas mixtures and reported that ilmenite actively oxidized H_2 and CO but had a low oxidation rate with CH_4.

Steam is generally used as a gasifying and fluidizing agent in coal CLC process, the conversion rate of coal with ilmenite increases as steam content increases [17]; however, it is difficult to separate the char gasification reaction and the volatiles' reaction with oxygen carriers or steam as they all take place in a single fluidized-bed reactor. Steam can work also as a reformer, inhibitor and oxidizer in the fuel reactor. For example, carbon deposition commonly caused by coal is prevented by steam. Concerning condensable hydrocarbons, further investigation remains important for the stable

operation of direct CLC with coal, although some CLC studies [31–33] have indicated that no tar deposits appeared in the outflow of the fuel reactor.

In this study, we focused on actual coal volatiles and aimed to investigate the combustion reactivity of ilmenite with the coal volatiles under the steam reforming atmosphere. Steam reforming experiments were carried out in a two-stage fixed-bed reactor. The influence of the pre-oxidation and of steam-to-carbon-in-coal-sample (S/C) ratios on conversion performance of ilmenite was investigated in comparison with that of a synthetic iron oxide carrier, Fe_2O_3/Al_2O_3.

2.2 Experimental

2.2.1 Samples and characterization

All samples used in this study were provided by JCOAL, Japan.
An Indonesian subbituminous coal with a particle size of 1.0 mm was employed as a source of coal volatiles. Proximate and ultimate analyses of a coal sample are shown in **Table 1**.

Table 1
Proximate (dry basis; d.b.) and ultimate analyses (dry ash-free basis; d.a.f.) of coal sample

Proximate analysis (wt%, d.b.)			Ultimate analysis (wt%, d.a.f.)				
V.M.	Ash	$F.C._{diff.}$	C	H	N	S	$O_{diff.}$
42.9	2.9	54.2	71.00	5.01	0.62	0.14	23.23

An Australian natural iron titanium ore, ilmenite, was used as an oxygen carrier; it is denoted as “Raw IL.” A pre-oxidized ilmenite sample, denoted as “Oxi IL,” was prepared by calcination at 1173 K in air for 2 h, followed by pulverization and sieving to about 150 μm prior to the experiments. The effect of the calcination time had been previously studied, and 2 h of pretreatment was found to be enough for full oxidation of ilmenite [28]. The chemical composition of the ilmenite samples is shown in Table 2. For a comparison with the ilmenite carriers, a synthetic iron oxide with alumina, 50 wt%

Fe_2O_3/Al_2O_3, denoted as "SD_{50}," and inactive river sand were also used as a reference iron-based oxygen carrier and an inert material, respectively.

Table 2

Chemical composition of Australian ilmenite

Type	FeO (wt%)	Fe_2O_3 (wt%)	TiO_2 (wt%)	Others (wt%)
Raw IL	34.8	12.2	49.3	3.7
Oxi IL	-	49.0	47.3	3.7

Oxygen carrier samples before and after the steam reforming experiment were characterized by X-ray diffraction (XRD) (SmartLab, Rigaku, Japan) to determine their crystalline phases. The microstructural changes on an external surface and a cross section of the oxygen carriers were observed by scanning electron microscopy (SEM) (SU-70, Hitachi, Japan). Element distribution mapping was also performed by energy dispersive X-ray spectroscopy (EDX).

2.2.2 Steam reforming experiments of coal volatiles with ilmenite and Fe_2O_3/Al_2O_3

Steam reforming experiments were conducted in a two-stage fixed-bed quartz reactor with an internal diameter of 22 mm and a main body length of 880 mm. A schematic illustration of the experimental setup is shown in Figure 10. Prior to the experiment, a carrier sample of 3.5 g and a coal sample of about 1 g wrapped with silica wool were placed in the lower and upper stages, respectively. As a heavy tar trap, some amount of silica wool was also packed under the lower stage of the reactor, and a water trap was set at the outlet of the reactor as well.

Temperatures at the two stages were programmed and controlled individually by two electric furnaces. First, the oxygen carrier stage was heated to 1173 K in nitrogen flow of 60 $ml \cdot min^{-1}$ from the top of the reactor and maintained at that temperature throughout the experiment. Then, steam with nitrogen gas was introduced into the lower stage through the branch gas inlet at atmospheric pressure. The total gas flow rate from the central and branch inlets was adjusted to 120 $ml \cdot min^{-1}$ including steam. Here, S/C ratios of 0.5, 1.0, 1.5, and 2.5, corresponding to 9.5%, 19.0%, 28.5%, and 47.5% steam

in nitrogen, respectively, were chosen to investigate the effect of steam content on the reforming performance of the carrier. Steam reforming was then commenced with heating of the coal sample to 1173 K for 90 min at a heating rate of 10 $K \cdot min^{-1}$. Volatiles produced via pyrolysis of the coal reacted with steam and oxygen carrier in the lower stage.

Gaseous products collected in a gasbag were analyzed using offline gas chromatographs (GC-2014B, Shimadzu, Japan) with a thermal conductivity detector and a flame ionization detector equipped with a methanizer. Gas yield was calculated and presented as the molar amount of each gas component. At the end of the steam reforming experiment, the other carbonaceous products from coal volatiles such as soot and tar, left in the reactor and on the tar trap, were combusted separately in oxygen. The carbon molar yield of each product was determined from the combustion gases using gas chromatography analysis. The carbon balance is defined as the molar percentage of elemental carbon in each product out of the total carbon of the volatiles.

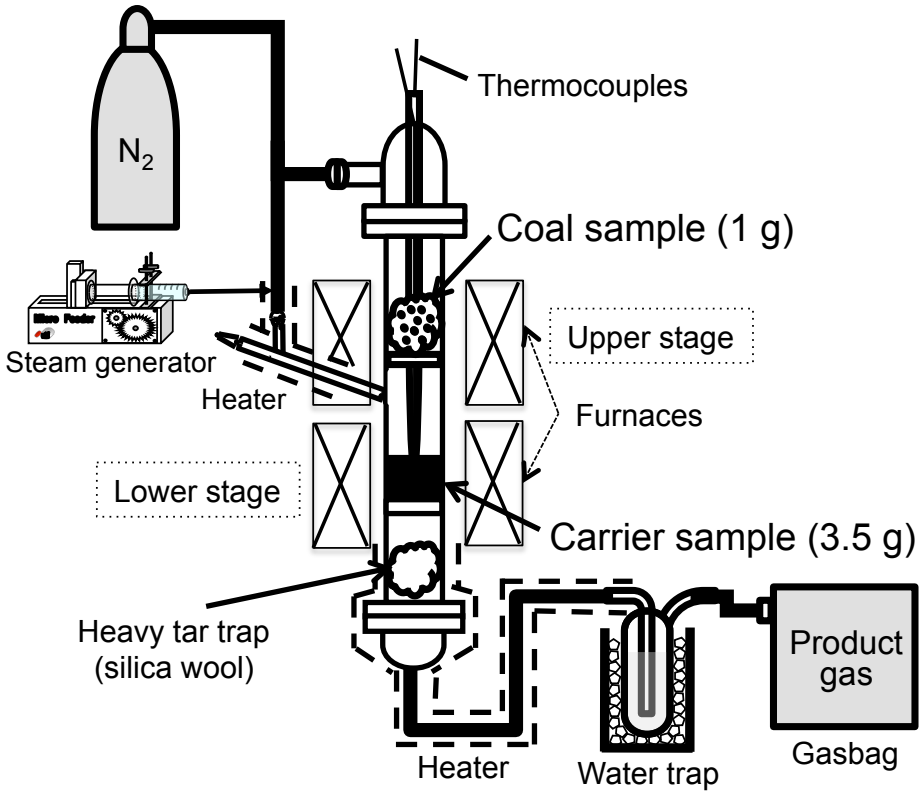

Figure 10. Schematic illustration of the experimental setup for the steam reforming experiments.

2.2.3 Redox reactivity tests of ilmenite and Fe_2O_3/Al_2O_3

Eight-redox cycles of pre-oxidized ilmenite and Fe_2O_3/Al_2O_3 were examined isothermally at 1173 K in a thermo gravimetric analyzer (TGD-7000RH, Ulvac Rico, Japan), as shown in Figure 11. 20 mg of the oxygen carrier sample was placed in a platinum pan and heated up to 1173 K in air. Then the carrier sample was reduced by 20 % H_2/N_2 with 100 ml·min^{-1} for 30 min and following which 100 ml·min^{-1} of air was introduced to oxidize the reduced carrier for another 10 min after N_2 purging for 2 min. The obtained TG data was used to calculate the reduction, X_{red}, and the oxidation, X_{ox}, of oxygen carriers during eight-redox cycles with following equations 1 and 2.

$$Xred = 1 - \left(\frac{m_{red} - m_{Fe}}{m_{Fe(III)} - m_{Fe}}\right) \quad \text{(Eq.1)}$$

$$Xox = \frac{m_{ox} - m_{Fe}}{m_{Fe(III)} - m_{Fe}} \quad \text{(Eq.2)}$$

where m_{red} and m_{ox} are the masses of carrier sample during the reduction and the oxidation, and m_{Fe} and $m_{Fe(III)}$ are the theoretical masses of reduced and oxidized carriers, respectively.

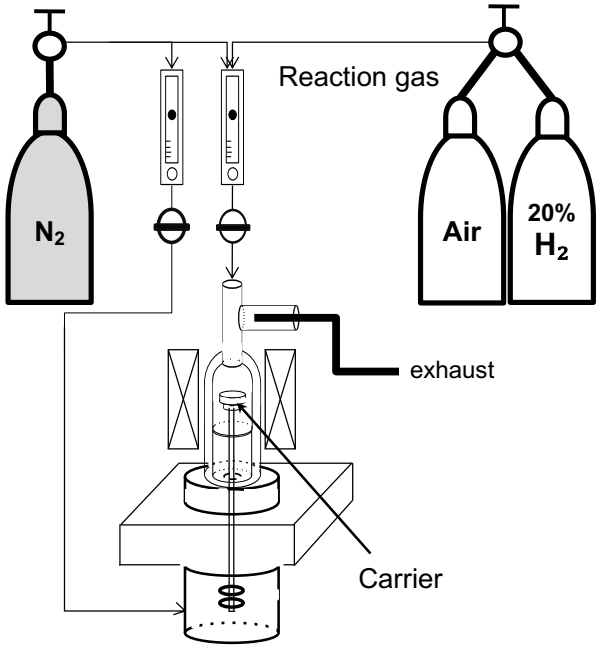

Figure 11. Schematic illustration of the experimental setup for the 8-cycle redox test

2.3 Results and discussion

2.3.1 Effect of the pre-oxidation on the combustion reactivity of ilmenite

To investigate the combustion performance of ilmenite during the steam reforming of coal volatiles, the carbon balance and product gas yield with natural and the pre-oxidized ilmenite were quantified and are shown in Figure 12(a) and (b), respectively. To provide a comparison of performance, the amounts of volatiles consumed and produced by ilmenite carriers during steam reforming are also presented as differences from the data of sand (Figure 12(c)).

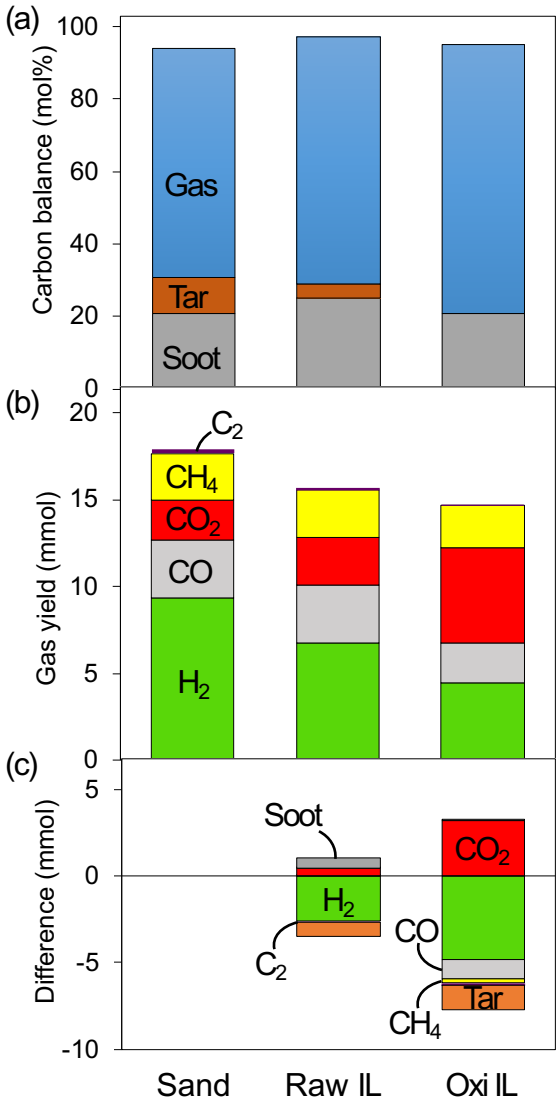

Figure 12. (a) Carbon balance and (b) product gas yield obtained with sand, natural ilmenite, and pre-oxidized ilmenite during the steam reforming (S/C ratio of 0.5) of coal volatiles, and (c) the difference in volatiles in Raw IL or Oxi IL compared with sand.

The total carbon balance of gas, soot, and heavy tar exceeded 93% in all of the samples investigated; the remaining minorities might correspond to those of heavy gases or water-soluble hydrocarbons, which were not measured at this time.

Based on the carbon balance for sand, higher hydrocarbons, e.g. tar included in the coal volatiles was approximately 10 mol%. The amount of tar declined to 4 mol% in natural ilmenite and almost 0 mol% in pre-oxidized ilmenite. Tar appeared on the tar traps of each medium is shown in Figure 13. Heavy tar formation is clearly visible in sand, but greatly reduced in natural ilmenite. Tar was almost completely decomposed during the steam reforming experiment of volatiles with pre-oxidized ilmenite. This is consistent with previous studies [31–33]. Accompanying the progress of tar decomposition, the yield of carbon-containing gas increased by 5–11 mol%.

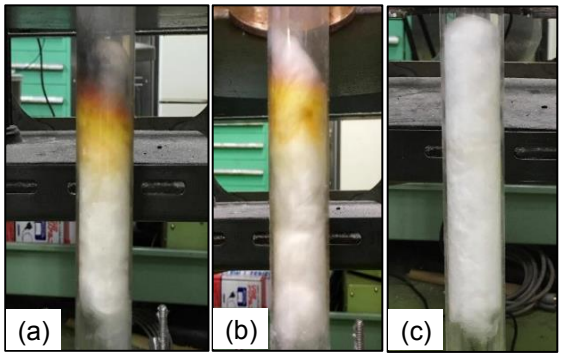

Figure 13. Photos of heavy tar traps after steam reforming of coal volatiles with (a) sand, (b) natural ilmenite and (c) pre-oxidized ilmenite.

In our study, a promotion of combustion reaction was identified by the increase in CO_2 and the decrease in flammable volatiles, such as H_2, CO, CH_4, and higher hydrocarbons by oxygen carriers in comparison with sand. Here, we assumed that the steam reforming effect is the same for all mediums. Figure 12(c) reveals that the CO_2 yield, coupled with a decline in flammable volatiles, substantially increased with pre-oxidized ilmenite. On the other hand, there was little change when ilmenite was naturally used, with the exception of a certain decrease in H_2 and tar. These results indicate that pre-oxidation treatment increases the combustion reactivity of ilmenite, meaning that it is directly related to its physicochemical properties. Figure 14 shows the XRD patterns of ilmenite particles before and after pre-oxidation and after used in the steam reforming

experiment. Natural ilmenite is composed mainly of $FeTiO_3$, indicating that the iron has the low oxidation number (II). The $FeTiO_3$ phase disappeared after pre-oxidation, but Fe_2TiO_5 with highly oxidized iron (III) and TiO_2 phase evolved according to reaction R16.

$$2FeTiO_3 + 1/2O_2 \rightarrow Fe_2TiO_5 + TiO_2 \qquad \text{(R16)}$$

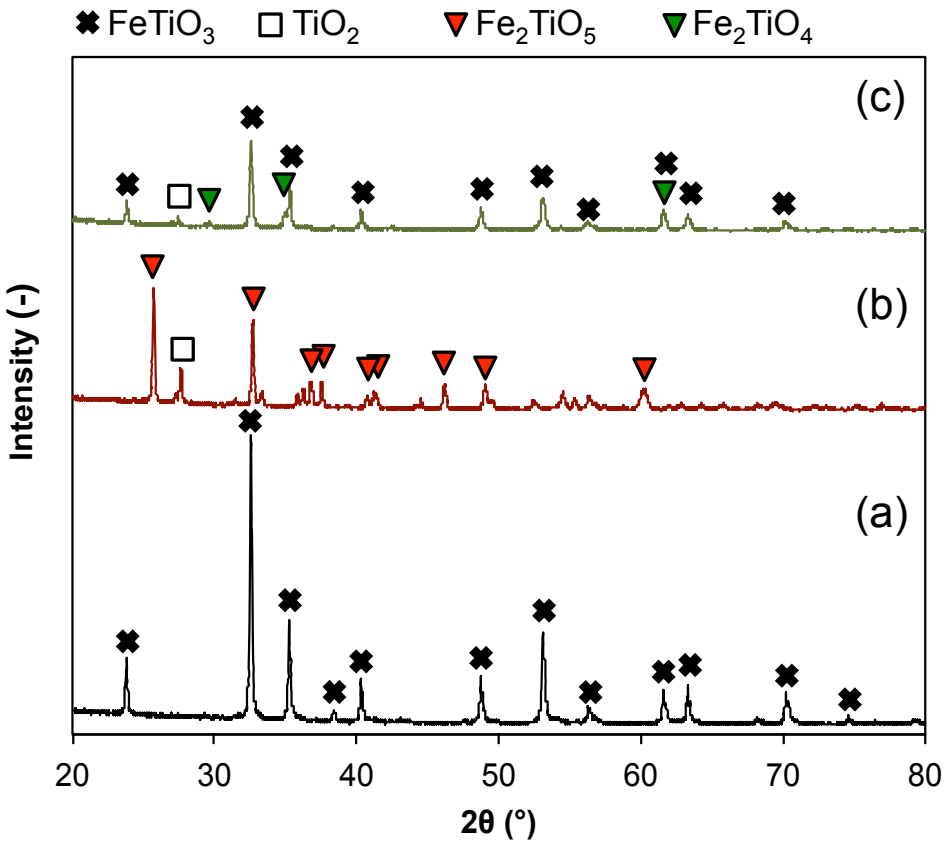

Figure 14. X-ray diffraction (XRD) patterns of (a) natural, (b) pre-oxidized, and (c) used ilmenite particles for steam reforming of coal volatiles.

The similar transformation of $FeTiO_3$ into pseudobrookite Fe_2TiO_5 has been reported under the same condition [34]. Figure 14(c) reveals that the phase change via reaction R16 is reversible when pre-oxidized ilmenite is exposed to coal volatiles. Fe_2TiO_5 phase was reduced into $FeTiO_3$ and/or Fe_2TiO_4 during reforming of coal volatiles. Fe_2TiO_4 with iron (II) valance state is one of intermediates produced at the early stage of the reduction of Fe_2TiO_5 in following reactions [35].

$$2Fe_2TiO_5 + Volatiles \rightarrow 2Fe_2TiO_4 + H_2O + CO_2 \quad (R17)$$

$$2Fe_2TiO_4 + 2TiO_2 + Volatiles \rightarrow 4FeTiO_3 + H_2O + CO_2 \quad (R18)$$

This almost completely reversible phase change strongly suggests that the lattice oxygen released from the Fe_2TiO_5 phase oxidizes coal volatiles efficiently according to the following reactions R19 to R23:

$$Fe_2TiO_5 + TiO_2 + H_2 \rightarrow 2FeTiO_3 + H_2O \quad (R19)$$

$$Fe_2TiO_5 + TiO_2 + CO \rightarrow 2FeTiO_3 + CO_2 \quad (R20)$$

$$4Fe_2TiO_5 + 4TiO_2 + CH_4 \rightarrow 8FeTiO_3 + CO_2 + 2H_2O \quad (R21)$$

$$6Fe_2TiO_5 + 6TiO_2 + C_2H_4 \rightarrow 12FeTiO_3 + 2CO_2 + 2H_2O \quad (R22)$$

$$(2m+n/2)Fe_2TiO_5 + (2m+n/2)TiO_2 + C_mH_n(Tar) \rightarrow (4m+n)FeTiO_3 + mCO_2 + n/2H_2O \quad (R23)$$

Based on the molar amounts of CO_2 generated and H_2 consumed, the amount of the lattice oxygen used by carriers during steam reforming was semi-quantitatively calculated. The result shows that an active phase Fe_2O_3 (TiO_2) of pre-oxidized ilmenite was entirely consumed during the experiments and completely reduced to FeO (TiO_2) by the end. However, the lattice oxygen consumption from Fe_2O_3 during the steam reforming of coal volatiles, was only 31% in the natural ilmenite.

In order to evaluate the reactivity difference of ilmenite samples, a morphological characterization was performed by SEM. Figure 15 represents the typical SEM images of external surfaces and cross sections of natural, pre-oxidized and used ilmenite particles for reforming experiments. As shown in Figure 15(A1)-(A3), natural ilmenite consists of relatively dense particles with granular surface, but some pores are observed in the bulk and at the surface. After pre-oxidation, ilmenite forms a pebble-like granular matrix with a dense bulk structure, as presented in Figure 15(B1)-(B3). After steam reforming of coal volatiles, the external surface morphology of ilmenite changed drastically into a porous structure with smaller grains, and some cracks also appeared in the external surface. The cross-sectional image, described in Figure 15(C3), also reveals that the used ilmenite had a porous structure not only at the surface but also in the bulk. In conjunction with XRD results presented in Figure 14, it is suggested that the numerous pores of the used ilmenite are formed by the release of lattice oxygen from the Fe_2TiO_5 phase during steam

reforming. These results strongly reveal that the relatively rapid evolution of the porous structure increases the solid–gas two-phase boundary, resulting in efficient utilization of the lattice oxygen from pre-oxidized ilmenite.

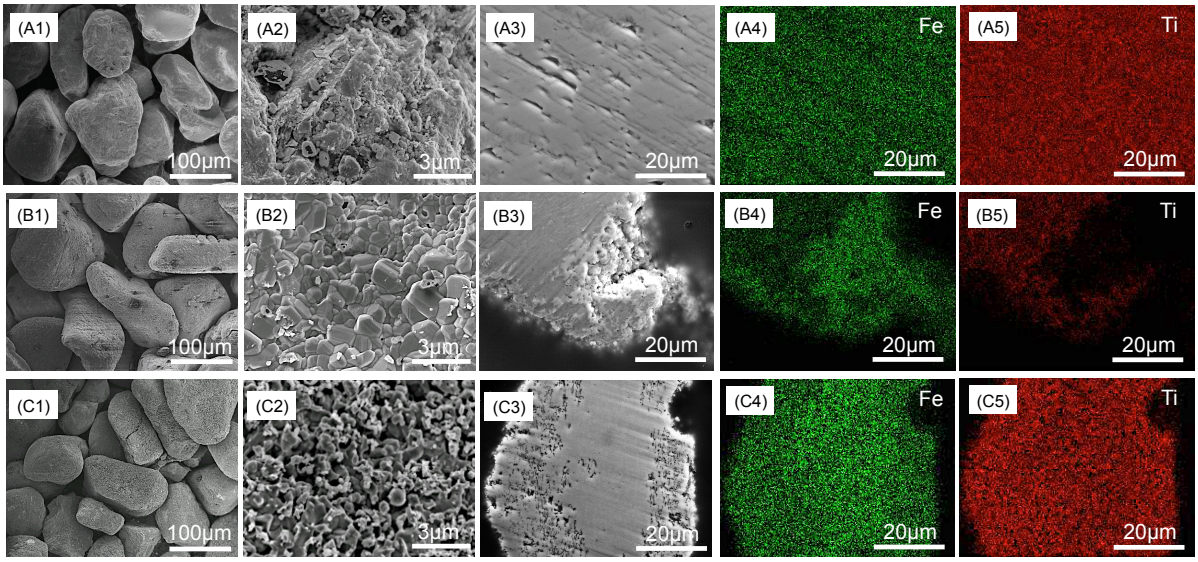

Figure 15. SEM images and element distribution maps of (A1)-(A5) natural, (B1)-(B5) pre-oxidized, and (C1)-(C5) used ilmenite samples for steam reforming with coal volatiles: (A1)-(C1) general overviews, (A2)-(C2) external surfaces, (A3)-(C3) cross sections, (A4)-(C4) Fe elements and (A5)-(C5) Ti elements, respectively.

In addition, EDX analyses were conducted to determine Fe and Ti elemental distributions over the ilmenite particles, as shown in Figure 15(A4)-C(5). The Fe and Ti elements in natural ilmenite were distributed uniformly over the entire particle. For pre-oxidized Oxi IL the elemental distribution was greatly changed in the outer part of the particle, where Fe element is more condensed, as clearly seen in Figure 15(B4). In conjunction with XRD results in Figure 14, it is insisted that during the pre-oxidation, ilmenite undergoes a migration phenomenon of the Fe towards external part of the particle to form Fe-rich Fe_2TiO_5 phase. In contrast, as shown in Figure 15(C4), those Fe condensed areas in the outer part of pre-oxidized ilmenite particles disappeared after steam reforming experiment and the distribution of Fe and Ti elements in the used ilmenite particles rather recovered. It might mean that when lattice oxygen released from the external Fe phases of ilmenite particles, Ti migrates towards the external part to prevent the oxygen release.

2.3.2 Redox reactivity of ilmenite and Fe_2O_3/Al_2O_3

The redox reactivity of pre-oxidized ilmenite was evaluated by eight redox cycles in TGA with 20% H_2/N_2 and air at 1173 K, in comparison with Fe_2O_3/Al_2O_3. The weight changes for ilmenite and Fe_2O_3/Al_2O_3 carriers during the eight redox cycles were presented in Figure 16(a) and (b), respectively. A weight value of 0% in Figure 16 is corresponding to the sample in its most oxidized state and the maximum theoretical weight loss value between Fe^{III} to Fe^0 in Oxi IL and SD_{50} is approximately 15%. As shown in Figure 16, the oxygen transfer capacity was relatively high for both of the oxygen carriers, because the values to almost fully reduced and oxidized states were observed in two carriers.

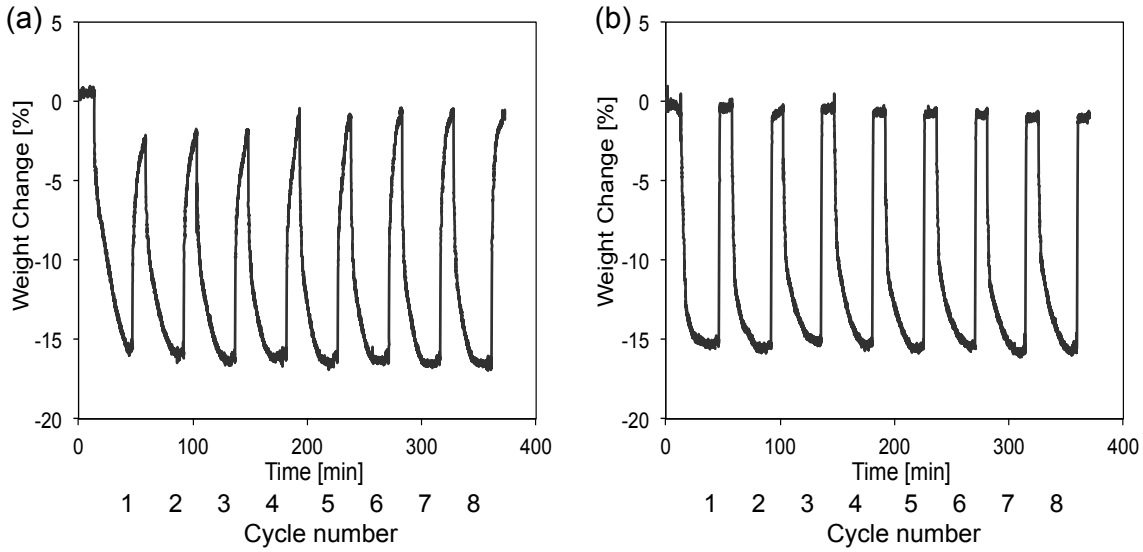

Figure 16. Eight-cycle thermogravimetric analyses of (a) pre-oxidized ilmenite and (b) Fe_2O_3/Al_2O_3 with 20% H_2/N_2 for 30 min and air for 10 min at 1173 K.

However, a different tendency of reactivity was observed in two carriers with higher cycle numbers. The redox reactivity of ilmenite increased as cycle number increased, while, in contrast, it decreased in Fe_2O_3/Al_2O_3. Figure 17 and Figure 18 show the conversion time profiles for the reduction and oxidation cycle number 1, 2, 5 and 8 of ilmenite and Fe_2O_3/Al_2O_3, respectively. To compare the reduction of Fe_2O_3/Al_2O_3, ilmenite initially presented rather low reduction rate, but it increased with the number of cycles. As can also be seen in Figure 17(a), the initial reduction rate of ilmenite was not high but gradually increased after next a few cycle. This redox activation behavior of ilmenite has been reported by others and is thought to be due to the development of

granulation and porosity [16, 28]. Meanwhile, Fe_2O_3/Al_2O_3 had achieved the maximum conversion rate in both reduction and oxidation at the beginning, but the reduction rate of Fe_2O_3/Al_2O_3 slightly decreased with the increased cycle numbers (Figure 17(b), Figure 18(b)). This reactivity loss might be attributed to the agglomeration of iron-based oxygen carriers when Fe_2O_3 is reduced to FeO or Fe phases because they have lower melting points and higher exothermic heat in the oxidation step.

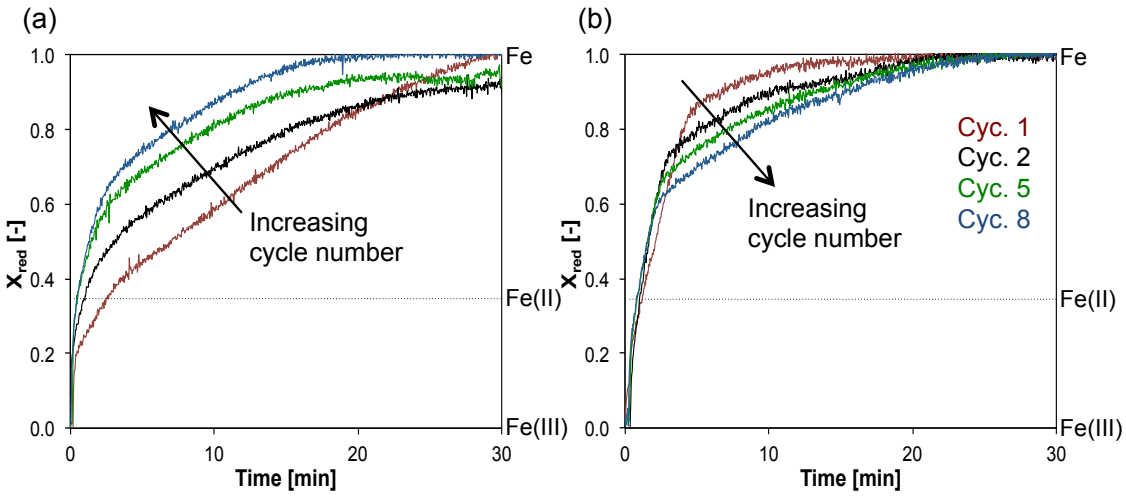

Figure 17. Reduction time profiles for cycle number 1, 2, 5 and 8 of (a) ilmenite and (b) Fe_2O_3/Al_2O_3 with 20 %H_2/N_2 for 30 min at 1173 K. Broken lines represent the theoretical conversion values to Fe(II).

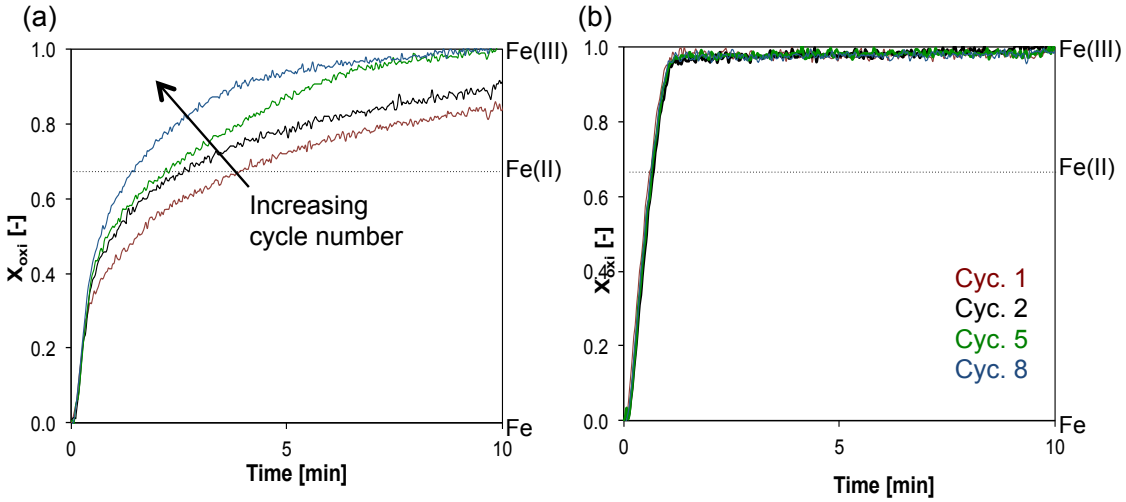

Figure 18. Oxidation time profiles for cycle number 1, 2, 5 and 8 of (a) ilmenite and (b) Fe_2O_3/Al_2O_3 with air for 10 min at 1173 K. Broken lines represent the theoretical conversion values to Fe(II).

Although the redox test here was carried out with only H_2 gas, we can confirm that pre-oxidized ilmenite and Fe_2O_3/Al_2O_3 are relatively efficient and reproducible oxygen carriers for CLC process.

2.3.3 Effect of S/C ratios on the combustion reactivity of ilmenite and Fe_2O_3/Al_2O_3 with coal volatiles

Steam plays an important role in direct CLC with coal, not only as a gasifying agent of coal char but also as a carbon deposition inhibitor. When carbon deposits on the oxygen carrier in the fuel reactor, it will transfer to air reactor, decreasing the CO_2 capture efficiency (R24). Therefore, effect of steam on the reaction between volatiles and oxygen carriers is also important factor to evaluate.

$$C(\text{deposited on oxygen carrier}) + O_2 \rightarrow CO_2 \qquad (R24)$$

The steam reforming experiments of pre-oxidized ilmenite and Fe_2O_3/Al_2O_3 were performed under various S/C ratios in the range 0–2.5 to investigate the influence of steam on the reactivity of the oxygen carriers. The carbon balance and product gas yield are shown in Figure 19(a) and (b). For the sake of comparison, the amounts of volatiles consumed and produced at various S/C ratios are also presented as differences from the data without steam (Figure 19(c)).

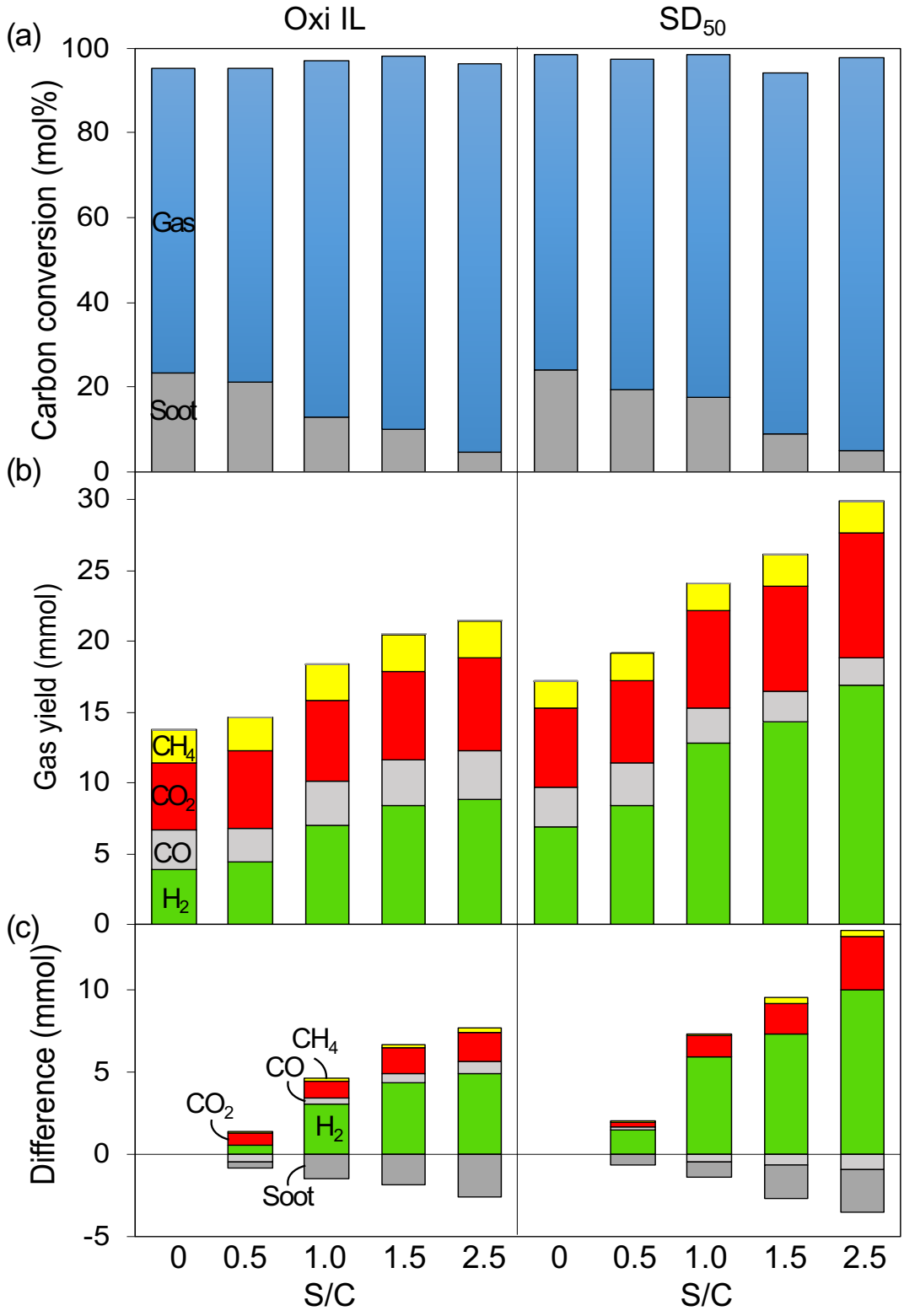

Figure 19. (a) Carbon balance and (b) product gas yield during the steam reforming of coal volatiles with pre-oxidized ilmenite and Fe_2O_3/Al_2O_3 under various S/C ratios, and (c) the differences in volatiles under various S/C ratios compared with no steam in ilmenite and Fe_2O_3/Al_2O_3.

As shown in Figure 19(a), the influence of the S/C ratio on carbon balance was similar for the both carriers and the carbon conversion of coal volatiles into carbon gases greatly increased without any formation of tar when the S/C ratio increased. At the same time, soot decomposition was observed for both carriers with higher steam ratios. The soot content for ilmenite and Fe_2O_3/Al_2O_3 in S/C ratio of 2.5 were almost 5 times as low as those without steam. Furthermore, it can also be seen in Figure 19(b) and (c) that the yields of H_2 and CO_2 for both carriers were coupled with the decrease in soot as the S/C ratio increased. Especially, H_2 gas substantially increased for Fe_2O_3/Al_2O_3 at the higher steam ratios, compared with that for ilmenite. A gain of H_2 is not favorable in respect to the total combustion efficiency of CLC process. Based on the results above, soot decomposition by steam could be one source for hydrogen generation.

In essence, conversion of soot into gaseous species by steam should proceed according to the following sequential reactions: carbon gasification R14 and the WGS reaction R15. In order to evaluate these contributions to gas product yield, the amounts of CO_2 and H_2 from reactions R14 and R15 were estimated from the yields of soot and CO at various S/C ratios and were compared with the experimental data (Figure 20). Here, we assumed that the higher levels of CO_2 and H_2 compared to the no-steam condition correspond to those produced through the above reactions. A negligible effect for methane reforming by steam was also assumed as its concentration was not very different with or without steam.

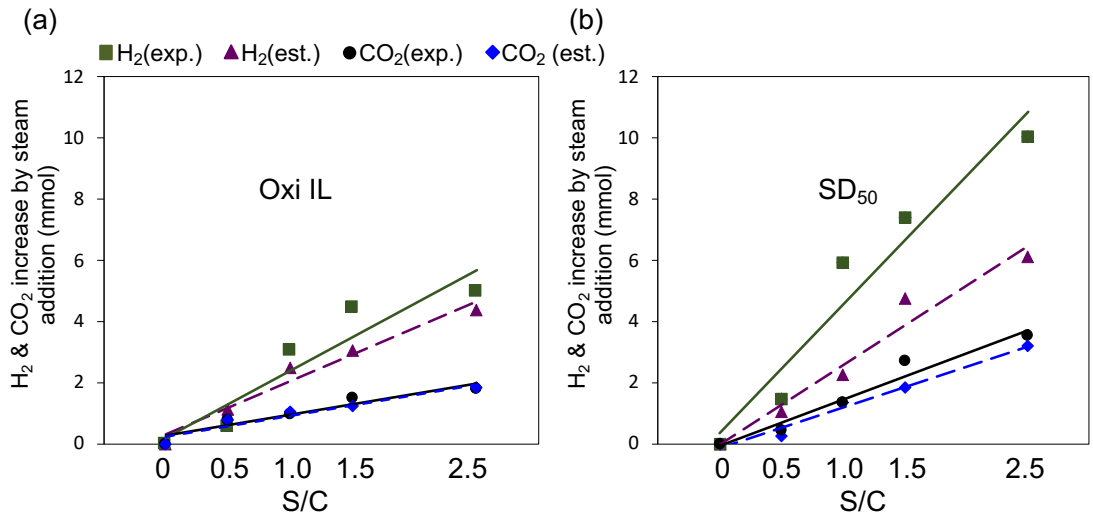

Figure 20. H_2 and CO_2 increase with increasing steam ratios; experimental (solid lines) and estimated (broken lines) in (a) ilmenite and (b) Fe_2O_3/Al_2O_3.

As shown in Figure 20(a), the estimated H_2 amount is only slightly lower than the experimental value and, in addition, the data for CO_2 show nearly perfect agreement on ilmenite. This fact strongly suggests that gasification of soot and the subsequent WGS reaction were promoted in ilmenite in this S/C range. In the case of Fe_2O_3/Al_2O_3, estimated and experimental data show relatively good agreement for CO_2, however, substantial differences were observed for H_2, especially at and above an S/C ratio of 1.0 (Figure 20(b)). Based on these results, some additional reactions related to H_2 generation might be being promoted in Fe_2O_3/Al_2O_3 besides the soot gasification R14 and the WGS reaction R15.

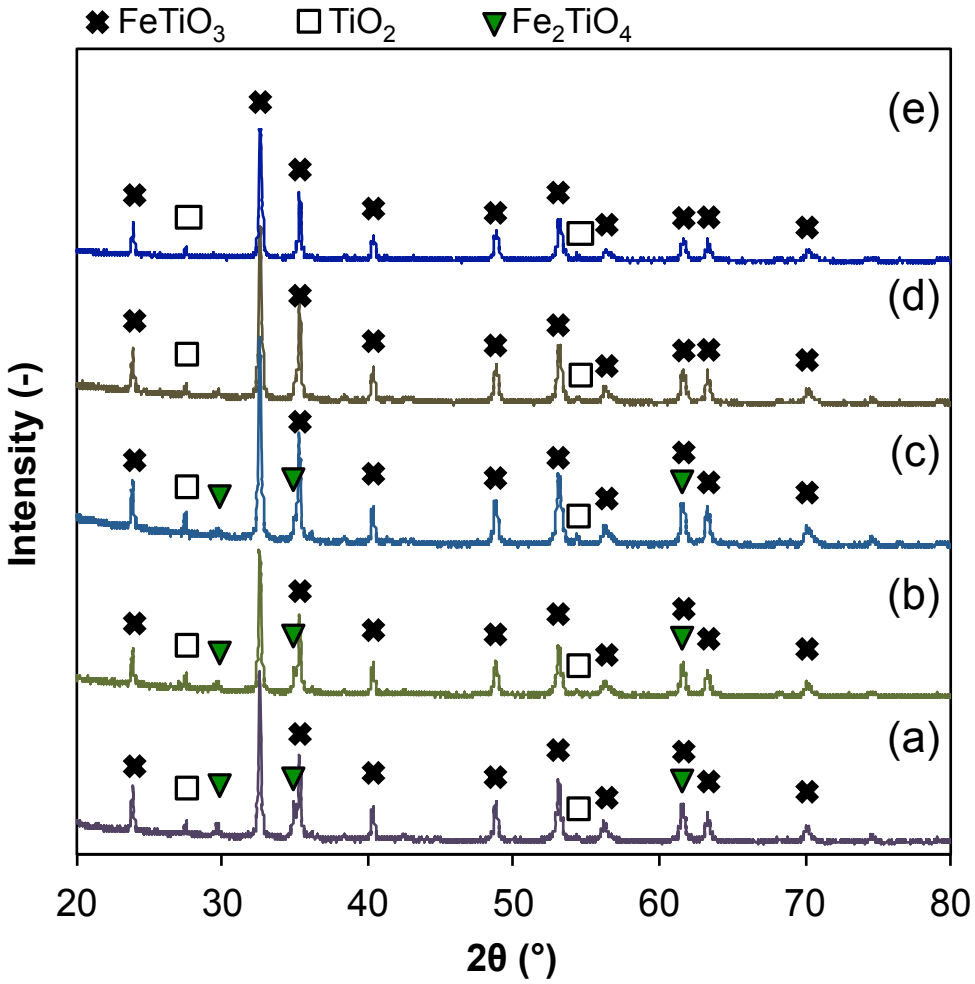

Figure 21. XRD patterns of used ilmenite particles after reforming (a) without steam, and with S/C ratio of (b) 0.5, (c) 1.0, (d) 1.5, and (e) 2.5.

XRD identification of oxygen carriers after steam reforming with various S/C ratios was performed in order to find the difference. Figure 21 shows XRD patterns of used ilmenite particles after reforming at various S/C ratios. It can be observed that pre-oxidized ilmenite is reduced into $FeTiO_3$ and/or Fe_2TiO_4 after reforming of coal volatiles with all S/C ratios from 0 to 2.5. This indicates that the iron (II) valance state formed via the reduction of ilmenite was retained during the reforming, regardless of the steam concentration. Furthermore, it was clearly visible on ilmenite in Figure 20(a) that the increase of H_2 and CO_2 during steam reforming of coal volatiles with various S/C ratios is mainly attributed to the soot gasification R14 and the WGS reaction R15. Based on these results, we can conclude that oxidation of volatiles with ilmenite, soot gasification and WGS reactions mainly proceed during steam reforming with higher S/C ratios and the reduced state $FeTiO_3$ of ilmenite is relatively stable with the steam addition.

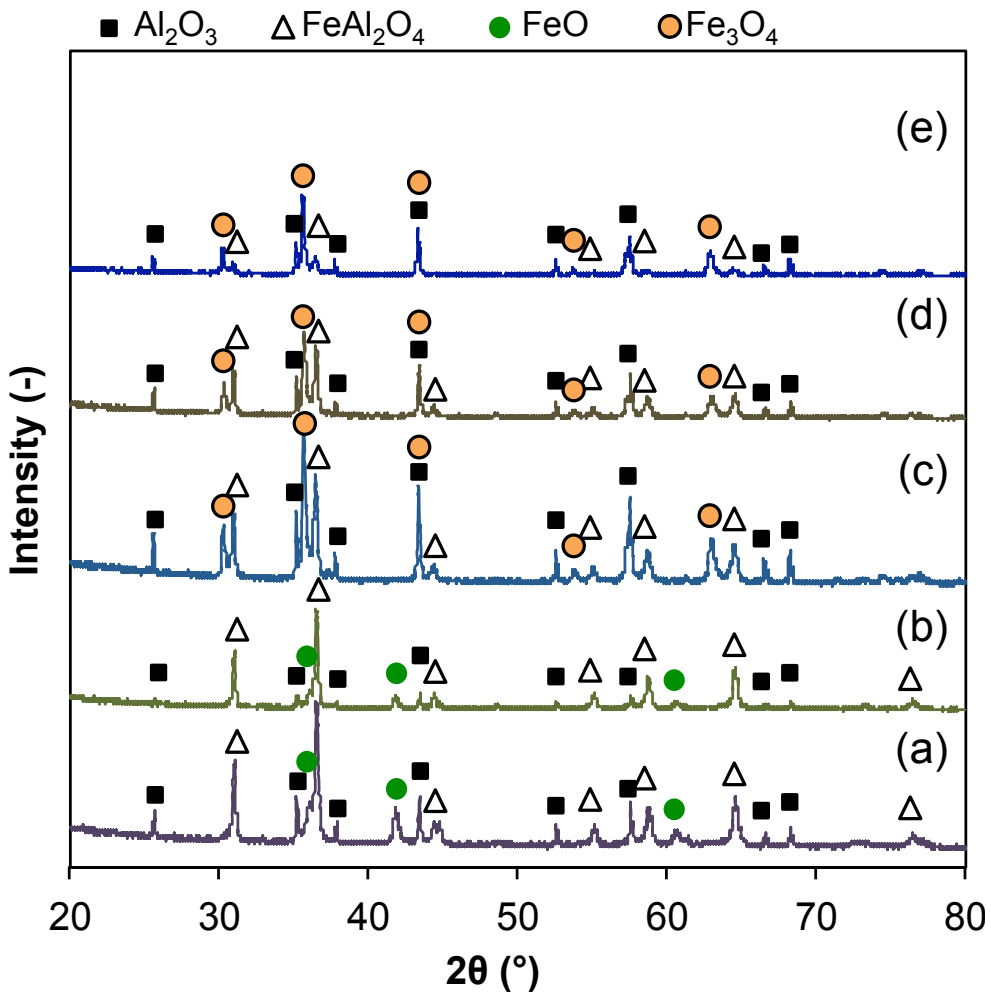

Figure 22. XRD patterns of used Fe_2O_3/Al_2O_3 particles after reforming (a) without steam, and with S/C ratio of (b) 0.5, (c) 1.0, (d) 1.5, and (e) 2.5.

Figure 22 shows XRD patterns of used Fe_2O_3/Al_2O_3 after reforming at various S/C ratios. Fe_2O_3/Al_2O_3 in the absence of steam was reduced by coal volatiles into FeO and $FeAl_2O_4$ with a valence of iron (II), which maintained until S/C ratio of 0.5.

$$Fe_2O_3/Al_2O_3 + \text{Volatiles} \rightarrow FeO + FeAl_2O_4 + H_2O + CO_2 \quad \text{(R25)}$$

However, Fe_3O_4 phase with mixed iron (II) and iron (III) valences, as shown in Figure 22(c) to (e), appeared in Fe_2O_3/Al_2O_3 oxygen carrier after steam reforming at S/C ratios of 1.0 and above, where FeO phase vanished. In addition, a relative intensity of the peaks corresponding to Fe_3O_4 phase became greater with the increase of S/C ratio, while one corresponding to $FeAl_2O_4$ became smaller. This indicates that oxidation from FeO and $FeAl_2O_4$ to Fe_3O_4 in synthetic Fe_2O_3/Al_2O_3 carrier is promoted by steam. According to the results of reforming experiments, not only soot gasification R14 and WGS reaction R15 proceed with higher steam ratios, but also some additional reaction related to hydrogen generation is promoted by synthetic Fe_2O_3/Al_2O_3 carrier. In a combination of the XRD and reforming experimental data, we can consider that the reduced FeO and $FeAl_2O_4$ particles of synthetic iron carrier are further re-oxidized by steam according to reactions R26 and R27 in addition to soot reactions R14 and R15. That could explain why a considerable amount of H_2 is produced during the steam reforming with S/C ratios of 1.0 and above.

$$3FeO + H_2O \rightarrow Fe_3O_4 + H_2 \quad \text{(R26)}$$

$$3FeAl_2O_4 + H_2O \rightarrow Fe_3O_4 + 3Al_2O_3 + H_2 \quad \text{(R27)}$$

In fact, these steam-iron reactions are discussed for chemical looping hydrogen generation process [36], suggesting that the reduced iron oxide is partly oxidized by steam to Fe_3O_4 with producing high concentration of hydrogen. On the other hand, thermodynamic equilibrium calculation [8] shows that the level of reduction of Fe_2O_3 to Fe_3O_4 or FeO strongly depends on the water/hydrogen ratio. When water/hydrogen ratios are higher than 2.8, reduction of Fe_2O_3 proceeds toward Fe_3O_4; otherwise, it is reduced to FeO or Fe. In the current experiments, water/hydrogen ratios were greater than 3 in all conditions. Therefore, it is reasonable for synthetic Fe_2O_3/Al_2O_3 carrier to form Fe_3O_4 at higher S/C ratios.

Overall, full conversion by oxygen carriers is a main objective in CLC with coal to achieve a high CO_2 capture and energy generation. In respect to the total combustion efficiency, pre-oxidized ilmenite showed the higher performance than Fe_2O_3/Al_2O_3 during the reforming of coal volatiles with various steam-to-carbon ratios, even though its redox reactivity was slower than Fe_2O_3/Al_2O_3. Furthermore, the carbon deposited from coal can be transferred to the air reactor with an oxygen carrier and combusted in the flue gas, causing efficiency loss for CO_2 capture. Based on the current results, carbon deposits can be reduced with the introduction of a sufficient amount of steam. However, extra steam in CLC could greatly encourage a reversible H_2 generation reaction in Fe_2O_3/Al_2O_3 oxygen carrier, while ilmenite can maintain the combustion reactivity at higher steam content levels.

2.3.4 Effect of oxygen carrier's circulation ratio on the combustion reactivity of ilmenite and Fe_2O_3/Al_2O_3 with coal volatiles

An oxygen carrier to coal weight ratio was 3.5 during the steam reforming experiments above. However, an oxygen carrier for a developing system of iG-CLC by JCOAL (Figure 8) was proposed to circulate at least 50 times higher amount than coal. Therefore, steam reforming experiments of coal volatiles (S/C 1.0) with ilmenite and Fe_2O_3/Al_2O_3 were also performed at an oxygen carrier/coal weight ratio of 50. The carbon balance and product gas yield are shown in Figure 23(a) and (b). For comparison, the amounts of volatiles consumed and produced at the oxygen carrier/coal ratios of 3.5 and 50 are also presented as differences from the Sand data in Figure 23(c).

When a weight ratio of oxygen carrier was 50 times higher than coal, most carbon gases and H_2 were converted to CO_2 and H_2O. As shown in Figure 23(c), CO_2 conversions of the released carbon gas were approximately 85% and 100% in ilmenite and Fe_2O_3/Al_2O_3, respectively. For Fe_2O_3/Al_2O_3, almost all the carbon gas releasing from fuel reactor was CO_2. In addition, there was a slightly decreasing tendency for soot formation, when the higher amount of oxygen carriers employed. The soot amount for ilmenite and Fe_2O_3/Al_2O_3 was 11 mol% and 15 mol% of total molar carbon in volatiles, respectively. No tar formation was observed.

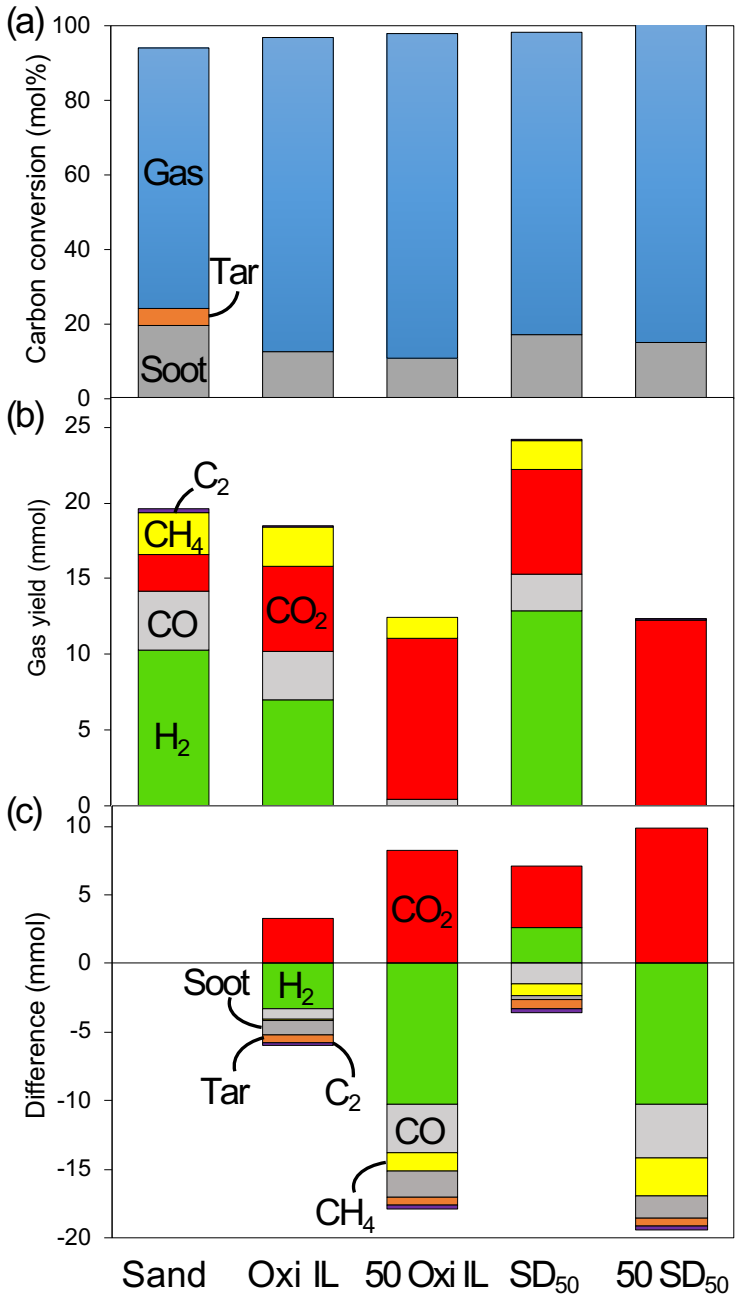

Figure 23. (a) Carbon balance and (b) product gas yield during the steam reforming (S/C 1.0) of coal volatiles with pre-oxidized ilmenite and Fe_2O_3/Al_2O_3 at oxygen carrier/coal weight ratios of 3.5 (Oxi IL, SD_{50}) and 50 (50 Oxi IL, 50 SD_{50}), and (c) the differences in volatiles compared with sand.

Based on these results at an oxygen carrier/coal ratio of 50, carbon balances of coal volatiles for the iG-CLC system with ilmenite and Fe_2O_3/Al_2O_3 were estimated and shown in Figure 24 and Figure 25. Furthermore, carbon balances with S/C ratio of 2.5 were estimated from the results described in Figure 19.

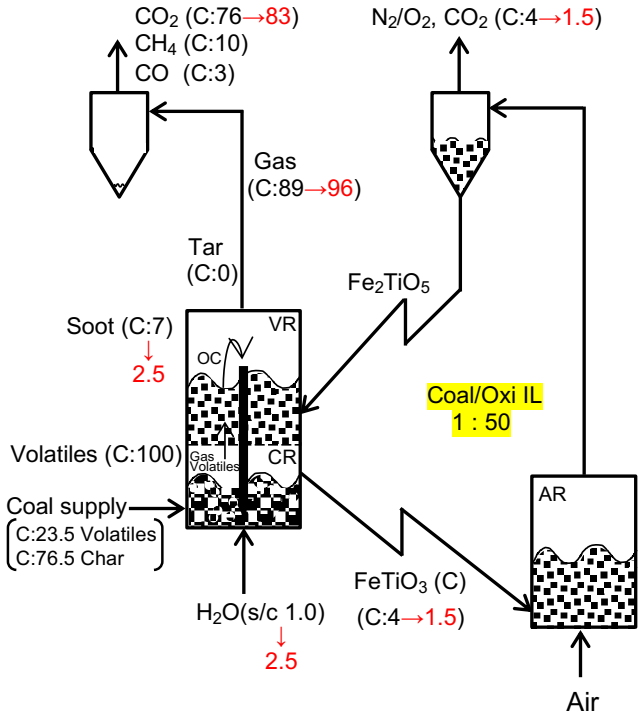

Figure 24. Carbon balance of coal volatiles with ilmenite circulated with an oxygen carrier weight ratio of 50 at S/C ratios 1.0 (black) and 2.5 (red) estimated for the proposed iG-CLC system. Carbon from char gasification is not accounted for estimation.

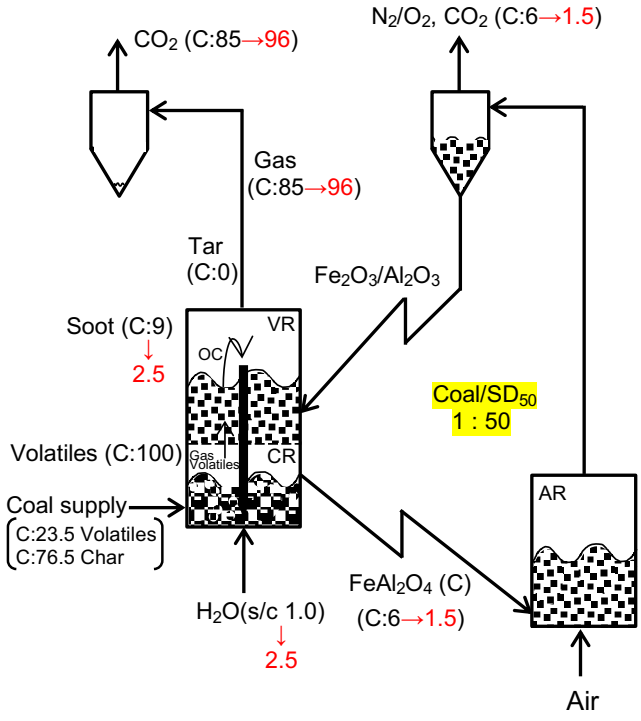

Figure 25. Carbon balance of coal volatiles with Fe_2O_3/Al_2O_3 (an oxygen carrier weight ratio of 50) at S/C ratios 1.0 (black) and 2.5 (red) estimated for the proposed iG-CLC system. Carbon from char gasification is not accounted for estimation.

For ilmenite, the gaseous specious from the fuel reactor accounted for 89% of the carbon from volatiles. The remaining carbon was either deposited in the volatiles reactor (7%), or existed from the air reactor (4%). Although 76% of the total carbon in volatiles was converted to CO_2 at S/C ratio of 1.0, it could be enhanced to 83% at S/C ratio of 2.5. The higher amount of steam is then provided, the smaller amount of carbon deposition will be formed. Comparing to ilmenite, a synthetic oxygen carrier Fe_2O_3/Al_2O_3 presented much greater CO_2 conversion. CO_2 conversions with Fe_2O_3/Al_2O_3 were 85% at 1.0 and 96% at 2.5 of S/C ratios, respectively.

For comparison, carbon balance of coal during the operation with ilmenite using the 100kWth three-tower iG-CLC plant developed by JCOAL was also shown in Figure 26.

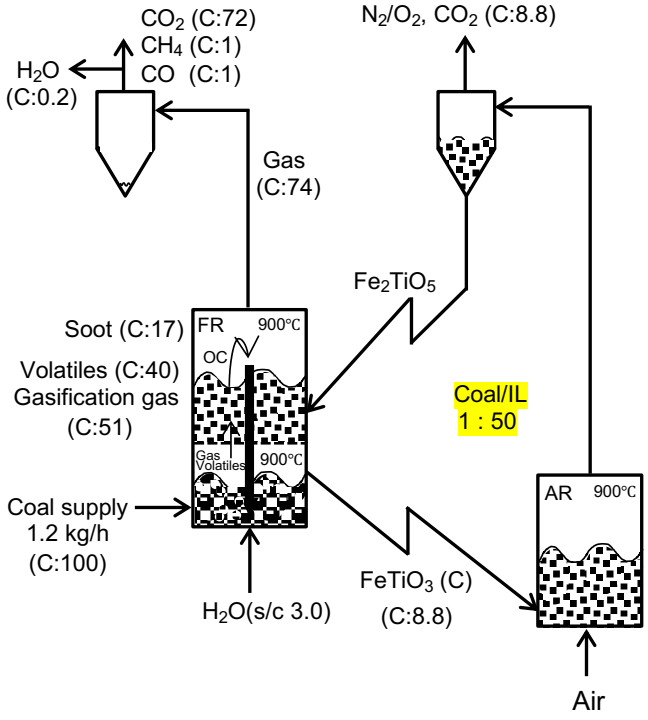

Figure 26. Carbon balance of coal during an operation with ilmenite of the 100kWth three-tower iG-CLC plant (S/C 3.0)

The S/C ratio of 3.0 was validated in the three-tower CLC plant operation, where 17% and 8.8 % of total carbon in coal were deposited in the fuel reactor and released from the air reactor, respectively. In the carbon balance of coal volatiles with ilmenite shown in Figure 24, only 1.5% of total carbon in volatiles is expected to release from the air reactor at S/C ratios of 2.5. This loss is expected to be much less in the S/C ratio of 3.0. Therefore, the estimated carbon deposits from volatiles in our study would be much lower than the real CLC plant. Hence, a carbon in char may be a big contribution to the carbon depositions in the three-tower CLC plant. Nevertheless, it is clear from our study that carbon depositions can be prevented by high steam amount.

2.4 Conclusions

The performance of ilmenite for steam reforming of coal volatiles was investigated using a two-stage fixed-bed reactor. The steam reforming experiments were conducted at 1173 K under various steam conditions. Natural ilmenite is mainly composed of the lower oxidation state of Fe (II), causing its reactivity for tar decomposition and volatile conversion to be lower. However, the combustion reactivity of ilmenite with coal volatiles greatly increased after pre-oxidation. There was no tar formation and CO_2 conversion was greatly enhanced due to the efficient utilization of the lattice oxygen in pre-oxidized ilmenite. Morphological changes on ilmenite carrier were also observed during the reaction with volatiles.

For both oxygen carriers of pre-oxidized ilmenite and Fe_2O_3/Al_2O_3, carbon deposits greatly decreased with increasing the steam content. At the same time, CO_2 conversion was promoted by gasification and WGS reactions. The reduced phase $FeTiO_3$ of ilmenite was relatively stable with the addition of steam, whereas a reversible reaction from reduced $FeAl_2O_4$ to Fe_3O_4 occurred on the Fe_2O_3/Al_2O_3 by steam in the higher steam ratios. When pre-oxidized ilmenite and Fe_2O_3/Al_2O_3 were used with an oxygen carrier to coal weight ratio of 50, carbon gases from volatiles were significantly converted to CO_2. Almost full CO_2 conversion was obtained in Fe_2O_3, whereas CO_2 conversions with ilmenite was approximately 85%. The results obtained in this study should be useful for the design and optimization of coal CLC.

References

[1] W.K. Lewis, E.R. Gilliland, M.P. Sweeney, Gasification of carbon-Metal oxides in a fluidized powder bed, Chem. Eng. Prog. 47 (1951) 251–256.

[2] H.J. Richter, K.F. Knoche, Reversibility of combustion processes, in: R.A. Gaggioli (Ed.), Efficiency and Costing, American Chemical Society, Washington, 1983, pp. 71–85.

[3] M. Ishida, H. Jin, A new advanced power-generation system using chemical-looping combustion, Energy 19 (1994) 415–422.

[4] M. Anheden, A.S. Naesholm, G. Svedberg, Chemical-looping combustion – efficient conversion of chemical energy in fuels into work, United States: 1995. web.

[5] A. Lyngfelt, B. Leckner, T. Mattisson, A fluidized-bed combustion process with inherent CO_2 separation; application of chemical-looping combustion, Chem. Eng. Sci. 56 (2001) 3101–3113.

[6] H. Jin, M. Ishida, A new type of coal gas fueled chemical-looping combustion, Fuel 83 (2004) 2411–2417.

[7] T. Mattisson, F. García-Labiano, B. Kronberger, A. Lyngfelt, J. Adánez, H. Hofbauer, Chemical-looping combustion using syngas as fuel, Int. J. Greenh. Gas Control 1 (2007) 158–169.

[8] A. Abad, F. García-Labiano, L.F. de Diego, P. Gayán, J. Adánez, Reduction kinetics of Cu-, Ni-, and Fe-based oxygen carriers using syngas ($CO + H_2$) for chemical-looping combustion, Energy & Fuels 21 (2007) 1843–1853.

[9] J. Adanez, A. Abad, F. Garcia-Labiano, P. Gayan, L.F. de Diego, Progress in chemical-looping combustion and reforming technologies, Prog. Energy Combust. Sci. 38 (2012) 215–282.

[10] J. Adánez, A. Abad, T. Mendiara, P. Gayán, L.F. de Diego, F. García-Labiano, Chemical looping combustion of solid fuels, Prog. Energy Combust. Sci. 65 (2018) 6–66.

[11] Y. Cao, W.P. Pan, Investigation of chemical looping combustion by solid fuels. 1. process analysis, Energy & Fuels 20 (2006) 1836–1844.

[12] S.A. Scott, J.S. Dennis, A.N. Hayhurst, T. Brown, *In situ* gasification of a solid fuel and CO_2 separation using chemical looping, AIChE J. 52 (2006) 3325–3328.

[13] H. Leion, T. Mattisson, A. Lyngfelt, The use of petroleum coke as fuel in

chemical-looping combustion, Fuel 86 (2007) 1947–1958.

[14] A. Lyngfelt, Chemical-looping combustion of solid fuels – status of development, Appl. Energy 113 (2014) 1869–1873.

[15] S.Y. Lin, T. Saito, K. Hashimoto, Development of the three-tower chemical looping coal combustion technology, Energy Procedia, 114 (2017) 414–418.

[16] A. Cuadrat, A. Abad, J. Adánez, L.F. de Diego, F. García-Labiano, P. Gayán, Behavior of ilmenite as oxygen carrier in chemical-looping combustion, Fuel Process. Technol. 94 (2012) 101–112.

[17] H. Leion, T. Mattisson, A. Lyngfelt, Solid fuels in chemical-looping combustion, Int. J. Greenh. Gas Control 2 (2008) 180–193.

[18] T.A. Brown, J.S. Dennis, S.A. Scott, J.F. Davidson, A.N. Hayhurst, Gasification and chemical-looping combustion of a lignite char in a fluidized bed of iron oxide, Energy & Fuels 24 (2010) 3034–3048.

[19] J. Adánez, C. Dueso, L.F. de Diego, F. García-Labiano, P. Gayán, A. Abad, Effect of fuel gas composition in chemical-looping combustion with Ni-based oxygen carriers. 2. fate of light hydrocarbons, Ind. Eng. Chem. Res. 48 (2009) 2509–2518.

[20] P. Gayán, C.R. Forero, L.F. de Diego, A. Abad, F. García-Labiano, J. Adánez, Effect of gas composition in Chemical-Looping Combustion with copper-based oxygen carriers: fate of light hydrocarbons, Int. J. Greenh. Gas Control 4 (2010) 13–22.

[21] M. Keller, H. Leion, T. Mattisson, H. Thunman, Investigation of natural and synthetic bed materials for their utilization in chemical looping reforming for tar elimination in biomass-derived gasification gas, Energy & Fuels 28 (2014) 3833–3840.

[22] F. Lind, M. Seemann, H. Thunman, Continuous catalytic tar reforming of biomass derived raw gas with simultaneous catalyst regeneration, Ind. Eng. Chem. Res. 50 (2011) 11553–11562.

[23] A. Larsson, M. Israelsson, F. Lind, M. Seemann, H. Thunman, Using ilmenite to reduce the tar yield in a dual fluidized bed gasification system, Energy & Fuels 28 (2014) 2632–2644.

[24] E. Jerndal, T. Mattisson, A. Lyngfelt, Thermal analysis of chemical-looping combustion, Chem. Eng. Res. Des. 84 (2006) 795–806.

[25] S. Rajendran, M. Wong, D. Stokie, S. Bhattacharya, Performance of a Victorian brown coal and iron ore during chemical looping combustion in a 10 kW_{th}

alternating fluidized bed, Fuel 183 (2016) 245–252.

[26] J. Ma, X. Tian, H. Zhao, S. Bhattacharya, S. Rajendran, C. Zheng, Investigation of two hematites as oxygen carrier and two low-rank coals as fuel in chemical looping combustion, Energy & Fuels 31 (2017) 1896–1903.

[27] M. Matzen, J. Pinkerton, X. Wang, Y. Demirel, Use of natural ores as oxygen carriers in chemical looping combustion: a review, Int. J. Greenh. Gas Control 65 (2017) 1–14.

[28] J. Adánez, A. Cuadrat, A. Abad, P. Gayán, L.F. de Diego, F. García-Labiano, Ilmenite activation during consecutive redox cycles in chemical-looping combustion, Energy & Fuels 24 (2010) 1402–1413.

[29] H. Leion, T. Mattisson, A. Lyngfelt, Use of ores and industrial products as oxygen carriers in chemical-looping combustion, Energy & Fuels 23 (2009) 2307–2315.

[30] H. Leion, A. Lyngfelt, M. Johansson, E. Jerndal, T. Mattisson, The use of ilmenite as an oxygen carrier in chemical-looping combustion, Chem. Eng. Res. Des. 86 (2008) 1017–1026.

[31] N. Berguerand, A. Lyngfelt, The use of petroleum coke as fuel in a 10 kW_{th} chemical-looping combustor, Int. J. Greenh. Gas Control 2 (2008) 169–179.

[32] A. Cuadrat, A. Abad, F. García-Labiano, P. Gayán, L.F. de Diego, J. Adánez, The use of ilmenite as oxygen-carrier in a 500 W_{th} Chemical-Looping Coal Combustion unit, Int. J. Greenh. Gas Control 5 (2011) 1630–1642.

[33] A. Cuadrat, A. Abad, F. García-Labiano, P. Gayán, L.F. de Diego, J. Adánez, Ilmenite as oxygen carrier in a chemical looping combustion system with coal, Energy Procedia 4 (2011) 362–369.

[34] D. Yamaguchi, L. Tang, K. Chiang, Pre-oxidation of natural ilmenite for use as an oxygen carrier in the cyclic methane–steam redox process for hydrogen production, Chem. Eng. J. 322 (2017) 632–645.

[35] Y. Ku, Y. Liu, P. Chiu, Y. Kuo, Y. Tseng, Mechanism of Fe_2TiO_5 as oxygen carrier for chemical looping process and evaluation for hydrogen generation, Ceram. Int. 40 (2014) 4599-4605.

[36] L. Zeng, F. He, F. Li, L.S. Fan, Coal-direct chemical looping gasification for hydrogen production: reactor modeling and process simulation, Energy and Fuels. 26 (2012) 3680–3690.

Chapter 3 EFFECT OF H_2S ON THE COMBUSTION REACITVITY OF ILMENITE WITH COAL VOLATILES UNDER STEAM REFORMING

3.1 Introduction and objectives

Coal is the world's most abundant and widely distributed fossil fuel, and most countries still depend on as an energy source. Carbon dioxide (CO_2) from coal-fired power plants accounts for the largest percentage (30%) of global CO_2 emissions. Due to increasing public concern over global warming and climate change, a transition to clean innovative coal technologies that reduce CO_2 emissions is urgently needed. Coal chemical-looping combustion (CLC) technology can be the best solution for satisfying both global energy and environmental requirements. A number of intensive lab-scale and pilot-scale CLC experiments using gaseous fuel have been performed, proving its capability for industrial application [1].

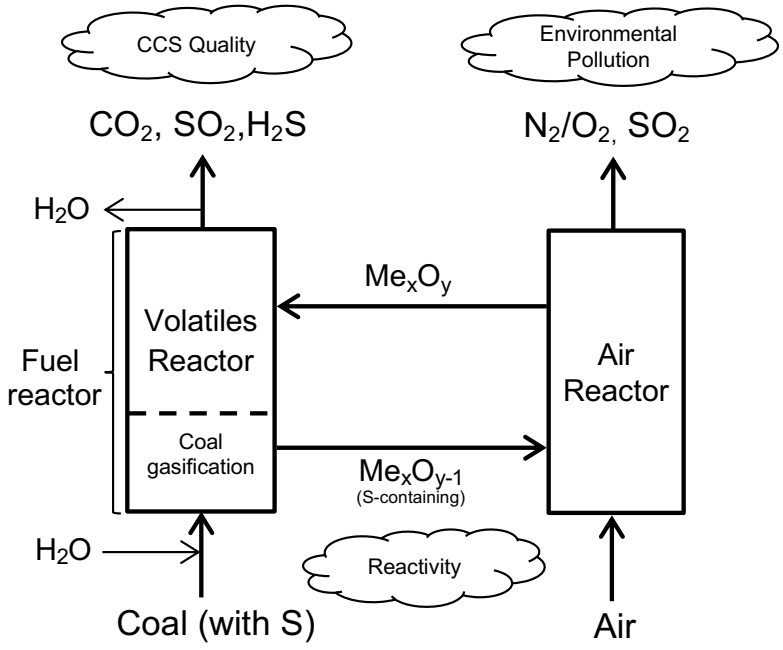

Figure 27. Schematic illustration of the direct CLC process with sulfur-containing coal.

However, when it comes to coal [2–7], unlike with gaseous fuels, it is important to consider various factors such as sulfurous impurities, nitrogen impurities, or higher hydrocarbons, because these pollutants could deteriorate the performance of CLC units. In the coal CLC system developed by Japan Coal Energy Center (JCOAL), sulfur impurity is also one of the critical issues, as shown in Figure 27 [7–10].

Because coal usually contains a high amount of sulfur contaminant (0.3-8%), which can lead to serious problems in CLC system. From an operational point of view, H_2S, the most common sulfurous species emitted from coal, can interact with oxygen carriers to form sulfides or sulfates. Those sulfur compounds on the oxygen carriers may then reduce the chemical looping conversion efficiency, or even deactivate the oxygen carriers. From an environmental point of view, sulfur can be released from both reactors. In the fuel reactor, oxygen carriers can convert sulfur contaminants such as H_2S, into SO_2, which then released with CO_2. If sulfur is accumulated on oxygen carrier particles during the reduction, the accumulated sulfur is transferred to the air reactor, where the sulfur is oxidized and released as SO_2. The quality of CO_2 capture and storage (CCS) is degraded by sulfur gases. Additionally, flue gas emissions with sulfur must fulfill strict environmental legislation. Therefore, it is very important to understand how the conversion performance and lifetime of oxygen carriers is affected by sulfur species, in addition to knowing in which reactor system this occurs and how much sulfurous gas is emitted. Understanding the behavior of sulfur impurities is useful for process design and optimization of coal CLC systems.

Numerous studies have been carried out on sulfur evolution in CLC. Jerndal *et al*. [11] performed theoretical thermal analyses of a number of different oxygen carriers in CLC with CH_4 in the presence of H_2S; they concluded that the H_2S contaminant is greatly converted to SO_2 for most of the CLC systems that use Cu- and Fe-based oxygen carriers. They also reported that Fe_2O_3/Fe_3O_4, which is thermodynamically the most suitable iron oxide for CLC, forms hardly any sulfide or sulphate at any concentration of sulfur-containing gas within the temperature ranges of CLC. Furthermore, Wang *et al*. [12] thermodynamically investigated the influences of various factors including pressure, temperature, oxygen availability (oxygen excess number), and gas composition on sulfur evolution in CLC with syngas; they determined that deposition of sulfur species on oxygen carriers is enhanced at higher pressure, lower temperature, and lower oxygen availability, and that the potential sulfur deposits on NiO, Fe_2O_3, Mn_3O_4, and CoO are Ni_3S_2, $Fe_{0.84}S$, $MnSO_4$ and $CoS_{0.89}$, respectively. In addition, de Diego *et al*. [13]

thermodynamically and experimentally investigated sulfur fate in the CLC process of Fe-based oxygen carriers with sour gas (containing 15% H_2S) over various ranges of oxygen carrier to fuel ratio values, ϕ. The oxygen carrier to fuel ratio $\phi = 1$ corresponds to the stoichiometric amount of oxygen carrier required for a full fuel conversion. De Diego *et al*. indicated that in CLC operating at oxygen carrier to fuel ratio values of ϕ>1.5, H_2S is completely combusted into SO_2 in the fuel reactor, while at lower ϕ values, iron sulfide $Fe_{0.877}S$ can be generated. Thermogravimetric analysis (TGA) experimental work [14] with bentonite-supported Fe, Ni, Mn, and Cu oxygen carriers also revealed that the sulfidation reaction with H_2S proceeds after further reduction to metal, whereas the metal sulfides can be removed by the oxidation. Furthermore, although metal sulfides can cause the sintering and defluidization of iron ore oxygen carriers due to their low melting points, steam addition and the use of a sulfur absorbent are effective in preventing those problems [15]. One positive effect of H_2S that has been reported is that the reduction rate of Fe-Mn oxygen carriers by syngas is enhanced in the presence of H_2S [16]. Chung *et al*. investigated the sulfur balance with iron-based oxygen carriers in a real 100 kW coal CLC unit [17]. They found that 69% of the total sulfur in coal was released as SO_2 and H_2S in reduction, while only 2.7% was released in oxidation. The remaining 28.3% of the sulfur was left behind in the coal ash.

As for the choice of oxygen carrier used in coal CLC, ilmenite, a natural iron titanium ore, has been found to be the most promising oxygen carrier due to its high mechanical strength and ability to resist agglomeration and attrition [7]. However, only a few studies have focused on sulfur evolution while using ilmenite in CLC. Linderholm *et al*. [18] conducted a 4.7 hour long CLC experiment with a subbituminous coal containing 0.6% sulfur and a mixture of ilmenite and manganese ore and showed that 72% of the sulfur was converted to sulfurous gases (mainly SO_2) in the fuel reactor and the rest was left on the elutriated solids. CLC experiments carried out by Moldenhauer *et al*. revealed that ilmenite is more reactive to sulfurous kerosene than to sulfur-free kerosene [19]. Tan *et al*. reported a similar positive effect of sulfur on ilmenite reactivity during pressurized TGA tests using CH_4 and ilmenite in the presence of H_2S under an atmosphere of CO_2 [20]. Using SEM-EDX analysis, they found that sulfur was locally deposited on the surfaces of the reduced ilmenite samples; however, the formation mechanism of the sulfur deposits was unclear. In addition, the reaction of ilmenite with actual coal volatiles in the presence of H_2S has not yet been studied.

In this work, we investigated the effect of sulfur gas on the combustion reactivity of ilmenite with coal volatiles under a steam reforming atmosphere in a two-stage fixed bed reactor. We used actual volatiles from coal pyrolysis as fuel, with the aim of studying the interaction of ilmenite and sulfur in more realistic steam environment. A TGA cycle study of ilmenite in the presence of H_2S was carried out for confirmation.

3.2 Experimental

3.2.1 Samples and characterization

Coal and oxygen carrier samples used in this work were the same as previous chapter 2. The natural ilmenite ore was calcined in a muffle furnace operating at 1173 K for 2 h in air and then pulverized and sieved to grain sizes below 150 μm before being used in the experiments. The chemical composition of the ilmenite is presented in Table 2. The crystalline phase of Fe_2TiO_5, the fully oxidized state of ilmenite, was confirmed by X-ray diffraction analysis. A synthetic iron oxide with alumina, Fe_2O_3/Al_2O_3 (50 wt% Fe_2O_3) was also used for a comparison with ilmenite.

An Indonesian subbituminous coal with a particle size of 1.0 mm was employed as a source of coal volatiles. Proximate and ultimate analyses of a coal sample are shown in Table 1. The sulfur content of the coal sample was very low, and the majority remained as inorganic and aromatic sulfur in the char pyrolysis [17] [21], so we consider its impact on the volatiles in our study to be negligible. Inactive river sand was used as an inert material in the experiment.

The crystalline phases of ilmenite particles before and after the experiment were characterized by X-ray diffraction (XRD) (SmartLab, Rigaku, Japan). The XRD apparatus was set to operate at 40 kV and 30 mA over a scanning range between 20° and 80° at a scanning rate of 0.03°/s.

The chemical states of the surface components of the used ilmenite particles were identified by an X-ray Photoelectron Spectrometer (XPS) (AXIS-NOVA, Shimadzu, Japan). Al Kα radiation (10 mA, 15 kV) was used as an X-ray source. Au powder (99.99%, Nilaco Corp., Japan) was mixed with the samples as an internal standard for measurement. Charge correction was made by setting the peak position of the Au $4f^{7/2}$ to 84.0 eV.

3.2.2 Steam reforming of coal volatiles with ilmenite and Fe_2O_3/Al_2O_3 in the presence of H_2S

Steam reforming experiments were conducted in a two-stage fixed-bed quartz reactor with an internal diameter of 22 mm and a main body length of 880 mm. A schematic illustration of the experimental setup is shown in Figure 28. The experimental setup was designed to conduct a slow coal pyrolysis in the upper stage of the reactor, and reforming and combustion of volatiles in the lower stage. Approximately 3.5 g of ilmenite or Fe_2O_3/Al_2O_3 oxygen carrier samples was placed on the lower stage, and 1 g of coal wrapped with silica wool was placed on the upper stage. A silica wool tar trap was packed under the lower stage of the reactor.

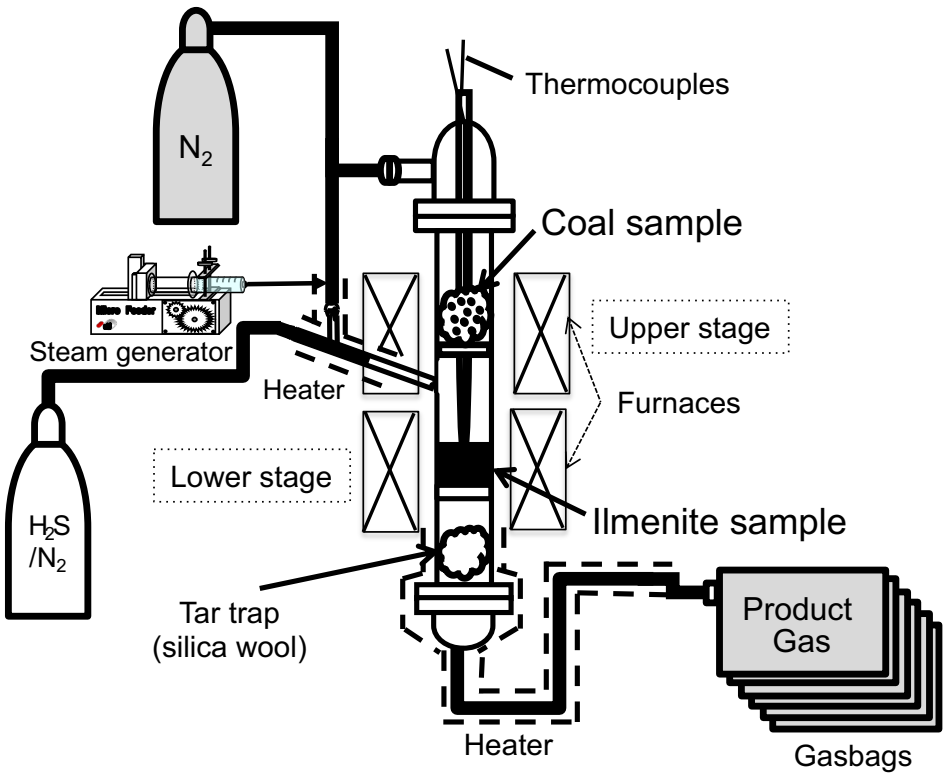

Figure 28. Schematic illustration of the experimental setup for the steam reforming experiments in the presence of H_2S.

Before the commencement of coal pyrolysis, the oxygen carrier stage was preheated to 1173 K at 20 $K \cdot min^{-1}$ in N_2; it remained at this temperature during the experiment. The N_2, provided from the top of the reactor with a flow rate of 60 $ml \cdot min^{-1}$

was used for coal pyrolysis. Steam and H_2S in N_2 were introduced into the lower stage through the branch gas inlet at atmospheric pressure. The steam to carbon in the coal (S/C) ratio was 0.5 (approximately 10 vol%). The H_2S concentrations used were 2000 ppm and 4000 ppm. The reforming experiment was commenced by heating the coal sample from 373 K to 1173 K at a rate of 10 $K \cdot min^{-1}$ for 90 min. Volatiles from the coal gradually devolatilized and reacted with the oxygen carrier in the lower stage, which was fixed at 1173 K under the presence of steam and H_2S.

In order to evaluate changes in the gases released over time and temperature, exhaust gas from the experiment was collected in 6 gas bags at intervals of 15 min and analyzed. The H_2 and carbon gases (such CO, CO_2, CH_4, C_2H_4, and C_2H_6) were analyzed using offline gas chromatographs (GC-2014, Shimadzu, Japan) with a thermal conductivity detector and a flame ionization detector equipped with a methanizer. The sulfurous gases, H_2S and SO_2, in the outlet gas were measured using a Gastec GV-100 gas sampling pump kit with Gastec Detector Tubes (Gastec Corporation, Japan; 4H for H_2S and 5M for SO_2). The gas yield was calculated according to Eq.3 and presented as the molar amount of each gas component.

$$molar\ yield\ of\ gas\ component\ i = \frac{x_i \times V_{N2}}{V_m \times (1 - \sum_i x_i)} \qquad \text{(Eq.3)}$$

where *i* represents H_2, CO, CO_2, CH_4, C_2 and the higher hydrocarbon gases, H_2S, and SO_2, and x_i is the volume percentage of released gas *i*.

At the end of the reforming experiment, the oxygen carrier particles and the reactor were individually oxidized at 1173 K for 1 h, and the amount of sulfur deposited on the ilmenite particles and in the reactor was determined from the amount of SO_2 detected in the combustion gas by Gastec detector tubes. The sulfur balance was calculated as the molar percentage of elemental sulfur in each product out of the total sulfur introduced. Similarly, the amount of carbon (soot) and tar deposited was determined from the amount of CO and CO_2 in the combustion gas using gas chromatographs. The carbon balance was presented as the molar percentage of elemental carbon in each product out of the total carbon of the volatiles.

$$carbon\ balance\ of\ carbon\ component\ j = \frac{C_j}{C_{coal} - C_{char}} \times 100\% \qquad \text{(Eq.4)}$$

where *j* represents product gas, tar and soot obtained at the end of experiment, and C_j is the molar amount of carbon in the carbon product j.

3.2.3 Cycle redox reactivity tests of ilmenite and Fe_2O_3/Al_2O_3 in the presence of H_2S

To obtain more information about the impact of H_2S on the CLC reactivity of ilmenite and Fe_2O3/Al_2O_3 oxygen carriers, 8 successive cycle tests were conducted at 1173 K in a thermogravimetric analyzer (TGD-7000RH, Ulvac Rico, Japan) combined with mass spectrometry (MS), as shown in Figure 29. For each test, approximately 20 mg of the carrier sample was placed in a platinum pan and preheated to 1173 K at a rate of 20 K min^{-1} in air; the sample remained at this temperature during the cycle test. For the reduction period, a reducing gas composed of 5% H_2 in Ar was introduced into the reactor at a flow rate of 100 ml·min^{-1}; H_2S with a concentration between 1000 and 4000 ppm was also added. For the oxidation period, air was provided at a flow rate of 100 ml·min^{-1}. Reduction and oxidation reactions for each cycle were carried out for 30 min and 10 min, respectively. To avoid the mixing of gases between the oxidation and reduction periods, the reactor was purged with Ar for 3 min after each stage of the cycle. For comparison, a cycle test was also conducted without H_2S. The test data for the weight change of the ilmenite was acquired at 1 s interval. The outlet gases from the TGA instrument were introduced to the online mass spectrometer by a line heated to 393 K, and mass signals corresponding to H_2 (m/z=2), H_2O (m/z=18), O_2 (m/z=32), H_2S (m/z=34), and SO_2 (m/z=64) were recorded.

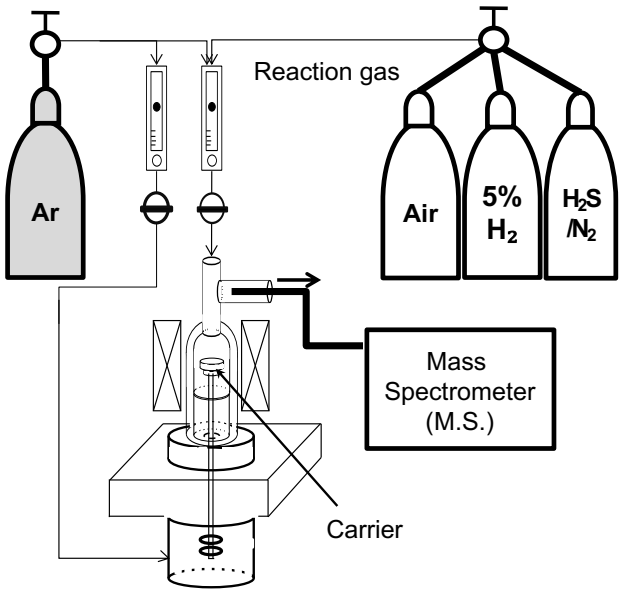

Figure 29. Schematic illustration of the experimental setup for the 8th cycle redox test in the presence of H_2S

3.3 Results and discussion

3.3.1 Effect of H_2S on the combustion reactivity of ilmenite over steam reforming of coal volatiles

Figures 25(a) and (b) show the total carbon balance and exhaust gas yield when steam reforming experiments of coal volatiles over ilmenite were carried out in the presence of 2000 and 4000 ppm H_2S. For comparison, data with sand and ilmenite are individually presented as well. In all cases, the carbon balance of the volatiles was more than 95%. The volatiles comprise mainly H_2, CO, CO_2, and CH_4, as well as unwanted carbon materials such as tar (higher hydrocarbons) and soot (carbon deposition) formed via coal pyrolysis.

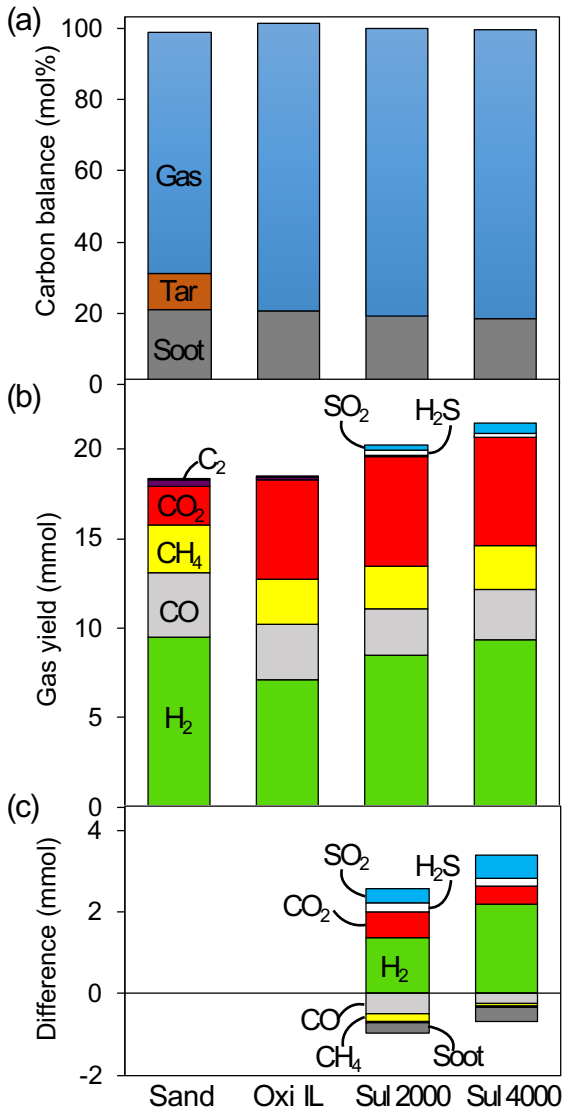

Figure 30. (a) Carbon balance and (b) exhaust gas yield obtained by the steam reforming (S/C 0.5) of coal volatiles over sand (Sand) and ilmenite in the absence (Oxi IL) and the presence of 2000 ppm (Sul 2000) and 4000 ppm H_2S (Sul4000). (c) Comparison of the volatiles with and without H_2S.

When using ilmenite for reforming experiments, the combustion reactions of the volatiles are promoted via reactions R19 through R23; this results in a substantial increase in CO_2 and a decline in other volatiles such as H_2, CO, CH_4, and the higher hydrocarbons (including tars) in the ilmenite. Similar to our previous work (chapter 2), the amount of lattice oxygen in ilmenite utilized for combustion was semi-quantitatively calculated, based on the molar amounts of CO_2 increase and H_2 decrease compared to those of sand. Approximately 85% of theoretical amount of lattice oxygen in ilmenite was utilized for volatiles' combustion in the absence of H_2S.

The differences in the data between ilmenite tested with and without H_2S, as shown in Figure 30(c), were used to evaluate the influence of sulfur gas on the combustion reactivity of ilmenite. When 2000 and 4000 ppm H_2S were introduced to the volatiles, the combustion reactivity of ilmenite was enhanced. Figure 30 shows that in the presence of H_2S, the carbon conversion to CO_2 increased while other carbon fractions such CO, CH_4, higher hydrocarbon gases, and soot decreased. In addition, no tar was obtained from the ilmenite tested with either 2000 or 4000 ppm H_2S. If only the increase in CO_2 were considered, the oxygen consumption of ilmenite would rise to about 97% with 2000 ppm H_2S, and to about 94% with 4000 ppm H_2S. These results suggest that the combustion reactivity of ilmenite may be activated in some way by H_2S.

In addition, we observed that hydrogen increased in correlation with an increase in H_2S concentration. A possible explanation for the increases in CO_2 and H_2 could be the promotion of soot gasification R14 and the subsequent WGS reaction R15 by H_2S. The decreases in soot and CO can be seen in Figure 30(c), and their contributions to CO_2 conversion may be very high. When steam is present, soot gasification reaction R14 can occur, but the subsequent WGS reaction R15 is not thermodynamically favorable at high temperatures. However, Saito *et al*. [9] revealed that the presence of an oxygen carrier promotes the WGS reaction R15 at high temperatures. Therefore, it can be assumed that H_2S activates ilmenite so that more lattice oxygen is available to promote CO_2 conversion.

Figure 31 shows the sulfur balance during the steam reforming experiments of coal volatiles over ilmenite in the presence of 2000 ppm and 4000 ppm of H_2S. The H_2S introduced during the experiments could be released as SO_2, H_2S, and COS in the outlet gas. COS was only present in a small amount (<5ppm) of the outlet gas; however, a large amount of SO_2 and H_2S were detected in the outlet gases for both of the H_2S cases. When 2000 ppm of H_2S were used, approximately 37% of the total sulfur was converted into SO_2; when 4000 ppm were used, the amount converted declined to 31%. On the other hand, in the presence of 2000 ppm H_2S, the sulfur deposited on the ilmenite particles after the experiment was approximately 14%. There was a sharp increase in sulfur deposition in the presence of 4000 ppm H_2S, where approximately 33% of total sulfur was deposited on the ilmenite particles, as shown in Figure 31. This increased accumulation of sulfur in 4000 ppm H_2S might lead to decreased activation of the combustion reactivity of ilmenite, which had greatly promoted CO_2 conversion in the presence 2000 ppm of H_2S (Figure 30c). The remaining amount of sulfur largely corresponded to the residual H_2S in the

exhaust gas and in the sulfur deposits in the reactor. The total sulfur balances, including the converted and deposited sulfurous fractions, were over 87% for both cases; the remainder might correspond to those sulfurs condensed in the water or on the reactor parts, such as the connectors and tubes, which were not measured.

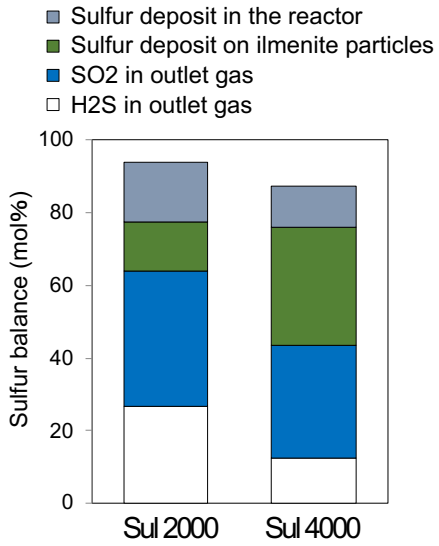

Figure 31. Sulfur balance obtained from steam reforming experiments of coal volatiles over ilmenite in the presence of 2000 ppm and 4000 ppm H_2S.

XRD and XPS analyses were performed on the used ilmenite samples in order to determine the crystal structures and chemical states of the sulfur deposits on the ilmenite particles. Figure 32 shows XRD profiles of the used ilmenite particles after CLC reforming experiments of volatiles with S/C 0.5, with and without H_2S. As shown in Figure 32(b), in the absence of H_2S the ilmenite particles were reduced by volatiles into $FeTiO_3$ and Fe_2TiO_4. A small peak of Fe_2TiO_4 represents an intermediate of ilmenite produced during an early stage of the reduction. In the presence of 4000 ppm H_2S, ilmenite particles were also mainly reduced to $FeTiO_3$, but pyrrhotite, an iron sulfide phase ($Fe_{1-x}S$), was also detected, as shown in Figure 32(d) (see also Appendix Figure A1). These results revealed that sulfidation could occur on the ilmenite by sulfur deposition. However, in the case of 2000 ppm H_2S, this sulfur phase was not confirmed (Figure 32(c)), despite the ilmenite particles having some sulfur accumulated on them. This might be due to low crystallinity of the sulfur phase or to the detection limit of the XRD apparatus.

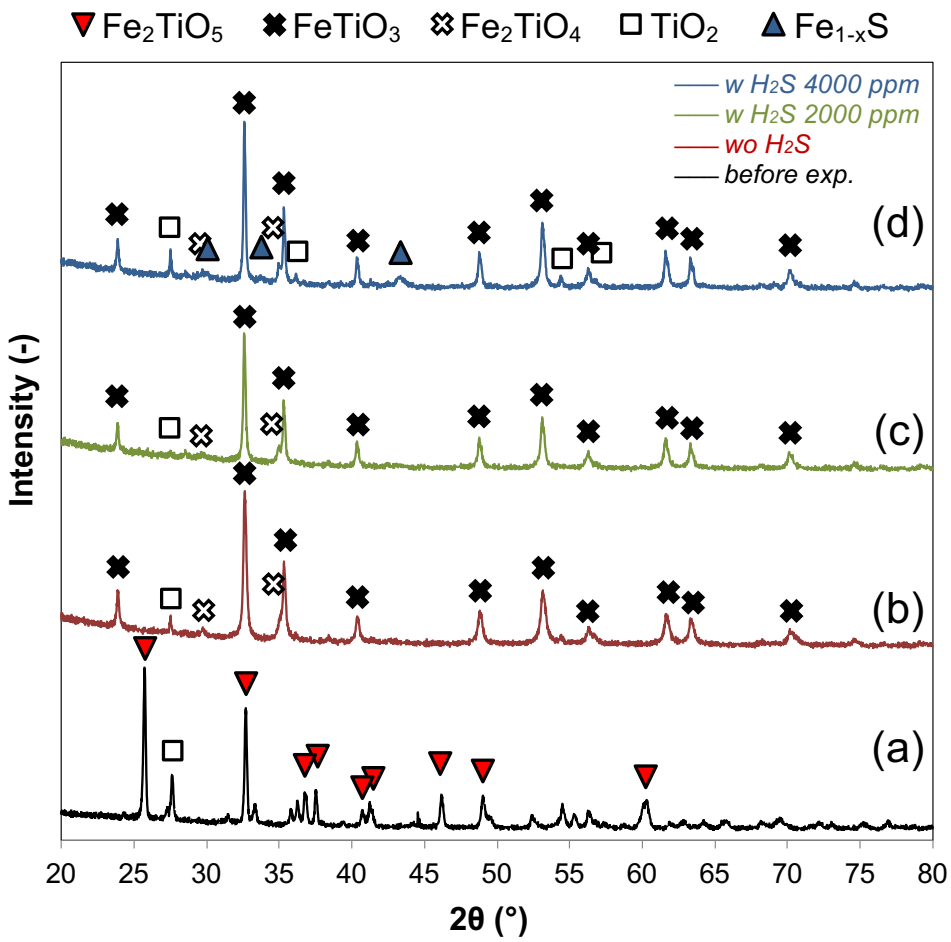

Figure 32. XRD profiles of the ilmenite particles after CLC steam reforming (S/C 0.5) of coal volatiles (a) before the experiment, (b) without H_2S, (c) with 2000 ppm H_2S, and (d) with 4000 ppm H_2S.

The XPS spectra of the S 2p binding energy of ilmenite particles used with various concentrations of H_2S are shown in Figure 33. For the ilmenite sample used in the presence 4000 ppm H_2S, the S 2p XPS spectra (Figure 33(c)) reveal three distinct peaks at 161.4, 162.6, and 168.8 eV; those peaks were also detected with very low intensities in samples used in the presence of 2000 ppm H_2S (Figure 33(b)). From comparison with the literature [14,22,23] and with references (see Appendix Figure A2), we determined that the binding energy values of 161.4 and 162.6 eV correspond, respectively, to the S $2p^{3/2}$ and S $2p^{1/2}$ of a monosulfide (FeS). The latter value also overlapped with the S $2p^{3/2}$ binding energy of a disulfide (FeS_2). This indicates that there was a mixture of FeS and FeS_2 present on the used ilmenite particles. The XPS results are consistent with the XRD results shown in Figure 32(d). The peak at 168.8 eV mainly resulted from the formation

of sulfate ($FeSO_4$), which could have been caused by oxidation. According to a study by de Diego *et al*. [13], the iron sulfide species $Fe_{0.84}S$ can be formed at low values of ϕ ($\phi < 1$). If the amount of carbon in the volatiles is taken into account, the value of ϕ in this study was approximately 0.4. Hence, iron sulfide was reasonably expected to form during our experiments.

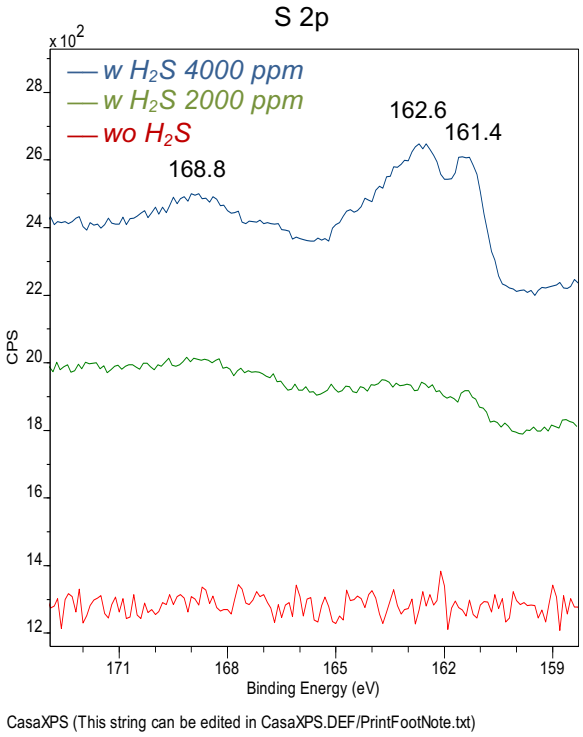

Figure 33. XPS spectra of the S 2p binding energy of the used ilmenite particles after CLC steam reforming (S/C 0.5) of coal volatiles (red) without H_2S, (green) with 2000 ppm H_2S, and (blue) with 4000 ppm H_2S.

All of the results discussed so far were obtained at the end of the CLC reforming experiments; they do not fully represent the sulfur fate during the experiment. In order to better understand the behavior of sulfur with ilmenite, samples of exhaust gas from the CLC reforming experiment were collected at intervals of 15 min, and the gas composition was analyzed. Figure 34 show the temporal changes in outlet gas composition over the elevated temperatures of coal pyrolysis during the steam reforming experiments. The data from the experiment conducted with sand shows that H_2 evaporated at approximately 823 K and 1123 K (Figure 34(a)). We consider the first peak of H_2 yield to be associated with the decomposition and reforming of the higher hydrocarbons, and the second one to be

due to the devolatilization of H_2 during carbonization of the coal. For other carbon volatile gases, such as CO, CH_4, CO_2, C_2H_4, and C_2H_6, volatilization mainly occurred at pyrolysis temperatures between 523 K and 1123 K. The higher hydrocarbons i.e., tar also releases at the temperature range between 523K and 823K, however, it is completely decomposed by ilmenite (Figure 30(a)). When only ilmenite was used in the experiment, volatiles were simultaneously oxidized by ilmenite, producing more CO_2. Figures 29(b) to (e) show that the combustion reactions of ilmenite with volatiles proceeded in the same temperature range, and that the CO_2 yield significantly increased with the declines in the other carbon gases.

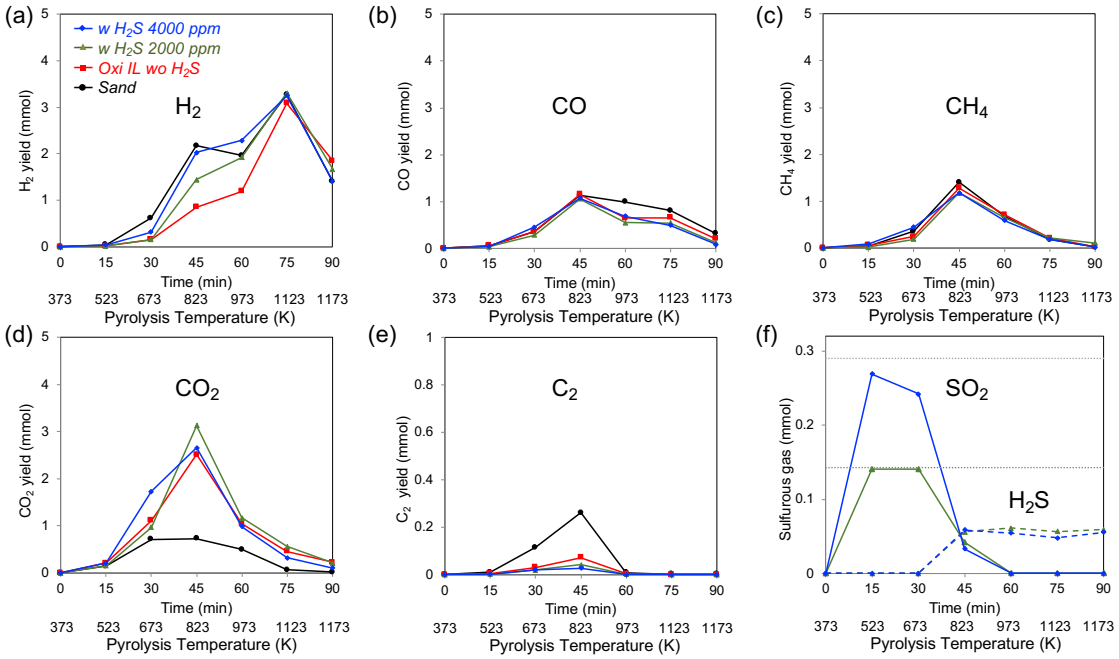

Figure 34. The temporal changes in outlet gas composition over the elevated temperatures of coal pyrolysis during the steam reforming of volatiles with ilmenite in the absence (red) and presence of 2000 ppm (green) and 4000 ppm H_2S (blue), compared to those of sand (black). (a) H_2, (b) CO, (c) CH_4, (d) CO_2, (e) C_2 carbon gases, and (f) sulfurous gases H_2S and SO_2.

On the other hand, the reaction behavior of sulfur in the presence of H_2S largely varied depending on the oxidizing condition of the ilmenite, as shown in Figure 34(f). First, at low pyrolysis temperatures up to 673 K (i.e., when no volatiles have been released), the introduced 2000 ppm and 4000 ppm H_2S were mostly combusted by ilmenite and converted to SO_2 (R28), as shown in Figure 34(f). Therefore, it seems that the direct sulfidation reaction of ilmenite by H_2S was negligible.

$3Fe_2TiO_5 + 3TiO_2 + H_2S \rightarrow 6FeTiO_3 + SO_2 + H_2O$ (R28)

Once the volatiles were released, the combustion reactions with ilmenite commenced; the CO_2 amount peaked at approximately 823 K, and sudden drops in the SO_2 yield were observed in the reforming experiments with both concentrations of H_2S (Figure 34(f)). Then, the SO_2 decreased further and eventually vanished, likely at the point when no further lattice oxygen was available from ilmenite. Although there was a small amount of residual H_2S, most of sulfur in the exhaust gas had disappeared. Those missing amounts of sulfur closely correlate with the amount of sulfur, estimated by sulfur balance (Figure 31), which was deposited on the ilmenite particles and in the reactor after the experiments with 2000 ppm and 4000 ppm H_2S. In addition, the majority of the sulfur deposits on the ilmenite were identified as iron sulfide by XRD and XPS analyses. Based on these results, we consider that sulfidation reactions took place on the reduced ilmenite particles after their initial reactions with the volatiles. In fact, a similar idea was presented from a TGA study with Ni, Cu, Fe, and Mn-based oxygen carriers by Tian *et al*. [14]. Others have also found that the reduction of Fe_2TiO_5 can occur in sequence, from $FeTiO_3$ to Fe, in a reducing environment [24]. Thus, the reduction and subsequent sulfidation reactions of ilmenite during the experiment can be expressed as follows:

$3Fe_2TiO_5 + 3TiO_2 + \text{Volatiles}(/H_2S) \rightarrow 6FeTiO_3 + CO_2 + H_2O$ (R29)

$3FeTiO_3 + \text{Volatiles}\ (/H_2S) \rightarrow 3Fe + 3TiO_2 + CO_2 + H_2O$ (R30)

$FeTiO_3 + H_2S \rightarrow FeS + TiO_2 + H_2O$ (R31)

$Fe + H_2S \rightarrow FeS + H_2$ (R32)

On the other hand, H_2 yield increased along with the increase in H_2S concentration at coal pyrolysis temperatures between 673 K and 1123 K, as shown in Figure 34(a). In other words, H_2S lowered the consumption of H_2 for reaction R20 with ilmenite. Figure 34(f) shows that ilmenite was reduced by H_2S up to a temperature of 673 K; then it was used threefold in the molar amount of SO_2, in accordance with reaction R28. This means that the reaction between H_2 and ilmenite could have decreased to the same extent. Another reason for the gain in H_2 could be soot gasification R14, and the WGS reaction R15. As discussed earlier in Figure 30(c), amounts of soot and CO over ilmenite decreased with H_2S addition, while the amount of CO_2 increased. Especially, the CO conversion to CO_2 was more encouraged with 2000 ppm of H_2S. Figure 34(b) also reveals

that CO_2 significantly increased up to 823K and then had decreasing trend. However, CO_2 was higher and moreover, CO decreased slightly more with 2000 ppm of H_2S after 823K, comparing with that case of ilmenite without H_2S. The rise in H_2 might be attributed to all of the above reactions.

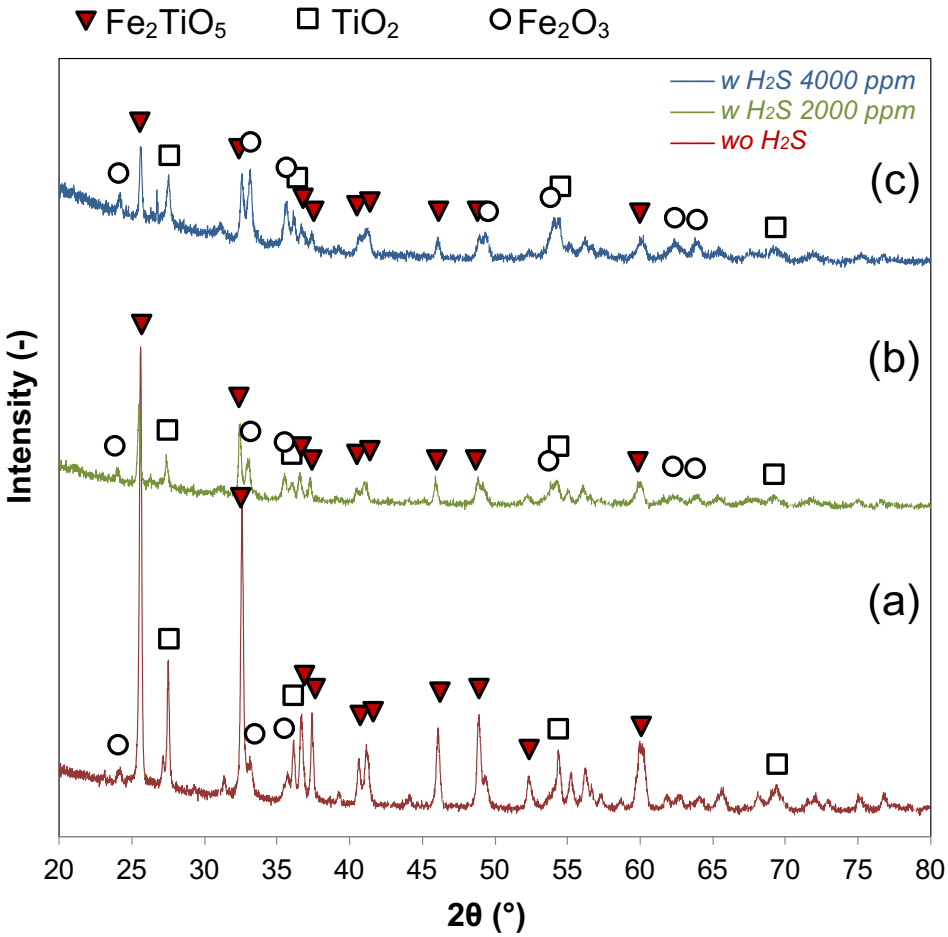

Figure 35. XRD profiles of the re-oxidized ilmenite particles after steam reforming (S/C 0.5) of coal volatiles (a) without H_2S, (b) with 2000 ppm H_2S, and (c) with 4000 ppm of H_2S.

Another explanation for the increase in H_2 could be the formation of more active iron species, such as Fe and FeO, by H_2S addition. It has been reported that the segregation of Fe from TiO_2 occurs on ilmenite particles during activation [25]. If the deeply reduced iron species Fe or FeO were partially moved from the bulk structure of ilmenite by further reduction of H_2S, then re-oxidation reactions by steam could occur instantaneously, generating H_2 [1, 26–28]. This is believed to be due to the fact that the

chemical phases of Fe and FeO are more reactive towards H_2O than the reduced $FeTiO_3$ phase of ilmenite [10]. The resulting re-oxidized iron species, i.e. the lattice oxygen might react again with volatiles or promote the gasification R14 and WGS reaction R15, enhancing CO_2 conversion. Probably, it would be much more plausible explanation for the increased amount of H_2 and CO_2 over ilmenite by the effect of H_2S. Furthermore, as shown in Figure 35, the XRD characterization of the further re-oxidized ilmenite particles after the reforming experiments in the presence of H_2S revealed a crystalline phase of Fe_2O_3 (other than Fe_2TiO_5) that had partially formed on the surface of the ilmenite particles. This implies that H_2S may induce the migration of iron species onto the surface of ilmenite.

Notably, some electrochemical studies show that iron sulfides in situ create a high active site of Fe-FeO_xS_y on their particles, which thermodynamically catalyzes the a water splitting reaction and generates H_2 [29]. Additionally, FeS_2 particles loaded on a TiO_2 catalyst enhance the water splitting reaction, because the heterostructure between TiO_2 and FeS_2 enables fast electron transfers. Although these electrochemical studies were conducted under completely different conditions than our study, the findings seem to relate to our experimental results.

3.3.2 Effect of H_2S on the redox reactivity of ilmenite

The effect of H_2S on the redox reactivity of ilmenite was evaluated by eight-cycle redox tests in TGA with 5% H_2 and air at 1173 K. The eight-cycle TGA profiles of ilmenite in the absence and presence of H_2S are shown in Figure 36. A weight value of 0% corresponds to the ilmenite sample in its most oxidized state, Fe_2TiO_5. The maximum theoretical weight loss values from Fe^{III}, to Fe^{II}, to Fe^0 are approximately 4.9 wt% and 14.7 wt%, respectively. Moreover, if a direct sulfidation reaction from Fe_2TiO_5 to FeS is possible, the maximum theoretical weight gain value must be approximately 4.9 wt%.

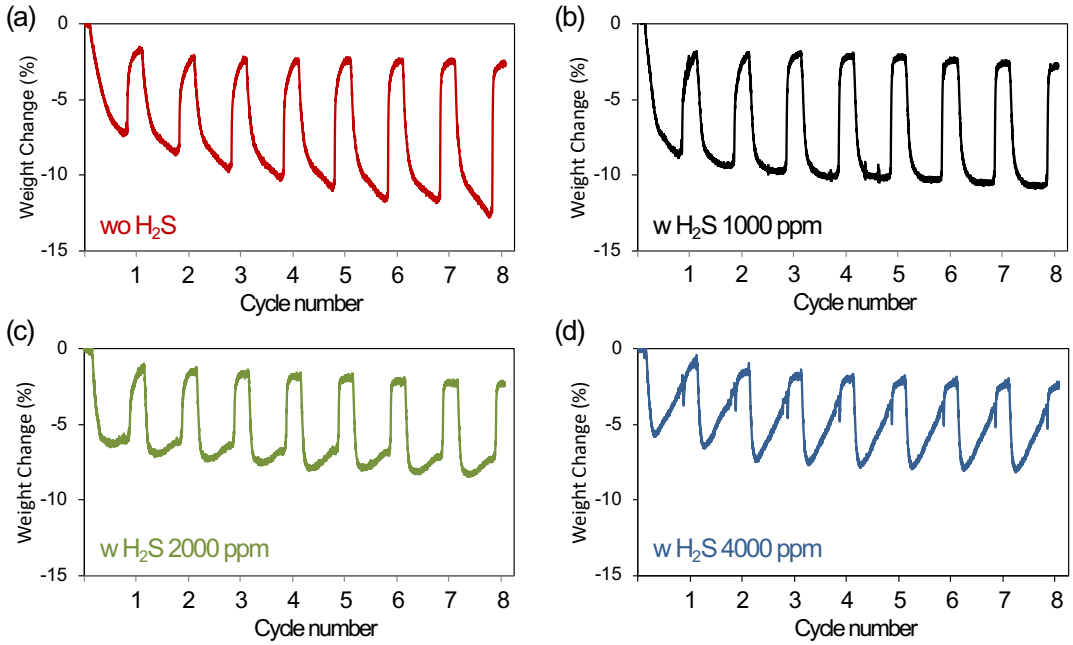

Figure 36. TGA profiles for eight redox cycles of ilmenite by 5% H_2 and air at 1173 K (a) without H_2S, (b) with 1000 ppm H_2S, (c) with 2000 ppm H_2S, and (d) with 4000 ppm of H_2S.

Ilmenite showed a weight loss of approximately 7.6 wt% from the first reduction with 5% H_2, but its performance increased with the number of cycles. This redox activation behavior of ilmenite was also observed in our previous study [10], and is reportedly due to the development of granulation and porosity in the ilmenite particles [16] [25]. In the presence of H_2S, similar activation performances were observed in the first 3 cycles, then the performance became relatively stable. Overall, compared to the reductions with only H_2, the total combustion reactivity of ilmenite greatly declined with the addition of 2000 ppm and 4000 ppm H_2S; and weight gain was even observed during the reduction period. However, the results were different with 1000 ppm H_2S.

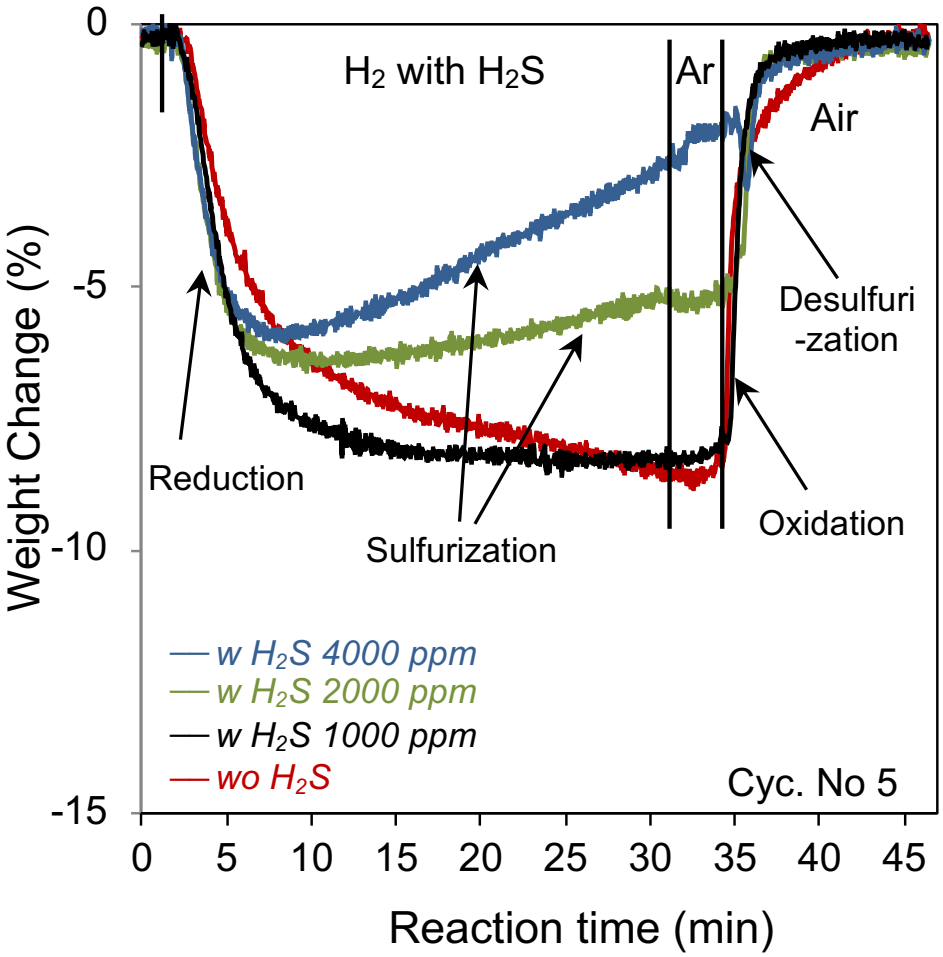

Figure 37. The 5th cycle TGA curves of ilmenite in 5% H_2 and air at 1173 K without H_2S (red), with 1000 ppm H_2S (black), with 2000 ppm H_2S (green), and with 4000 ppm H_2S (blue).

To evaluate the effect of H_2S on the performance of ilmenite, the TGA profiles of the fifth cycles with and without H_2S were compared; they are shown overlapped in Figure 37. No increases in weight at the initial time of reduction were observed in the TGA curves in any of the H_2S cases. Considering the sulfur gas result shown earlier in Figure 34(f), as well as the current results, the direct sulfidation of oxidized ilmenite by H_2S is unlikely to happen. In addition, it seems that initial reduction of Fe_2TiO_5 to $FeTiO_3$ occurred much faster with H_2S than that without H_2S. It took nearly 6.2 min to reach a reduction to $FeTiO_3$ (-4.9 wt%) in the absence of H_2S; whereas it only required approximately 4.8 min, 4.5 min and 4.7 min for 1000 ppm, 2000 ppm, and 4000 ppm of H_2S, respectively. This implies that initial reaction rate of ilmenite increases with the addition of H_2S. Moreover, the lowest amount of H_2S (1000 ppm) encouraged the further

reaction of ilmenite with H_2. As shown in Figure 37, the total reduction of ilmenite (up to 8.3 wt% of weight loss) proceeded twice as fast in the presence of 1000 ppm of H_2S than without H_2S. This finding shows that a small amount of H_2S impurity can greatly improve the reactivity of ilmenite.

On the other hand, a negative impact of H_2S was observed at 2000 ppm and 4000 ppm; in those cases, the total combustion capacity of ilmenite significantly declined because even though the initial weight loss was accelerated, some weight gain reaction took place during the reducing period. If we assume that the final weight loss point of ilmenite without H_2S was 100% (-8.7 wt% by the red curve in Figure 37), then the percentages in the cases with H_2S must be calculated in a similar way. Consequently, the combustion capacity of ilmenite greatly declined to 76% in 2000 ppm H_2S, to 70% in 4000 ppm H_2S, and only slightly to 98% in 1000 ppm H_2S. After those points, ilmenite experienced a weight gain in the cases of 2000 ppm and 4000 ppm of H_2S. The higher the concentration of H_2S introduced, the more weight gain we observed, as shown by the green and blue curves in Figure 37. The weight gain is considered to occur due to sulfidation reactions R31 and R32. As discussed in the previous section, ilmenite was initially reduced; then the sulfidation reactions took place simultaneously with reduction on the reduced ilmenite particles and finally dominated over reduction. That resulted in weight gain with the increased amount of H_2S. Notably, the weight gain appeared to start from a region of reduction to Fe^0 for the both H_2S cases. It can be inferred that the sulfidation reaction of ilmenite may take place more through the reduced metallic iron, Fe^0, (R32) than through $FeTiO_3$ (R31).

Samples at the end of reduction after 5 redox cycles with and without H_2S addition were subjected to XRD analysis. Figure 38(a) shows that the ilmenite particles had been reduced to $FeTiO_3$ and Fe phases after the fifth reduction. The formation of a metallic iron of Fe^0 was possible via the reduction of ilmenite. As confirmed by the previous reforming experiments, the iron sulfide pyrrhotite ($Fe_{1-x}S$) was also found on the surface of the ilmenite particles in the presence of H_2S (Figures 33(b)-(d)). Even more interesting, the relative intensities of the peaks corresponding to the $Fe_{1-x}S$ phase increased with the increase in H_2S concentration, while the intensities of the peaks corresponding to Fe^0 decreased. This result strongly supports the idea that the sulfidation of ilmenite goes through Fe^0 formation.

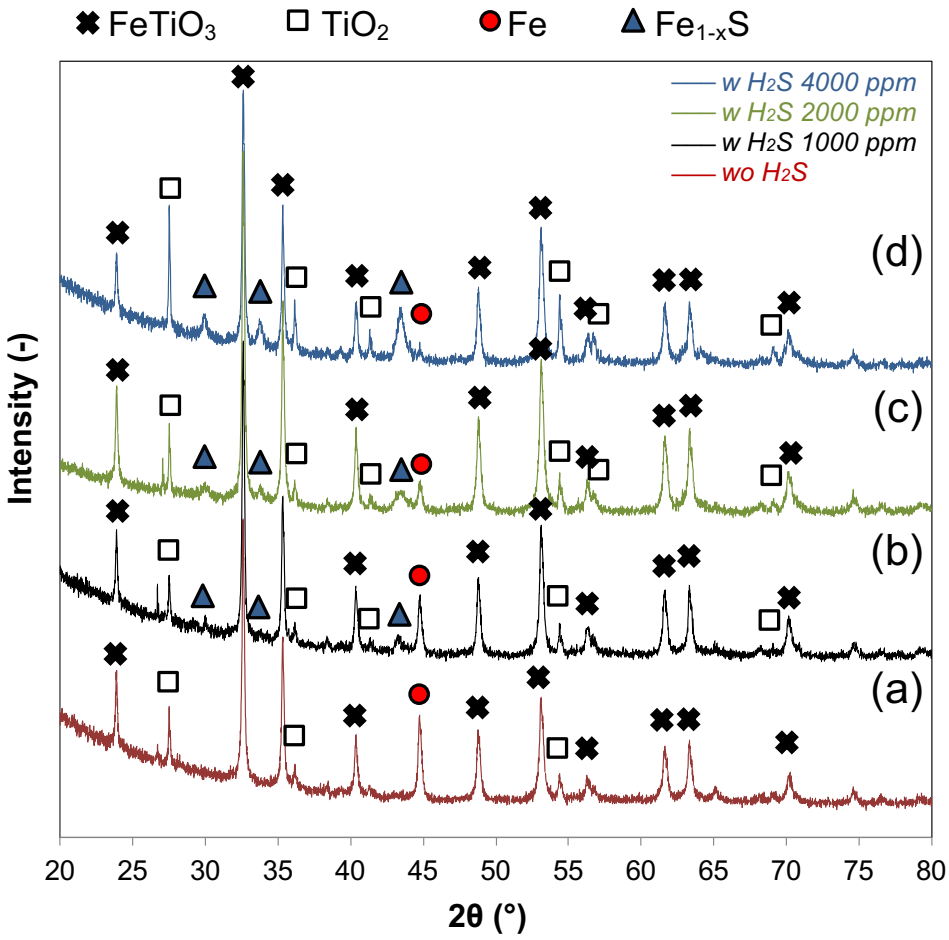

Figure 38. XRD patterns of the used ilmenite particles after reduction by 5% H_2 (a) without H_2S, (b) with 1000 ppm H_2S, (c) with 2000 ppm H_2S, and (d) with 4000 ppm H_2S.

XPS spectra of S 2p on the used ilmenite were also presented in Figure 39. As presented in the previous section, the peaks of S 2p centered at 161.3, 162.5 and 168.5 eV were also obtained more apparently on the ilmenite particles reduced by H_2 with H_2S. Their intensities have also increased with the higher H_2S. A similar comparison with the literature and references was conducted. Similar to the results discussed in the previous section, the presence of sulfur iron species such as FeS, FeS_2 and $FeSO_4$ was confirmed on the ilmenite particles used with H_2 and H_2S.

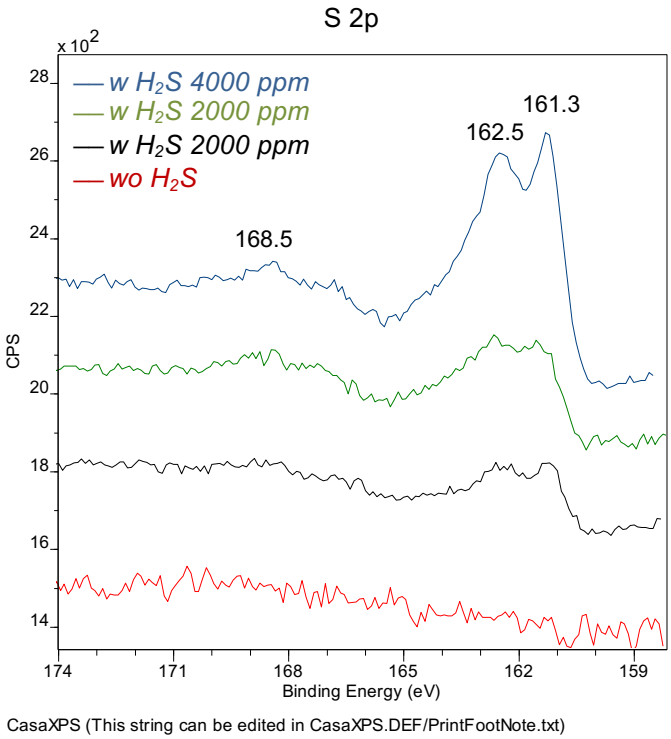

Figure 39. XPS patterns of the used ilmenite particles after reduction by 5% H_2 (a) without H_2S, (b) with 1000 ppm H_2S, (c) with 2000 ppm H_2S, and (d) with 4000 ppm H_2S.

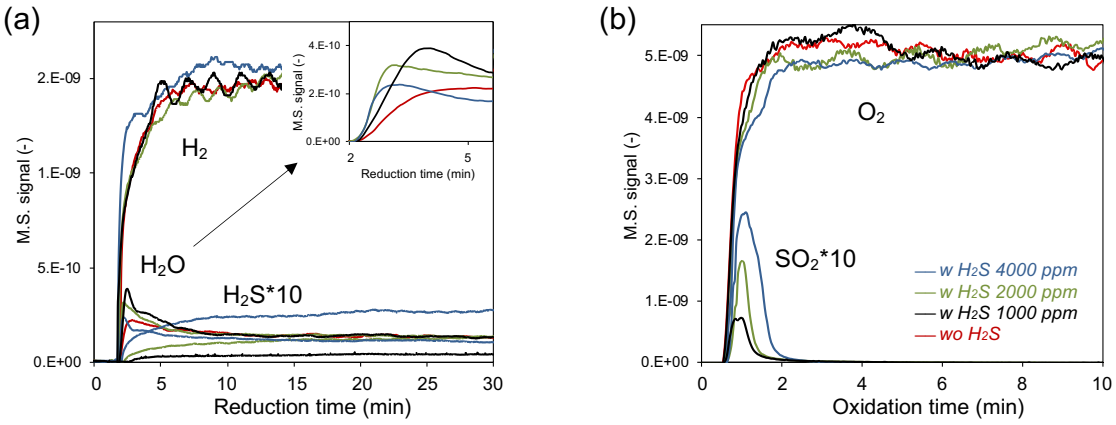

Figure 40. Mass profiles for the 5th cycles of ilmenite in 5% H_2 and air at 1173 K in the absence (red) and the presence of 1000 ppm (black), 2000 ppm (green), and 4000 ppm (blue) of H_2S for (a) H_2, H_2S and H_2O in the reducing period, and (b) SO_2 and O_2 in the oxidizing period.

MS data of the product gases from the 5th cycle tests were obtained for the evaluation of H_2S effect and are shown in Figure 40. During the reducing period, the MS signal of H_2O represents an initially rapid increase, forming a small peak and then becoming stable in the presence of H_2S and H_2 over ilmenite. This result revealed that the H_2S promoted the initially fast reduction of ilmenite (R33 and R34).

$$Fe_2TiO_5 + TiO_2 + H_2(/H_2S) \rightarrow 2FeTiO_3 + H_2O \quad (R33)$$

$$FeTiO_3 + H_2(/H_2S) \rightarrow Fe + TiO_2 + H_2O \quad (R34)$$

During the oxidation period, SO_2 peaks were detected for all samples with H_2S, as shown in Figure 40(b). The higher the concentration of H_2S introduced to the reduction, the larger the SO_2 peak area detected upon the next oxidation of ilmenite. This result demonstrates that the desulfurization reaction took place in correlation to the amount of H_2S used in the previous reduction. Moreover, in the case of 4000 ppm H_2S, there was a sharp weight loss at the beginning of oxidation, then the weight increased due to oxidation with air (blue curve in Figure 37). This weight loss, in conjunction with the MS results shown in Figure 40(b), is considered to be due to the release SO_2 from the iron sulfide species on the ilmenite (R35). However, this phenomenon was not observed in the cases of 2000 ppm and 1000 ppm H_2S; that might be because oxidation R36 and desulfurization R35 took place simultaneously, so that a minor weight loss from the release of SO_2 was masked by a weight gain from oxidation for in those cases. In addition, as shown in Figure 37, the reduced and sulfurized ilmenite finally regained its original weight through oxidation in all of the H_2S cases, indicating that the ilmenite particles finally recovered their oxygen carrier reactivity via sulfur removal and oxidation.

$$2FeS + 7/2O_2 \rightarrow Fe_2O_3 + 2SO_2 \quad (R35)$$

$$2FeTiO_3 + 1/2O_2 \rightarrow Fe_2TiO_5 + TiO_2 \quad (R36)$$

Although the reducing gases used in the TGA tests of ilmenite were only H_2 and H_2S, with no steam was involved, we obtained similar findings with reforming experiments. One important finding is that the combustion reactivity of ilmenite was activated by a small addition of H_2S. We observed that using fuel that contains a small amount of sulfur gas caused no significant damage to the combustion reactivity of ilmenite. Instead, the reactivity was greatly improved with a minor amount of added

sulfur. This activation behavior of ilmenite in the presence of H_2S has also been experimentally confirmed by others [19, 20]. Their thermodynamic calculations suggest that the TiO_2 present in ilmenite may have an inhibiting effect on iron sulfidation. Furthermore, based on our TGA results, the reduction capacity of ilmenite from Fe^{III} to Fe^{II} appears to be unaffected, or even promoted, by the presence of H_2S. This is similar to the thermodynamic results of Jerndal *et al*. [11], which implied that the Fe_2O_3/Fe_3O_4 oxygen carrier forms no sulfur compounds under any concentration of sulfurous gas at high temperature.

In addition, we confirmed that the sulfide species $Fe_{1-x}S$ can be created after formation of the further reduced iron species on ilmenite under an extra reducing atmosphere of H_2. If a further reduction to Fe^0 proceeds on ilmenite, sulfidation by H_2S can occur, resulting in the deterioration of the total combustion reactivity of ilmenite. Hence, it is concluded that controlling the reduction level of ilmenite during the CLC process is essential to preventing sulfur deposition and the reactivity loss of ilmenite. Values of the oxygen carrier to fuel ratios in the reforming and TGA experiments were extremely low, so the oxygen availability of ilmenite was not enough to prevent deep reduction and sulfidation. However, in real coal CLC processes, the ratio of oxygen carrier to coal is expected to be much larger than those of this study, allowing the prevention of further reduction and sulfidation.

3.3.3 Effect of H_2S on the combustion reactivity of Fe_2O_3/Al_2O_3 over steam reforming of coal volatiles

The same reforming experiments of coal volatiles using Fe_2O_3/Al_2O_3 were also carried out in the presence of 2000 and 4000 ppm H_2S. Figures 41 show the total carbon balance, exhaust gas yield and the differences in the data between Fe_2O_3/Al_2O_3 tested with and without H_2S. Data with sand are presented as a reference.

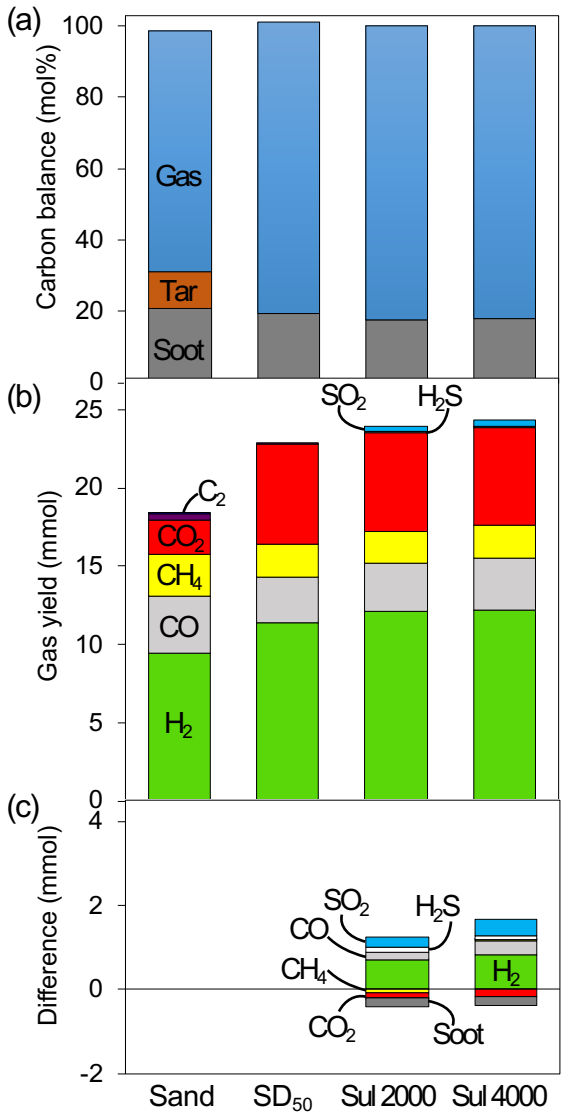

Figure 41. (a) Carbon balance and (b) exhaust gas yield obtained by the steam reforming (S/C 0.5) of coal volatiles over sand and Fe_2O_3/Al_2O_3 in the absence and the presence of 2000 ppm and 4000 ppm H_2S. (c) Comparison of the volatiles over Fe_2O_3/Al_2O_3 with and without H_2S.

When using synthetic oxygen carrier Fe_2O_3/Al_2O_3 for reforming experiments, the combustion reactions of the volatiles are promoted via reactions R37 through R41; that results in a substantial increase in CO_2 and a decline in other volatiles such as H_2, CO, CH_4, and the higher hydrocarbons (including tars) in Fe_2O_3/Al_2O_3. Furthermore, as discussed in the previous chapter, re-oxidation with steam in situ takes place in the reduced $FeAl_2O_4$ to increase the H_2 content (R42).

$Fe_2O_3/Al_2O_3 + H_2 \rightarrow 2FeAl_2O_4 + H_2O$ (R37)

$Fe_2O_3/Al_2O_3 + CO \rightarrow 2FeAl_2O_4 + CO_2$ (R38)

$4Fe_2O_3/Al_2O_3 + CH_4 \rightarrow 8FeAl_2O_4 + CO_2 + 2H_2O$ (R39)

$6Fe_2O_3/Al_2O_3 + C_2H_4 \rightarrow 12FeAl_2O_4 + 2CO_2 + 2H_2O$ (R40)

$(2m+n/2)Fe_2O_3/Al_2O_3 + C_mH_n \rightarrow (4m+n)FeAl_2O_4 + mCO_2 + n/2H_2O$ (R41)

$3FeAl_2O_4 + H_2O \rightarrow Fe_3O_4/3Al_2O_3 + H_2$ (R42)

Similar to our previous section 3.3.1, the amount of lattice oxygen in Fe_2O_3/Al_2O_3 utilized for combustion was semi-quantitatively calculated, based on the molar amounts of CO_2 and H_2 different from those of sand. Approximately 60% of theoretical amount of lattice oxygen in Fe_2O_3/Al_2O_3 was utilized for volatiles' combustion in the absence of H_2S.

The differences in the data between Fe_2O_3/Al_2O_3 tested with and without H_2S were used to evaluate the influence of sulfur gas on the combustion reactivity of Fe_2O_3/Al_2O_3. Figure 41(c) reveals that when 2000 and 4000 ppm H_2S were introduced to the volatiles, the carbon conversion to CO_2 slightly declined, meaning that the combustion reactivity of Fe_2O_3/Al_2O_3 diminished. It also shows that in the presence of H_2S, yields of other carbon fractions such CH_4, higher hydrocarbon gases and soot decreased, but CO and H_2 increased. No tar was formed with either 2000 or 4000 ppm H_2S. If only the decrease in CO_2 were considered, the oxygen consumption of Fe_2O_3/Al_2O_3 would decline to around 58% with 2000 ppm H_2S, and to around 57% with 4000 ppm H_2S. These results suggest that the combustion reactivity of Fe_2O_3/Al_2O_3 is somehow deactivated by H_2S, which was opposite compared to the ilmenite. As shown in Figure 30, the combustion reactivity of ilmenite was activated in the same condition.

We also observed some amount of H_2 increase with Fe_2O_3/Al_2O_3, however it did not seem to be in direct correlation with an increase in H_2S concentration. The H_2 gain might be attributed soot gasification R14. Because soot decrease accompanied with CO increase was observed in the sulfur cases of Figure 41(c). However, the subsequent WGS reaction R15 might not proceed during the volatiles' steam reforming experiments with Fe_2O_3/Al_2O_3 and H_2S. The WGS reaction is generally not thermodynamically promoted at high temperatures, unless there is lattice oxygen more available from oxygen carrier [9].

Figure 42 shows the sulfur balance during the steam reforming experiments of coal volatiles over Fe_2O_3/Al_2O_3 in the presence of 2000 ppm and 4000 ppm of H_2S. The H_2S introduced during the experiments could be released as SO_2, H_2S, and COS in the

outlet gas. COS was only present in a small amount (<5ppm) of the outlet gas; When 2000 ppm of H_2S were used, approximately 30% of the total sulfur was converted into SO_2 over Fe_2O_3/Al_2O_3; when 4000 ppm were used, the amount converted declined to 23%. On the other hand, the sulfur deposited on the Fe_2O_3/Al_2O_3 particles after the experiment were approximately 35% in 2000 ppm and 51% in 4000 ppm of H_2S, respectively. The sulfur deposition on Fe_2O_3/Al_2O_3 sharply increased with increasing the amount of H_2S. In addition, these sulfur deposits on Fe_2O_3/Al_2O_3 are apparently very high, compared to those on ilmenite particles shown in Figure 31. Hence, this increased accumulation of sulfur on Fe_2O_3/Al_2O_3 might lead to deactivation, which degraded the combustion reactivity of Fe_2O_3/Al_2O_3 in the presence of H_2S (Figure 41(c)). The remaining amount of sulfur corresponded to the residual H_2S in the exhaust gas and in the sulfur deposits in the reactor. The total sulfur balances, including the converted and deposited sulfurous fractions, were over 90% for Fe_2O_3/Al_2O_3; the remainder might correspond to those sulfurs condensed in the water or on the reactor parts, such as the connectors and tubes, which were not measured.

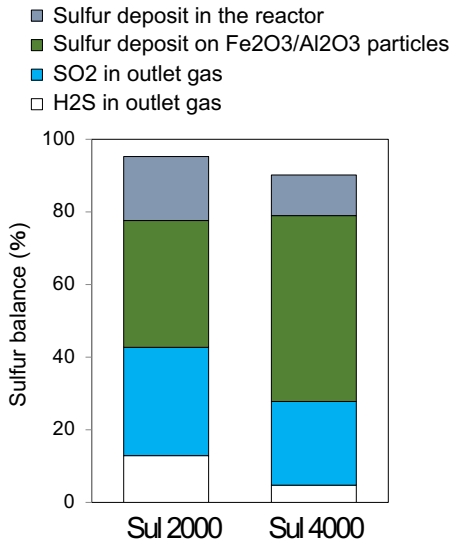

Figure 42. Sulfur balance obtained from steam reforming experiments of coal volatiles over Fe_2O_3/Al_2O_3 in the presence of 2000 ppm and 4000 ppm H_2S.

XRD and XPS analyses were also performed on the used Fe_2O_3/Al_2O_3 particles in order to determine the crystal structures and chemical states of the sulfur deposits on the Fe_2O_3/Al_2O_3 particles. Figure 43 shows XRD profiles of the used Fe_2O_3/Al_2O_3

particles after reforming experiments of volatiles with S/C 0.5, with and without H_2S. As shown in Figure 43(b), in the absence of H_2S the Fe_2O_3/Al_2O_3 particles were reduced by volatiles into $FeAl_2O_4$ and FeO. A small shoulder peak of Fe_3O_4 represented that some amount of $FeAl_2O_4$ or FeO was in situ re-oxidized by steam. In the presence of H_2S, Fe_2O_3/Al_2O_3 particles were also mainly reduced to $FeAl_2O_4$, but pyrrhotite, an iron sulfide phase ($Fe_{1-x}S$), was also detected in 4000 ppm H_2S, as shown in Figure 43(d), revealing the chemical states of sulfur depositions on the Fe_2O_3/Al_2O_3. In the case of 2000 ppm H_2S, this sulfur phase was not confirmed (Figure 43(c)), due to low crystallinity of the sulfur phase or to the detection limit of the XRD apparatus.

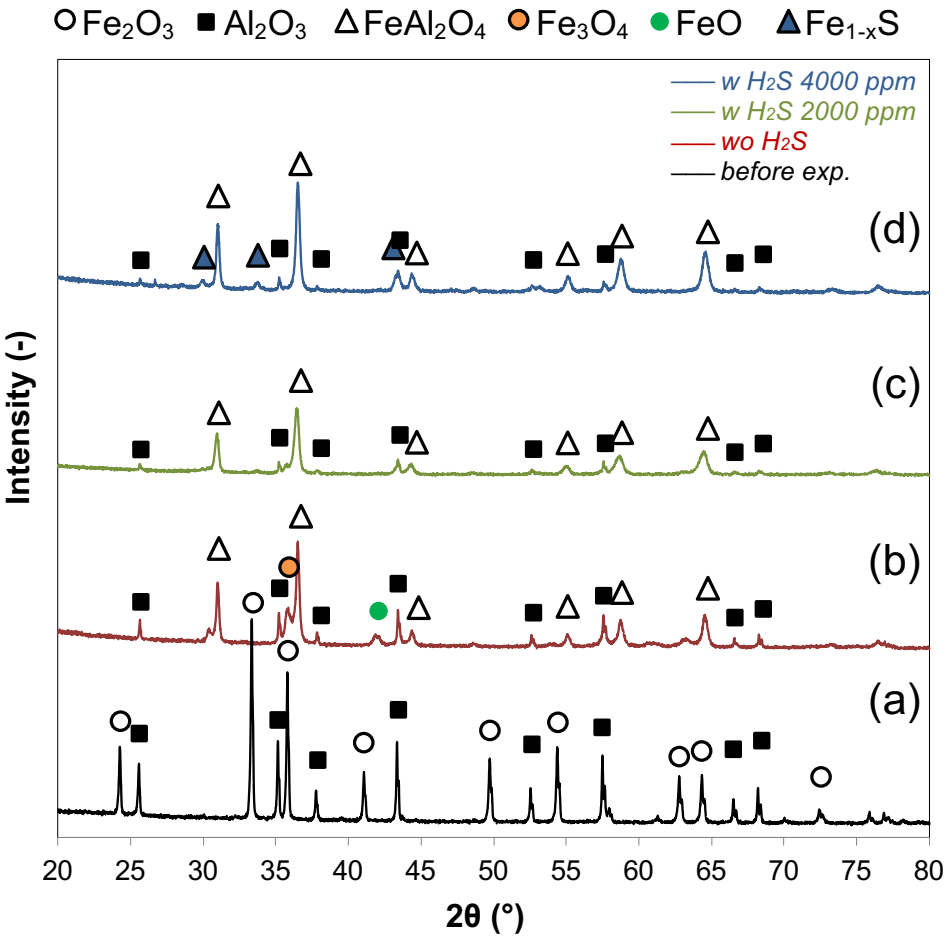

Figure 43. XRD profiles of the Fe_2O_3/Al_2O_3 particles after CLC steam reforming (S/C 0.5) of coal volatiles (a) before the experiment, (b) without H_2S, (c) with 2000 ppm H_2S, and (d) with 4000 ppm H_2S.

The XPS spectra of the S 2p binding energy of Fe_2O_3/Al_2O_3 particles used with various concentrations of H_2S are shown in Figure 44. For the Fe_2O_3/Al_2O_3 particles used with the presence of H_2S, three distinct peaks appeared at 161.3, 162.5, and 168.8 eV in the S 2p XPS spectra. Similar to previous sections, from comparison with the literature [14,22,23] and with references (see Appendix Figure A2), the presence of FeS, FeS_2 and $FeSO_4$ were determined on the used Fe_2O_3/Al_2O_3 particles. It is consistent with the XRD results shown in Figure 43(d). The iron sulfide species $Fe_{0.84}S$ can be formed at low values of ϕ ($\phi < 1$). The value of ϕ was approximately 0.4 in this study, and so it is reasonable to form iron sulfides.

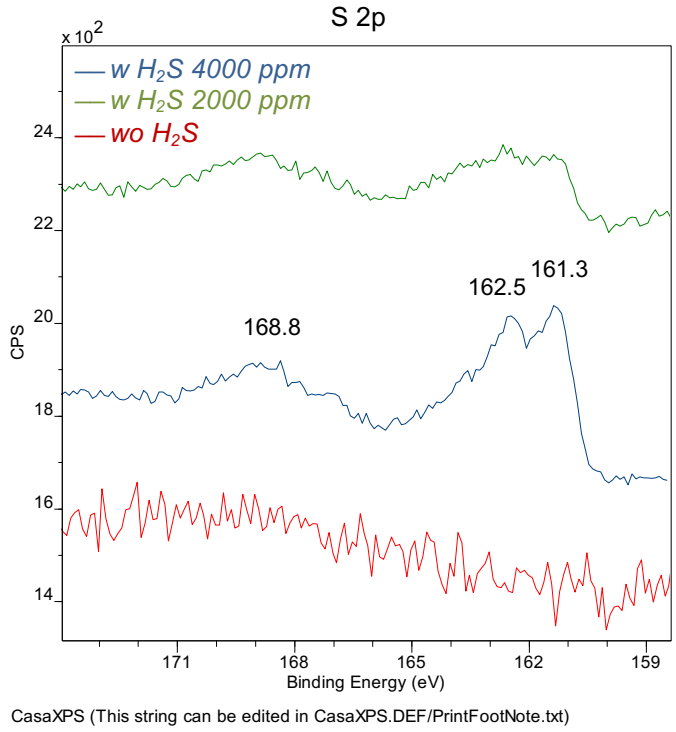

Figure 44. XPS spectra of the S 2p binding energy of the used Fe_2O_3/Al_2O_3 particles after steam reforming (S/C 0.5) of coal volatiles (red) without H_2S, (green) with 2000 ppm H_2S, and (blue) with 4000 ppm H_2S.

In order to better understand the behavior of sulfur with Fe_2O_3/Al_2O_3, samples of exhaust gas from the CLC reforming experiment were collected at intervals of 15 min, and the gas composition was analyzed. Figure 45 show the temporal changes in outlet gas composition over the elevated temperatures of coal pyrolysis during the steam reforming experiments over Fe_2O_3/Al_2O_3 with and without H_2S. Figures 40 show that

when Fe_2O_3/Al_2O_3 was used for reforming experiments, the combustion reactions of volatiles, and re-oxidation of Fe_2O_3/Al_2O_3 proceeded in the same temperature ranges with coal devolatilization. The CO_2 and H_2 yields significantly increased at 823K. However, when H_2S was introduced, it was observed that the carbon conversion to CO_2 declined whereas H_2 and CO rose by the effect of H_2S.

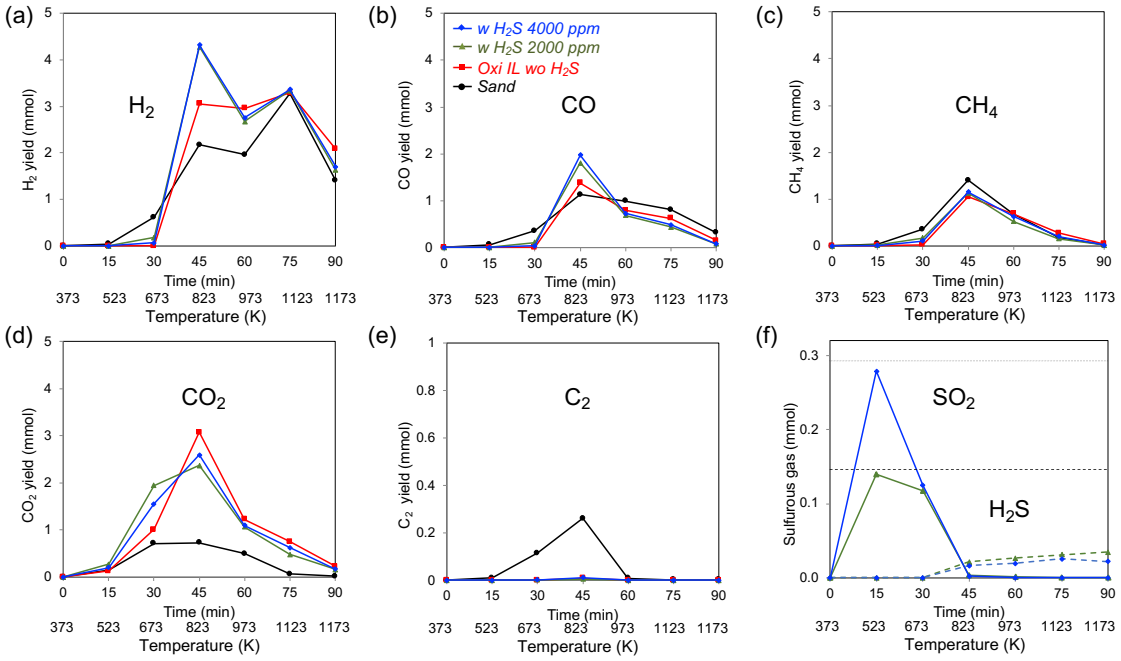

Figure 45. The temporal changes in outlet gas composition over the elevated temperatures of coal pyrolysis during the steam reforming of volatiles with Fe_2O_3/Al_2O_3 in the absence and presence of 2000 ppm and 4000 ppm H_2S, compared to those of sand. (a) H_2, (b) CO, (c) CH_4, (d) CO_2, (e) C_2 carbon gases, and (f) sulfurous gases H_2S and SO_2.

As discussed in the section 3.3.1, behavior of sulfur gas largely depends on the oxidizing condition of the Fe_2O_3/Al_2O_3, shown in Figure 45(f). First, when almost no volatiles have been released, the introduced H_2S were mostly oxidized to SO_2 (R43).

$$3Fe_2O_3/Al_2O_3 + H_2S \rightarrow 6FeAl_2O_4 + SO_2 + H_2O \quad \text{(R43)}$$

Once the volatiles were released, SO_2 yield suddenly dropped with beginning of the combustion reactions of volatiles with Fe_2O_3/Al_2O_3 and eventually disappeared, likely at the point when no further lattice oxygen was available from Fe_2O_3/Al_2O_3. Although there

was a small amount of residual H_2S, most of sulfur in the exhaust gas had disappeared after 823K. Those missing amounts of sulfur mostly correlate with the amount of sulfur deposited on the Fe_2O_3/Al_2O_3 particles (Figure 42), and moreover, the majority of them were identified as iron sulfides by XRD and XPS analyses. As a result, it can be considered that sulfidation of Fe_2O_3/Al_2O_3 took place on the reduced iron particles via reactions with the volatiles. Assuming that the reduction of Fe_2O_3/Al_2O_3 proceed to Fe, the sulfidation reactions would proceed as follows:

$$3Fe_2O_3/Al_2O_3 + \text{Volatiles}(/H_2S) \rightarrow 6FeAl_2O_4 + CO_2 + H_2O \quad \text{(R44)}$$

$$3FeAl_2O_4 + \text{Volatiles}\ (/H_2S) \rightarrow 3Fe + 3Al_2O_3 + CO_2 + H_2O \quad \text{(R45)}$$

$$FeAl_2O_4 + H_2S \rightarrow FeS + Al_2O_3 + H_2O \quad \text{(R46)}$$

$$Fe + H_2S \rightarrow FeS + H_2 \quad \text{(R47)}$$

On the other hand, H_2S lowered the lattice oxygen utilization of Fe_2O_3/Al_2O_3 for volatiles. The increased amount of H_2 by 2000 ppm of H_2S addition was almost the same to the expected amount by reactions R37 and R43. In case of 4000 ppm of H_2S, it was relatively less than expected. This may be due to that the reaction R42 is also negatively affected by higher amount of H_2S. Furthermore, CO amount rose by the effect of H_2S at temperatures between 673K and 973K (Figure 45 (b)), which was mostly associated with the decomposition of the higher hydrocarbons and the subsequent carbon (soot) gasification. As mentioned before, the WGS reaction R15 from CO to CO_2 is not favorable at higher temperature without the lattice oxygen from oxygen carrier. As seen in Figure 45(d), the conversion for CO_2 declined in either case of H_2S, compared to that without H_2S. That is to say that lattice oxygen from Fe_2O_3/Al_2O_3 was not available at this point for a promotion of WGS reaction. The main reason for the deactivation of Fe_2O_3/Al_2O_3 was formation of sulfides, which easily occurred on the reduced iron particles of Fe_2O_3/Al_2O_3 by H_2S and prevented the reactions with volatiles.

Compared to Fe_2O_3/Al_2O_3, it was an opposite tendency in the ilmenite. the combustion reactivity of ilmenite with volatiles was positively affected during the steam reforming experiments with H_2S. We discussed in the previous section 2.3.1 that when lattice oxygen released from the external Fe phases of ilmenite particles, Ti migrates towards the external part to prevent the oxygen release. Based on this phenomenon, it is presumed that such externally migrated Ti phase may inhibit sulfidation reaction on ilmenite particles.

3.3.4 Effect of H_2S on the redox reactivity of Fe_2O_3/Al_2O_3

The effect of H_2S on the redox reactivity of synthetic Fe_2O_3/Al_2O_3 was also evaluated by eight-cycle redox tests in TGA with 5% H_2 and air at 1173 K. The eight-cycle TGA profiles of Fe_2O_3/Al_2O_3 in the absence and presence of H_2S are shown in Figure 46. A weight value of 0% corresponds to the most oxidized state, Fe_2O_3/Al_2O_3. The maximum theoretical weight loss values from Fe^{III}, to Fe^{II}, to Fe^0 are approximately 5 wt% and 15 wt%, respectively. Moreover, if a direct sulfidation reaction from Fe_2O_3 to FeS is possible, the maximum theoretical weight gain value must be approximately 5 wt%.

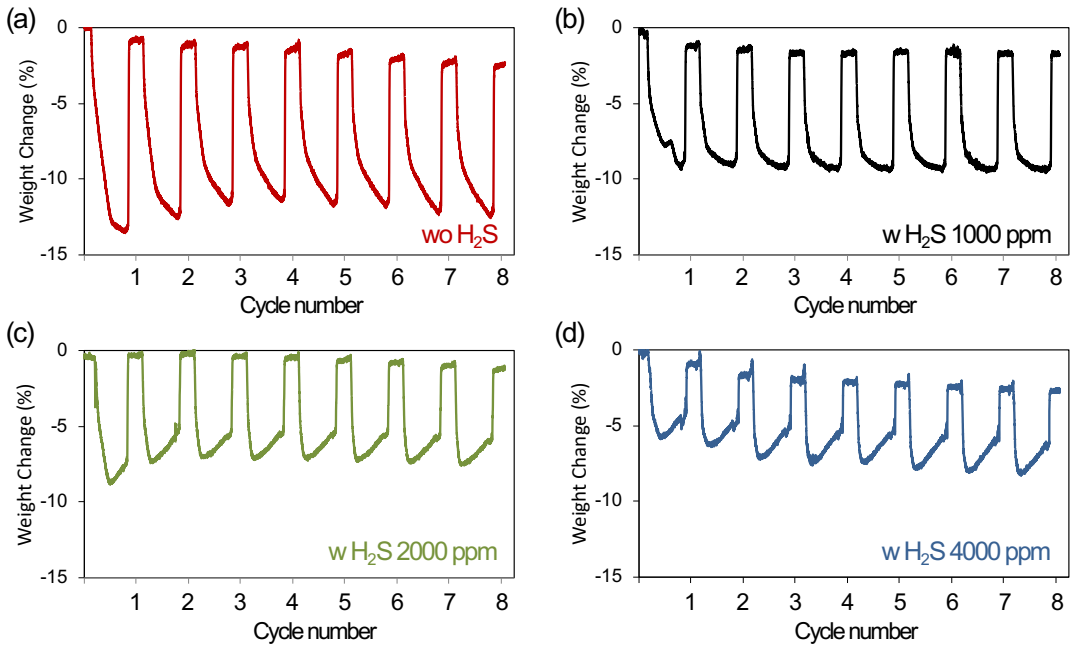

Figure 46. TGA profiles for eight redox cycles of Fe_2O_3/Al_2O_3 by 5% H_2 and air at 1173 K (a) without H_2S, (b) with 1000 ppm H_2S, (c) with 2000 ppm H_2S, and (d) with 4000 ppm of H_2S.

Fe_2O_3/Al_2O_3 showed a weight loss of 13.6 wt% from the first reduction with 5% H_2, but its performance decreased with the number of cycles. This redox deactivation behavior of Fe_2O_3/Al_2O_3 was also observed in our previous results in chapter 2, and is due to the agglomeration of iron-based oxygen carriers at the high temperature. In the presence of H_2S, similar deactivation were observed as well. The total combustion reactivity of Fe_2O_3/Al_2O_3 significantly declined with the addition of H_2S and weight gain

was even observed during the reduction period in the cases of 2000 ppm and 4000 ppm H_2S.

For evaluation of the effect of H_2S on the performance of Fe_2O_3/Al_2O_3, the TGA profiles of the fifth cycles with and without H_2S were compared and overlapped in Figure 47. There were no direct weight increases at the initial time of reduction on the TGA curves in any cases of H_2S, insisting that the direct sulfidation of Fe_2O_3/Al_2O_3 by H_2S is unlikely to happen. Similar to ilmenite samples, a weight loss by reduction of Fe_2O_3 firstly occurred, and then a weight gain by sulfidation followed with 2000 ppm and 4000 ppm of H_2S. The weight gain became much greater with the higher concentration of H_2S. From some point of the reduction, sulfidation reactions took place simultaneously and finally dominated over the reduction, which resulted in weight gain.

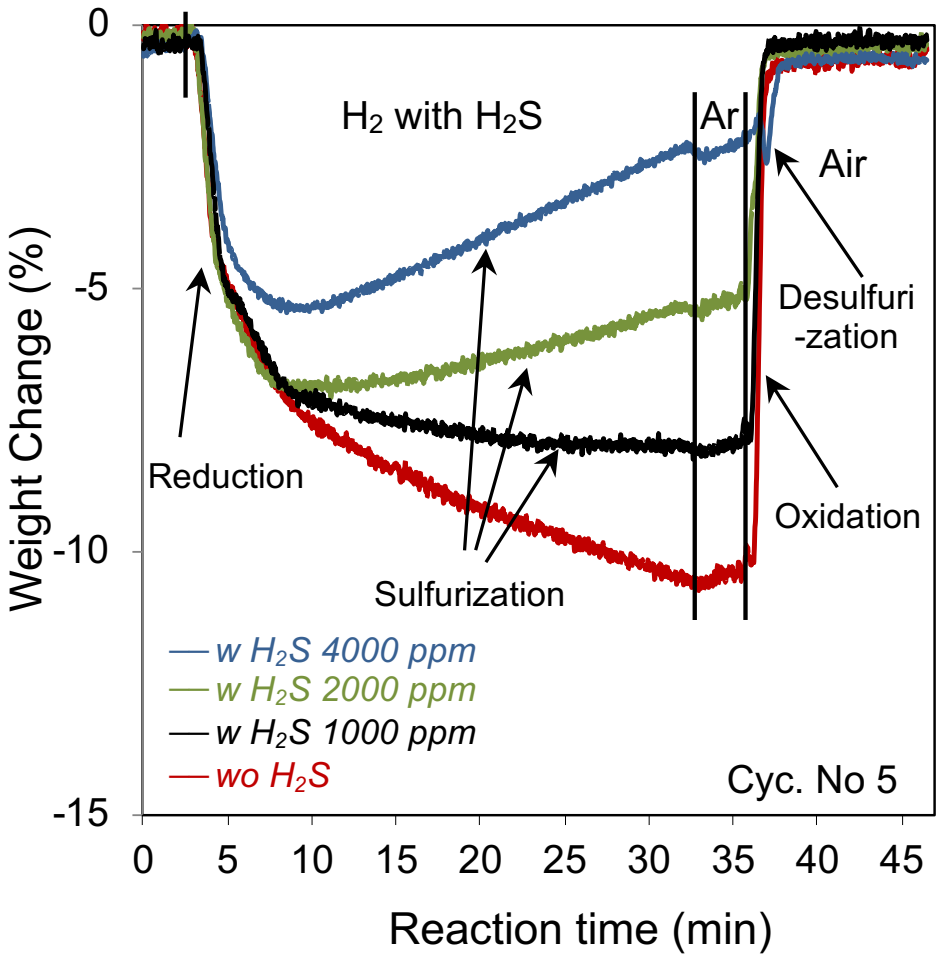

Figure 47. The 5th cycle TGA curves of Fe_2O_3/Al_2O_3 in 5% H_2 and air at 1173 K without H_2S (red), with 1000 ppm H_2S (black), with 2000 ppm H_2S (green), and with 4000 ppm H_2S (blue).

Overall, it was seen that the initial reduction rate to a weight loss of 3.1 wt% was not significantly changed by H_2S, which roughly corresponds to Fe_3O_4/Al_2O_3. This result strongly supports that the Fe_2O_3/Fe_3O_4 oxygen carrier forms no sulfur compounds under any concentration of sulfurous gas at high temperature [11]. After that, however, the combustion capacity of Fe_2O_3/Al_2O_3 negatively affected by H_2S. If the final reduction weight loss point (10.7 wt%) of Fe_2O_3/Al_2O_3 without H_2S is assumed to be 100%, the percentages in the cases with H_2S would be calculated in a similar way from the final reduction points. Consequently, the combustion capacity of Fe_2O_3/Al_2O_3 are around 76%, 65%, and 50% in 1000 ppm, 2000 ppm, and 4000 ppm of H_2S, respectively.

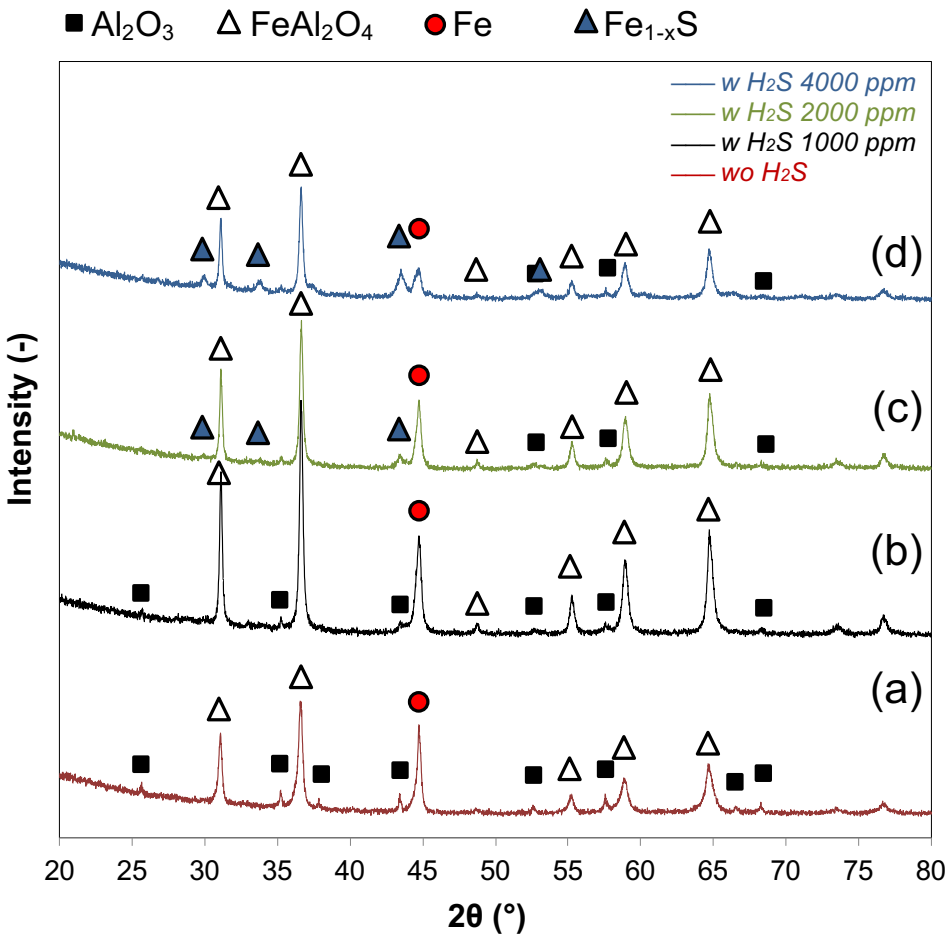

Figure 48. XRD patterns of the used Fe_2O_3/Al_2O_3 particles after reduction by 5% H_2 (a) without H_2S, (b) with 1000 ppm H_2S, (c) with 2000 ppm H_2S, and (d) with 4000 ppm H_2S.

The used samples of Fe_2O_3/Al_2O_3 at the end of reduction after 5 redox cycles with and without H_2S addition were subjected to XRD and XPS analyses. As seen in Figure 48(a), the Fe_2O_3/Al_2O_3 particles had been reduced to $FeAl_2O_4$ and Fe phases under the extra reducing atmosphere. A metallic iron of Fe^0 formed via the reduction of Fe_2O_3/Al_2O_3. Similarly, the iron sulfide pyrrhotite ($Fe_{1-x}S$) was also found on the surface of the Fe_2O_3/Al_2O_3 particles in the presence of H_2S (Figures 43(c)-(d)). In addition, the relative intensities of the peaks corresponding to the $Fe_{1-x}S$ phase increased with the increase in H_2S concentration, while the intensities of the peaks corresponding to Fe^0 decreased. This behavior was the same as the ilmenite particles, insisting that sulfidation goes through Fe^0 formation, in accordance with R47. As shown in Figure 49, XPS analysis also confirmed the presence of sulfur iron species such as FeS, FeS_2 and $FeSO_4$ on the Fe_2O_3/Al_2O_3 particles used with H_2 and H_2S.

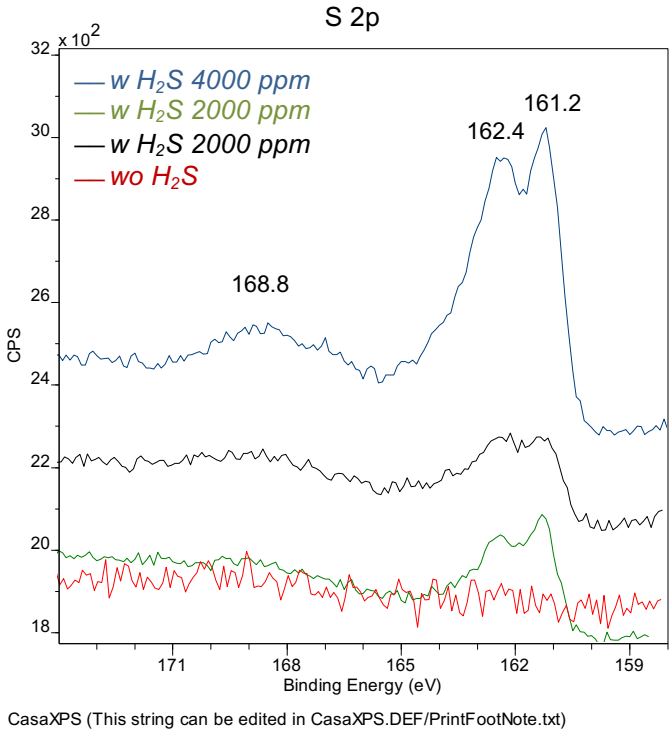

Figure 49. XPS patterns of the used Fe_2O_3/Al_2O_3 particles after reduction by 5% H_2 (a) without H_2S, (b) with 1000 ppm H_2S, (c) with 2000 ppm H_2S, and (d) with 4000 ppm H_2S.

MS data of the product gases from the 5th cycle tests with Fe_2O_3/Al_2O_3 were obtained for the evaluation of H_2S effect and are shown in Figure 50. During the reducing

period, there was no significant difference on the initial reduction of Fe_2O_3/Al_2O_3 with and without H_2S. During the oxidation period, SO_2 peaks were detected for all samples with H_2S, as shown in Figure 50(b). The higher the concentration of H_2S introduced to the reduction, the larger the SO_2 peak area detected upon the next oxidation of Fe_2O_3/Al_2O_3. This result reveals that the desulfurization reaction R48 took place in correlation to the amount of H_2S used in the previous reduction during the oxidation R49.

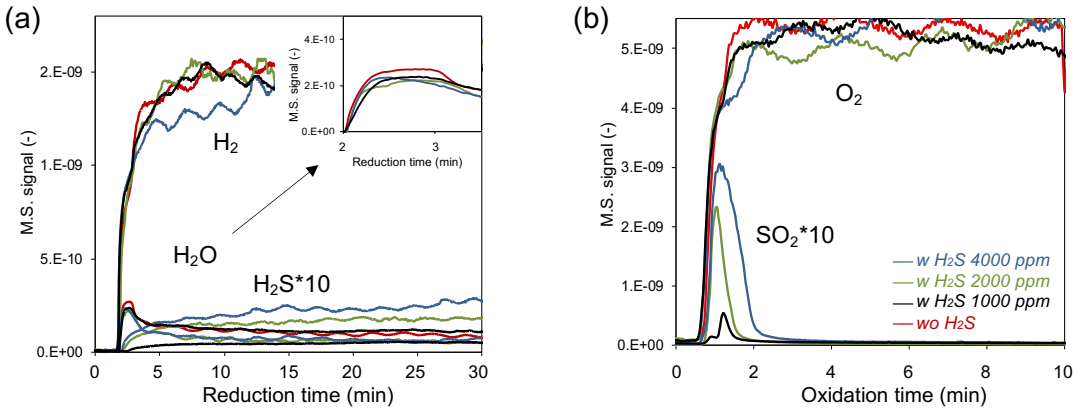

Figure 50. Mass profiles for the 5th cycles of Fe_2O_3/Al_2O_3 in 5% H_2 and air at 1173 K in the absence (red) and the presence of 1000 ppm (black), 2000 ppm (green), and 4000 ppm (blue) of H_2S for (a) H_2, H_2S and H_2O in the reducing period, and (b) SO_2 and O_2 in the oxidizing period.

$$2FeS + 7/2O_2 \rightarrow Fe_2O_3 + 2SO_2 \quad \text{(R48)}$$

$$2FeAl_2O_4 + 1/2O_2 \rightarrow Fe_2O_3 + 2Al_2O_3 \quad \text{(R49)}$$

Moreover, as shown with blue curve in Figure 47, there was a sharp weight loss at the beginning of oxidation in the case of 4000 ppm H_2S with Fe_2O_3/Al_2O_3. In conjunction with the MS results shown in Figure 50(b), it is due to the release SO_2 from the $Fe_{1-x}S$ phase on the Fe_2O_3/Al_2O_3. Finally, the reduced and sulfurized Fe_2O_3/Al_2O_3 carrier recovered their oxygen carrier reactivity via sulfur removal and oxidation.

3.3.5 The expected sulfur fate during the iG-CLC operation under a deficient oxygen condition

The carbon and sulfur balances of coal volatiles over ilmenite and Fe_2O_3/Al_2O_3 without and with 2000 ppm of H_2S was roughly estimated and presented in Figure 51 and Figure 52. In this study, the sulfur effect on the reactivity of ilmenite and Fe_2O_3/Al_2O_3 with coal volatiles was investigated under a oxygen deficient condition (less than the stoichiometric amount). Oxygen carriers were used approximately 40% of the stoichiometric amount required for a full conversion of volatiles (ϕ=0.4). This oxygen deficiency made it clear that sulfur behavior in the CLC system greatly depends on the oxidizing condition of the oxygen carrier particles. If a lattice oxygen of ilmenite is sufficient, most of the sulfur is converted to SO_2 (S:30). Simultaneously, CO_2 conversion over ilmenite are promoted (around 5%) by the effect of sulfur gas. That may be due to activation of ilmenite and WGS reaction. If a lattice oxygen is deficient, which mostly corresponds to formation of the deeply reduced iron phase on the ilmenite, sulfur depositions on the ilmenite particles (14%) and in the volatiles reactor (19%) take place by the sulfurization. Sulfur deposit on the ilmenite particles is mainly present as iron sulfide species $Fe_{1-x}S$.

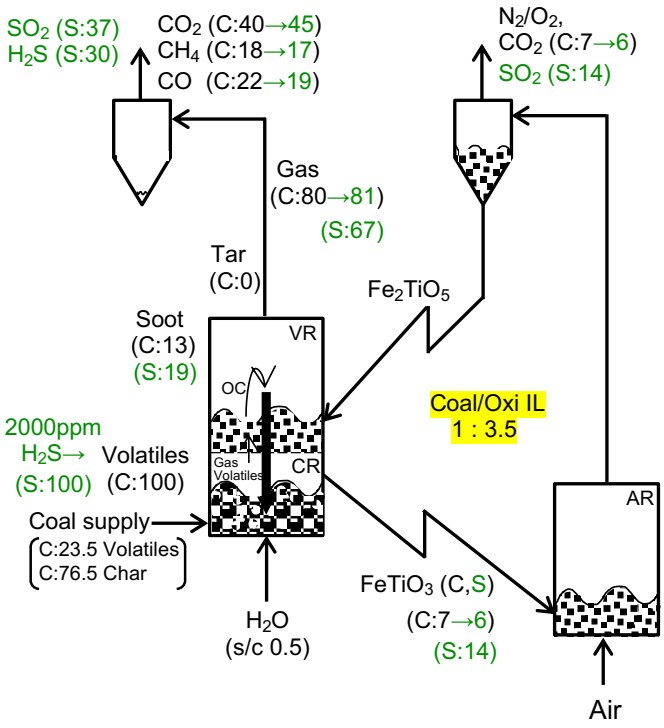

Figure 51. Carbon and sulfur balances of coal volatiles with ilmenite (S/C 0.5) without (black) and with 2000 ppm of H_2S (green) under an oxygen deficient condition (Oxi IL/Coal 3.5). Carbon from char gasification is not accounted for estimation.

However, tens of times higher amount of oxygen carrier to coal (50) is proposed for the iG-CLC system. That means that CLC process is mostly operated under a sufficient oxygen condition. Hence, sulfur impurities from coal are not big issues as long as the CLC system is run under a sufficient amount of oxygen carrier. Instead, sulfur can be promoting effect on the CO_2 conversion over ilmenite oxygen carrier.

A similar sulfur behavior dependent on oxidizing condition of Fe_2O_3/Al_2O_3 is presented in Figure 52. However, CO_2 conversion over Fe_2O_3/Al_2O_3 is not promoted by the effect of sulfur. That is because sulfidation is more easily occurred on the Fe_2O_3/Al_2O_3 particles than ilmenite under an extra reducing atmosphere. Therefore, sulfur deposit on the Fe_2O_3/Al_2O_3 particles is significantly high (35%). When high sulfur-containing fuel is employed in iG-CLC system, the reduction level of the oxygen carriers should be carefully controlled in order to avoid sulfur problems.

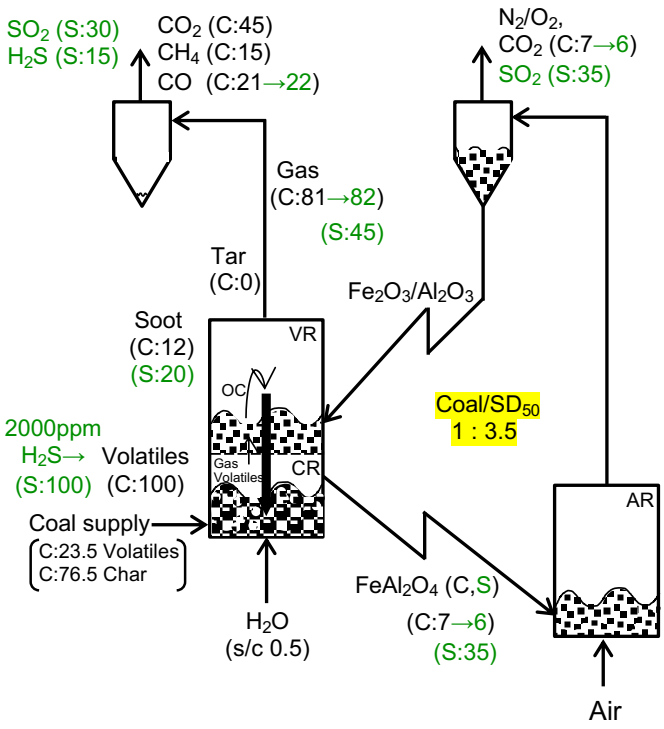

Figure 52. Carbon and sulfur balances of coal volatiles over Fe_2O_3/Al_2O_3 (S/C 0.5) without (black) and with 2000 ppm of H_2S (green) under an oxygen deficient condition (SD_{50}/Coal 3.5). Carbon from char gasification is not accounted for estimation.

3.4 Conclusions

The effect of H_2S on the combustion reactivity of ilmenite with coal volatiles under a steam reforming atmosphere was examined in a fixed-bed reactor. Actual volatiles from coal pyrolysis were used as fuel to react with the ilmenite. The results of the steam reforming experiments showed that ilmenite converted more carbon volatiles into CO_2 in the presence of H_2S than in the absence of H_2S. However, the enhancement to the combustion reactivity of ilmenite decreased with a higher concentration of H_2S due to the formation of iron sulfide species such as $Fe_{1-x}S$ on the reduced ilmenite particles. Based on TGA results, it can be inferred that once the ilmenite was reduced to the Fe^0 phase, its sulfidation by H_2S took place instantaneously in the reducing atmosphere. The TGA analysis also showed that the presence of H_2S greatly enhanced the initial reduction rate of ilmenite. In particular, the combustion reactivity of ilmenite can be improved by a small amount of added H_2S. While a higher amount of H_2S could cause sulfidation on ilmenite under an extra reducing environment, the iron sulfides and sulfur accumulation on ilmenite can be removed by oxidation.

Compared the ilmenite, it was a different tendency in the synthetic Fe_2O_3/Al_2O_3 carrier. The combustion reactivity of Fe_2O_3/Al_2O_3 with volatiles was declined by effect of H_2S, because sulfidation easily occurred on reduced particles of Fe_2O_3/Al_2O_3. The TGA results also showed the same deactivation behavior of Fe_2O_3/Al_2O_3 by H_2S.

Although many studies suggest that the formation of sulfides is not a problem as long as the CLC process is run under a sufficient amount of oxygen carriers, all aspects of sulfur behavior with oxygen carriers under various conditions are important to overall CLC process design and optimization. Based on the results of this study, if the reduction level of ilmenite by sulfur-containing fuel is carefully controlled, sulfur problems can be avoided.

References

[1] J. Adanez, A. Abad, F. Garcia-Labiano, P. Gayan, L.F. De Diego, Progress in chemical-looping combustion and reforming technologies, Prog. Energy Combust. Sci. 38 (2012) 215–282.

[2] Y. Cao, W.P. Pan, Investigation of chemical looping combustion by solid fuels. 1. Process analysis, Energy and Fuels. 20 (2006) 1836–1844.

[3] H. Leion, T. Mattisson, A. Lyngfelt, The use of petroleum coke as fuel in chemical-looping combustion, Fuel. 86 (2007) 1947–1958.

[4] H. Leion, T. Mattisson, A. Lyngfelt, Solid fuels in chemical-looping combustion, Int. J. Greenh. Gas Control. 2 (2008) 180–193.

[5] T.A. Brown, J.S. Dennis, S.A. Scott, J.F. Davidson, A.N. Hayhurst, Gasification and chemical-looping combustion of a lignite char in a fluidized bed of iron oxide, Energy and Fuels. 24 (2010) 3034–3048.

[6] C. Linderholm, M. Schmitz, Chemical-looping combustion of solid fuels in a 100 kW dual circulating fluidized bed system using iron ore as oxygen carrier, J. Environ. Chem. Eng. 4 (2016) 1029–1039.

[7] J. Adánez, A. Abad, T. Mendiara, P. Gayán, L.F. de Diego, F. García-Labiano, Chemical looping combustion of solid fuels, Prog. Energy Combust. Sci. (2018).

[8] S.Y. Lin, T. Saito, K. Hashimoto, Development of the Three-Tower Chemical Looping Coal Combustion Technology, in: Energy Procedia, 2017.

[9] T. Saito, S. Lin, Coal Char Reaction with Oxygen Carrier in Chemical Looping Combustion, Energy and Fuels. (2019).

[10] B. Tsedenbal, N. Kannari, K. Sato, H. Abe, H. Shirai, T. Takarada, Reforming of coal volatiles over ilmenite ore, Fuel Process. Technol. (2019).

[11] E. Jerndal, T. Mattisson, A. Lyngfelt, C. Combustion, O. After, Chemical Engineering Research and Design 2006-Thermal Analysis of Chemical-Looping Combustion, (2006).

[12] B. Wang, R. Yan, D.H. Lee, D.T. Liang, Y. Zheng, H. Zhao, C. Zheng, Thermodynamic investigation of carbon deposition and sulfur evolution in chemical looping combustion with syngas, Energy and Fuels. 22 (2008) 1012–1020.

[13] L.F. De Diego, F. García-Labiano, P. Gayán, A. Abad, A. Cabello, J. Adánez, G. Sprachmann, Performance of Cu- and Fe-based oxygen carriers in a 500 Wth CLC

unit for sour gas combustion with high H2S content, Int. J. Greenh. Gas Control. 28 (2014) 168–179.

[14] H. Tian, T. Simonyi, J. Poston, R. Siriwardane, Effect of hydrogen sulfide on chemical looping combustion of coal-derived synthesis gas over bentonite-supported metal-oxide oxygen carriers, Ind. Eng. Chem. Res. (2009).

[15] H. Gu, L. Shen, J. Xiao, S. Zhang, T. Song, D. Chen, Evaluation of the effect of sulfur on iron-ore oxygen carrier in chemical-looping combustion, Ind. Eng. Chem. Res. 52 (2013) 1795–1805.

[16] E. Ksepko, R. V. Siriwardane, H. Tian, T. Simonyi, M. Sciazko, Effect of H 2S on chemical looping combustion of coal-derived synthesis gas over Fe-Mn oxides supported on sepiolite, ZrO 2, and Al 2O 3, Energy and Fuels. 26 (2012)

[17] C. Chung, Y. Pottimurthy, M. Xu, T.L. Hsieh, D. Xu, Y. Zhang, Y.Y. Chen, P. He, M. Pickarts, L.S. Fan, A. Tong, Fate of sulfur in coal-direct chemical looping systems, Appl. Energy. 208 (2017) 678–690.

[18] C. Linderholm, M. Schmitz, P. Knutsson, A. Lyngfelt, Chemical-looping combustion in a 100-kW unit using a mixture of ilmenite and manganese ore as oxygen carrier, Fuel. 166 (2016) 533–542.

[19] P. Moldenhauer, M. Rydén, T. Mattisson, M. Younes, A. Lyngfelt, The use of ilmenite as oxygen carrier with kerosene in a 300W CLC laboratory reactor with continuous circulation, Appl. Energy. 113 (2014) 1846–1854.

[20] Y. Tan, Z. Sun, A. Cabello, D.Y. Lu, R.W. Hughes, Effects of H 2 S on the Reactivity of Ilmenite Ore as Chemical Looping Combustion Oxygen Carrier with Methane as Fuel, Energy and Fuels. 33 (2019) 585–594.

[21] N. Tsubouchi, Y. Mochizuki, Y. Ono, K. Uebo, Functional Forms of Nitrogen and Sulfur in Coals and Fate of Heteroatoms during Coal Carbonization, Tetsu-to-Hagane. 98 (2012) 161–169.

[22] D. Mandrino, XPS and SEM of Unpolished and Polished FeS Surface. Mater. Tehnol. 45 (2011) 325–328.

[23] M. Y. Morales-Gallardo, A. M. Ayala, M. Pal, M. A. Cortes Jacome, J. A. Toledo Antonio, N. R. Mathews, Synthesis of Pyrite FeS2 Nanorods by Simple Hydrothermal Method and Its Photocatalytic Activity. *Chem. Phys. Lett.* 660 (2016) 93–98.

[24] Y. Ku, Y.C. Liu, P.C. Chiu, Y.L. Kuo, Y.H. Tseng, Mechanism of Fe2TiO5 as oxygen carrier for chemical looping process and evaluation for hydrogen

generation, Ceram. Int. (2014).

[25] J. Adánez, A. Cuadrat, A. Abad, P. Gayán, L.F.D. Diego, F. García-Labiano, Ilmenite activation during consecutive redox cycles in chemical-looping combustion, Energy and Fuels. 24 (2010) 1402–1413.

[26] L. Zeng, F. He, F. Li, L.S. Fan, Coal-direct chemical looping gasification for hydrogen production: Reactor modeling and process simulation, in: Energy and Fuels, 2012.

[27] M. Pujara, M. Sheth, N. Rachchh, R. Bhoraniya, Chemical Looping Reforming (CLR) System for H 2 Production — A Review, (2020).

[28] Y. Zhongliang, Y. Yanyan, Y. Song, Z. Qian, Z. Jiantao, F. Yitian, H. Xiaogang, G. Guoqing, Iron-based oxygen carriers in chemical looping conversions: A review, Carbon Resour. Convers. 2 (2019) 23-34.

[29] D. Heift, Iron sulfide materials: Catalysts for electrochemical hydrogen evolution, Inorganics. (2019).

Chapter 4 CONCLUSIONS AND RECOMMENDATIONS

4.1 Results overview

In this work, the combustion reactivity of ilmenite with the coal volatiles under steam reforming and sulfur gas atmosphere was investigated, in comparison with Fe_2O_3/Al_2O_3, in order to evaluate the behavior of sulfur impurities, higher hydrocarbons (e.g., tar) and carbon depositions.

The main conclusions obtained in this study are:

- Based on this work, the higher hydrocarbons (tar) would not be a problem, when the coal CLC system runs under oxygen sufficiently supplied by the oxygen carrier.

- The carbon deposits on the oxygen carrier and in the fuel reactor can be avoided with higher concentration of steam.

- Sulfur gas behavior in the CLC system greatly depends on the oxidizing state of the oxygen carrier. If a lattice oxygen from oxygen carrier is sufficient, most of the sulfur can be converted to SO_2 and released from the fuel reactor. Simultaneously, CO_2 conversion over ilmenite is promoted by the effect of sulfur gas.

- If a lattice oxygen is deficient, sulfur depositions and sulfidation may proceed in the fuel reactor and on the oxygen carrier, respectively. Sulfur deposits on the ilmenite and Fe_2O_3/Al_2O_3 particles are mainly present as iron sulfide species such as $Fe_{1-x}S$.

- The tendency for sulfurization was dependent on the reduced level of ilmenite. Therefore, the reduction level of ilmenite by sulfur-containing coal should be carefully controlled in the iG-CLC system in order to prevent sulfur problems.

The other results obtained in this study are:

- Natural ilmenite was mainly composed of the lower oxidation state of Fe (II), causing its reactivity for tar decomposition and volatile conversion to be lower.

- The reactivity of ilmenite with coal volatiles over steam reforming was significantly enhanced after oxidation pretreatment, showing the higher conversion to CO_2 and no tar formation.

- After pre-oxidation, ilmenite forms a granular dense structure with Fe-condensed in the external surface. However, the internal and external porosity of ilmenite increases after the steam reforming of coal volatiles due to the efficient utilization of the lattice oxygen in ilmenite.

- The formation of carbon depositions was clearly correlated to the steam amount. Carbon deposits decreased considerably as steam ratios increased.

- The reduced phase $FeTiO_3$ of ilmenite was maintained with the higher steam concentration, and its reactivity was relatively stable compared with Fe_2O_3/Al_2O_3.

- A reversible reaction from reduced $FeO/FeAl_2O_4$ to Fe_3O_4 occurred on the Fe_2O_3/Al_2O_3 carrier by the higher steam ratios. Along with Fe_3O_4 formation, the H_2 content in flue gas substantially increased during the steam reforming.

- The redox reactivity of ilmenite increased with higher cycle numbers, whereas Fe_2O_3/Al_2O_3 reactivity decreased with increasing the cycles.

- The combustion reactivity of ilmenite with coal volatiles was positively affected by H_2S. Ilmenite converted more carbon volatiles into CO_2 in the presence of H_2S than in the absence of H_2S. However, the activation of ilmenite decreased with a higher concentration of H_2S due to the formation of iron sulfide species .

- In a comparison with ilmenite, Fe_2O_3/Al_2O_3 showed a decline of CO_2 conversion in the presence of H_2S during steam reforming of coal volatiles. H_2S significantly decreases the combustion reactivity of Fe_2O_3/Al_2O_3.

- The tendency for sulfurization was dependent on the reduced level of ilmenite. Sulfidation may not proceed during the reduction of ilmenite from Fe_2TiO_5 to $FeTiO_3$. Probably, sulfurization may occur from the reduced level of Fe^0 on the ilmenite particles in the reducing atmosphere.

- H_2S greatly enhanced the initial reduction rate of ilmenite. In particular, the combustion reactivity of ilmenite can be improved by a small amount of H_2S.

- Although a higher amount of H_2S causes sulfidation on ilmenite and Fe_2O_3/Al_2O_3 under an extra reducing environment, those iron sulfides and sulfur accumulation can be removed by next oxidation.

4.2 Recommendations for future works

Based on this work, the higher hydrocarbons (tar) would not be a problem, when the coal CLC system runs under oxygen sufficiently supplied by the oxygen carrier. The carbon deposition can be avoided with higher concentration of steam. The combustion reactivity of ilmenite with volatiles was not affected by the increased amount of steam, compared with Fe_2O_3/Al_2O_3. However, the cycle redox reactivity of ilmenite was not assessed under steam atmosphere in this study. That is strongly recommended for future investigation in order to confirm the effect of steam on ilmenite.

The behavior of sulfur gas significantly depended on the oxidized level of ilmenite. The sulfur gas is converted into SO_2 as long as oxygen available in the system. The initial reduction of ilmenite was activated by H_2S, which probably leaded to higher combustion reactivity of ilmenite under steam reforming of coal volatiles. However, the detailed activation mechanism of H_2S on ilmenite was not determined in this study. That

is strongly recommended for future investigation in order to confirm the effect of H_2S on the reactivity of ilmenite.

The combustion reactivity of ilmenite decreased with a higher concentration of H_2S due to the formation of iron sulfide species such as $Fe_{1-x}S$. Sulfidation appeared not to proceed during the reduction of ilmenite from Fe_2TiO_5 to $FeTiO_3$. Once the reduced level Fe^0 formed on the ilmenite particles, sulfidation took place. Based on these results of this study, the reduction level of ilmenite by sulfur-containing coal should be carefully controlled to prevent sulfur problems. They are also very important to assess the feasibility of using sulfur-containing coal for a real application as well as to estimate overall CLC process design and optimization.

Moreover, the reaction between steam and the reduced iron species discussed in this study is interesting for chemical looping hydrogen generation process. Especially, hydrogen generation should pay more attention on a synthetic oxygen carrier of Fe_2O_3/Al_2O_3.

Appendix

Table A1. CO_2 capture technologies in developmental stages

Capture technologies	Test stage
Post-Combustion	
Amine-based solvents	Demo
Advanced amine-based solvents	Pilot
Amino-Acid salt solvent	Pilot
Aqueous Ammonia solvent	Demo
Precipitating solvents	Lab/Bench
Two-phase liquid solvents	Lab/Bench
Catalyzed enhanced solvents	Lab/Bench
Ionic liquids	Lab/Bench
Temperature or Pressure Swing Adsorption with solid sorbents (TSA/PSA)	Pilot
Calcium Looping (CaL)	Pilot
Membranes	Pilot
Cryogenic CO_2 separation	Lab/Bench
Pre-Combustion	
Physical solvents	Demo
Ionic liquids	Lab/Bench
Temperature or Pressure Swing Adsorption with solid sorbents (TSA/PSA)	Lab/Bench
Sorption Enhanced Water Gas Shift (SEWGS)	Pilot
Sorption Enhanced Reforming (SER)	Pilot
Water Gas Shift Reactor (WGSR) membranes	Lab/Bench
Membranes	Piot
Cryogenic CO_2 separation	Concept
Oxy-Combustion	
Atmospheric pressure oxy-combustion	Demo
Ion Transport Membranes (ITM)	Pilot
Oxygen Transport Membranes (OTM)	Lab/Bench
Pressurized oxy-combustion	Pilot
Chemical Looping combustion (CLC)	Pilot

Table A2. Chemical compositions of coal tar, analyzed by GCMS

Peak **RT**	**Name of compounds**	**Formula**	**M.w.**
12.2	2-Pentanone, 4-hydroxy-4-methyl-	C6H12O2	116
41.5	Acenaphthylene	C12H8	152
44.2	Dibenzofuran	C12H8O	168
46.9	Fluorene	C13H10	166
54.5	Phenanthrene	C14H10	178
54.8	Anthracene	C14H10	178
59.3	4H-Cyclopenta[def]phenanthrene	C15H10	190
60.9	2-Phenylnaphthalene	C16H12	204
64.0	Pyrene	C16H10	202
64.7	Fluoranthene	C16H10	202
65.7	Pyrene	C16H10	202
75.2	Benzo[c]phenanthrene	C18H12	228
75.6	Chrysene	C18H12	228
85.2	Benzo[e]pyrene	C20H12	252
85.5	Perylene	C20H12	252
94.2	Benzo[ghi]perylene	C22H12	276

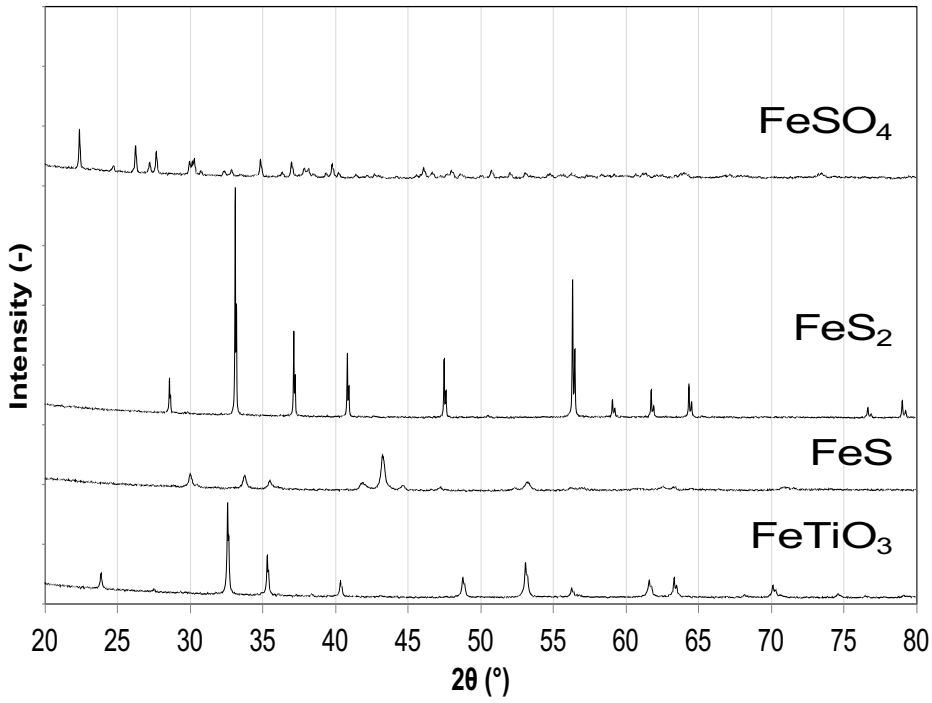

Figure A1. XRD spectra of $FeTiO_3$, FeS, FeS_2, and $FeSO_4$ particles

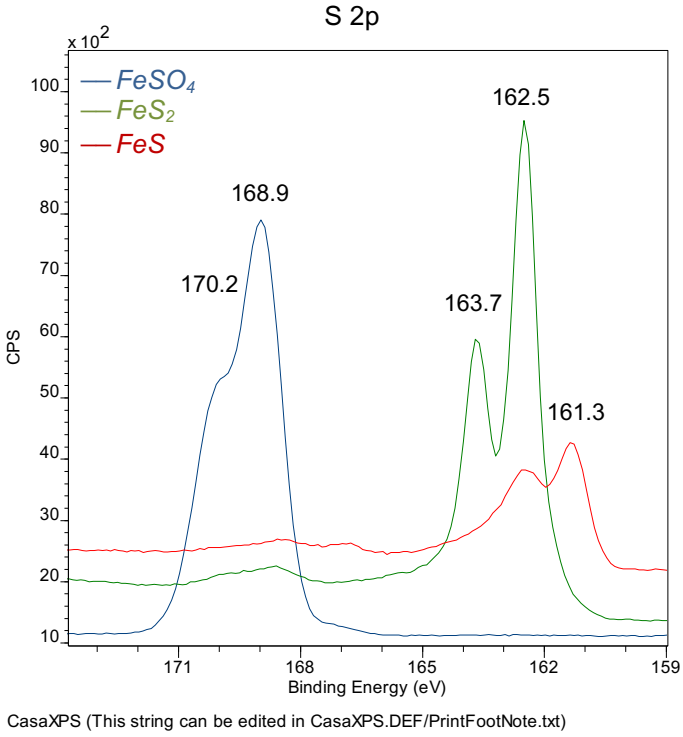

Figure A2. XPS spectra of the S 2p binding energy of $FeTiO_3$, FeS, FeS_2, and $FeSO_4$

LIST OF RESEARCH ARTICLES

1. Battsetseg Tsedenbal, Naokatsu Kannari, Kazuyoshi Sato, Hiromi Shirai, Takayuki Takarada, 'Effect of hydrogen sulfide on the combustion reactivity of ilmenite ores with coal volatiles under steam reforming'. *Energy & Fuels.* (just accepted).

2. Battsetseg Tsedenbal, Naokatsu Kannari, Kazuyoshi Sato, Hiroya Abe, Hiromi Shirai, Takayuki Takarada, 'Reforming of coal volatiles over ilmenite ore'. *Fuel Processing Technology*. 192 (2019) 96-104.

LIST OF PRESENTATIONS

1. Battsetseg Tsedenbal, Naokatsu Kannari, Kazuyoshi Sato, Hiromi Shirai, Takayuki Takarada, 'Steam reforming of coal volatiles by using iron-based chemical looping carriers'. *The 14th China-Japan Symposium on Coal and C1 Chemistry*. Sapporo, Hokkaido, Japan. September 2018.

2. Battsetseg Tsedenbal, Naokatsu Kannari, Takayuki Takarada, 'Effect of sulphur gas on iron-based oxygen carriers in chemical-looping process' The 2nd Australia-Japan Symposium on Carbon Resource Utilisation, Oral presentation. Brisbane, Australia, April 2018.

3. Battsetseg Tsedenbal, Naokatsu Kannari, Takayuki Takarada, 'Steam reforming of coal tar by chemical-looping carriers' 26th Annual Meeting of the Japan Institute of Energy tournament, Oral presentation. Aichi, Japan, August 2017.

4. Battsetseg Tsedenbal, Naokatsu Kannari, Takayuki Takarada, 'Steam reforming of coal tar using chemical-looping carriers' The 1st Australia-Japan Symposium on Carbon Resource Utilisation, Oral presentation. Melbourne, Australia, November 2016.
5. Battsetseg Tsedenbal, Naokatsu Kannari, Takayuki Takarada, 'Steam reforming of tar in coal using chemical-looping carriers' The 10th Kyung Hee-Gunma Joint

International Symposium on Green Energy, Oral presentation. Kusatsu, Japan, September 2016.

6. B. Kongsomart, B. Tsedenbal, S, Komatsu, N. Kannari, T. Takarada, 'Low temperature catalytic gasification of brown coal using empty fruit bunch'. *Gunma Conference*, *The society of chemical engineers in Japan*. Oral presentation. Gunma, Japan, December 2015.

7. B. Kongsomart, B. Tsedenbal, S, Komatsu, N. Kannari, T. Takarada, 'Low temperature catalytic gasification of brown coal using biomass'. *The 3rd Joint Meeting of Strategic Japanese Chinese Joint Research.* Poster presentation. Kanagawa, Japan, October 2015.

8. B. Kongsomart, B. Tsedenbal, S, Komatsu, N. Kannari, T. Takarada, 'Low temperature catalytic gasification of brown coal using chicken droppings'. *The 13th China-Japan Symposium on Coal and C1 Chemistry*. Poster presentation. Dunhuang, Gansu, China. August 2015.

9. B. Kongsomart, B. Tsedenbal, S, Komatsu, N. Kannari, T. Takarada, 'Low temperature catalytic gasification of brown coal using empty fruit bunch'. *The 13th China-Japan Symposium on Coal and C1 Chemistry*. Oral presentation. Dunhuang, Gansu, China. August 2015.